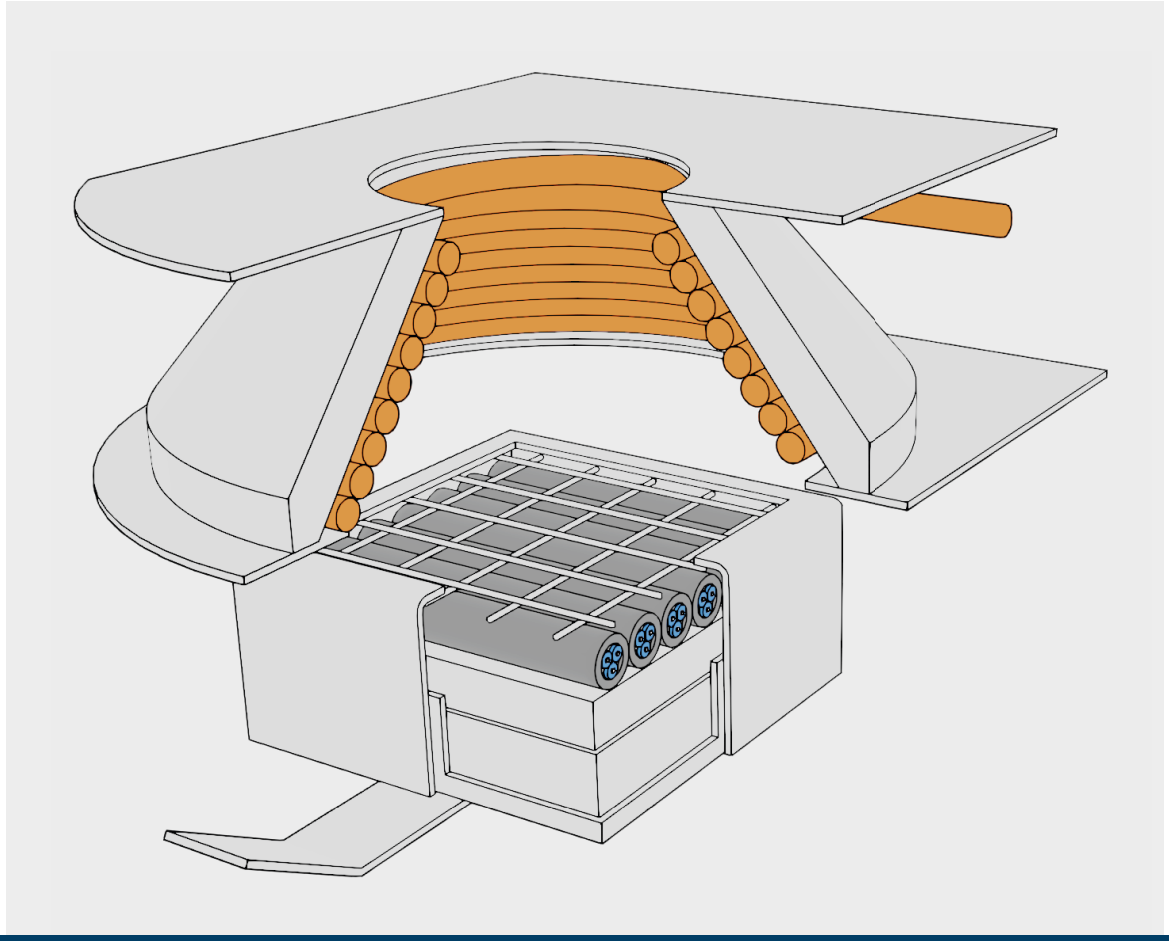

Simulation of Fire Propagation, Based on Material Pyrolysis

Tristan Hehnen

IAS Series
Band / Volume 75
ISBN 978-3-95806-875-9

Mitglied der Helmholtz-Gemeinschaft

JÜLICH
Forschungszentrum

Schriften des Forschungszentrums Jülich
IAS Series Band / Volume 75

Forschungszentrum Jülich GmbH
Institute for Advanced Simulation (IAS)
Zivile Sicherheitsforschung (IAS-7)

Simulation of Fire Propagation, Based on Material Pyrolysis

Tristan Hehnen

Schriften des Forschungszentrums Jülich
IAS Series

Band / Volume 75

ISSN 1868-8489

ISBN 978-3-95806-875-9

Bibliografische Information der Deutschen Nationalbibliothek.
Die Deutsche Nationalbibliothek verzeichnet diese Publikation in der
Deutschen Nationalbibliografie; detaillierte Bibliografische Daten
sind im Internet über http://dnb.d-nb.de abrufbar.

Herausgeber und Vertrieb:	Forschungszentrum Jülich GmbH Zentralbibliothek, Verlag 52425 Jülich Tel.: +49 2461 61-5368 Fax: +49 2461 61-6103 zb-publikation@fz-juelich.de www.fz-juelich.de/zb
Umschlaggestaltung:	Grafische Medien, Forschungszentrum Jülich GmbH
Druck:	Grafische Medien, Forschungszentrum Jülich GmbH
Copyright:	Forschungszentrum Jülich 2025

Schriften des Forschungszentrums Jülich
IAS Series, Band / Volume 75

D 468 (Diss. Wuppertal, Univ., 2024)

ISSN 1868-8489
ISBN 978-3-95806-875-9

Vollständig frei verfügbar über das Publikationsportal des Forschungszentrums Jülich (JuSER)
unter www.fz-juelich.de/zb/openaccess.

Abstract

Uncontrolled fires in buildings pose significant threats to occupants, the environment, property, and the continuity of operations. Fire risk assessments are critical tools used to identify hazards, determine the likelihood of their occurrence, assess potential consequences, and propose mitigation measures. Several methods exist for quantitative analysis, ranging from simple hand calculations to advanced computational fluid dynamics (CFD) simulations. Typically, heat release rates are prescribed in these assessments and are static. Primarily because the modelling of thermal decomposition (pyrolysis) of combustible materials is difficult.

This dissertation consists of three publications that deal with the design of parameter sets that allow the simulation of pyrolysis, based on the heat feedback to a sample material. From common small-scale fire experiments, data are used to create the material models.

The first publication deals with the simulation of fire propagation in cable tray installations. A proof of concept for a methodology is presented in which material parameters can be determined in an inverse modelling process (IMP). This IMP uses experimental data as the target.

The second publication builds on the work of the first publication and improves it. Several adjustments needed to be made in the previous work after the IMP concluded to enable fire propagation. These adjustments are here directly implemented in the IMP. Further improvements are implemented to the process, such as higher fluid cell resolution during the parameter estimation process.

The third publication moves away from the complex structure of electrical cables and focuses on a pure polymer: poly (methyl methacrylate) (PMMA). Further improvements are conducted with even higher fluid cell resolution. Furthermore, a wider range of experimental data sets is available, which is used to improve the parameter estimation.

Zusammenfassung

Brände in Gebäuden stellen erhebliche Bedrohungen für die Bewohner, die Umwelt, das Eigentum und die Weiterführung des Betriebs dar. Brandschutzkonzepte sind wichtige Werkzeuge, um Gefahren zu identifizieren, die Wahrscheinlichkeit ihres Auftretens zu bestimmen, mögliche Konsequenzen zu bewerten und Maßnahmen zur Minderung vorzuschlagen. Für die quantitative Analyse existieren verschiedene Methoden, die von einfachen Handrechenverfahren bis hin zu fortgeschrittenen numerischen Strömungsmechanik-Simulationen (CFD) reichen. Typischerweise werden in diesen Bewertungen Wärmefreisetzungsraten vorgeschrieben, die statisch sind. Dies liegt hauptsächlich daran, dass die Modellierung der thermischen Zersetzung (Pyrolyse) von brennbaren Materialien aufwändig ist.

Diese Dissertation besteht aus drei Veröffentlichungen, die sich mit der Entwicklung von Parametersätzen befassen, welche die Simulation der Pyrolyse basierend auf der Wärmeübertragung zu einem Probenmaterial ermöglichen. Aus gängigen kleinskaligen Brandversuchen werden Daten verwendet, um die Materialmodelle zu erstellen.

Die erste Veröffentlichung behandelt die Simulation der Brandausbreitung in Kabelinstallationen. Ein Konzept für eine Methodik wird vorgestellt, wie Materialparameter in einem inversen Modellierungsprozess (IMP) bestimmt werden können. Dieser IMP verwendet experimentelle Daten als Zielvorgaben.

Die zweite Veröffentlichung baut auf der Arbeit der ersten Veröffentlichung auf und verbessert diese. Einige Anpassungen mussten in der vorherigen Arbeit nach Abschluss des IMP vorgenommen werden, um die Brandausbreitung zu ermöglichen. Diese Anpassungen werden hier direkt im IMP implementiert. Weitere Verbesserungen am Prozess werden vorgenommen, wie z.B. eine höhere Auflösung der Fluidzellen während der Parameterbestimmung.

Die dritte Veröffentlichung entfernt sich von der komplexen Struktur elektrischer Kabel und konzentriert sich auf ein reines Polymer: Poly(methylmethacrylat) (PMMA). Weitere Verbesserungen werden mit noch höherer Auflösung der Fluidzellen durchgeführt. Darüber hinaus steht eine größere Bandbreite an experimentellen Datensätzen zur Verfügung, die zur Verbesserung der Parameterbestimmung verwendet werden.

Acknowledgements

This work would have been far more difficult than it was, if it had not been for the support and encouragement from many people, in big and small ways. The work started out with the goal to model flame spread in cable tray arrangements. In the end, cables were too complex and experimental data too limited. Thus, the topic shifted to more fundamental behaviour with a supposedly simpler material: PMMA – work that is still ongoing.

Along the way, a broad range of roadblocks were encountered. In the beginning, it became clear that the inverse modelling required substantial computing and access to them was limited. Hacker attacks on the Jülich Supercomputing Centre led initially to blocked and later to limited access during office hours for many weeks. Other computing clusters were plagued with emergency shutdowns due to issues with the cooling system. Software updates on the computing cluster and the simulation software led to setbacks and the need to rerun the material parameter estimation. At some point the internal structure of FDS changed, which prevented its parallel execution inside our inverse modelling scheme. In the end, the fix was fairly simple, but getting there was not. Ransomware rendered a lab computer unusable and required recovery. The fractured landscape of experimental data highlighted early on the need for experiments across all length scales with the same material. However, obtaining funding for such campaigns is difficult, especially on short notice. This lack of information was partly remedied toward the end of the work by data collected in the MaCFP pyrolysis effort. Thus, everything took way longer than intended and many people played a part in helping me stay on track. Some of their contributions are mentioned below.

To my parents and my brother, I would like to extend my gratitude for their continued support. They always encouraged me to keep going when I grew tired of school and pursued an apprenticeship. Later, when I decided to go back to school to earn the qualification needed to study at a university the support continued and it did not end when I decided to go abroad on a Phd scholarship, which eventually brought me here. Thank you very much!

I would like to thank the graduation committee – Armin, Lukas, Fabian and Jaan-Willem – for their time in reviewing and grading my work!

I am grateful to Lukas and Armin, for accepting me for a PhD position and their continued support during this endeavour. In particular, Lukas provided mentorship and supervision throughout. He put a lot of effort into making sure that computing resources were available, helped me to learn Python, and patiently edited and reviewed my monster-papers. He has always been available for discussions, and his views on open science are greatly appreciated.

Despite his busy schedule, Saverio always made time to talk about the progress of the work and other topics – music, quantum fire dynamics, adventures of the famous agent i or the crazy guy who tried to bring two knives onto a plane.

Fabian supported me with conversations about cone calorimeter simulations and modelling of modelling, and kindly agreed to act as the second reviewer of this thesis.

I would like to thank the Wolfgang-Gentner-Programme for giving me the opportunity of a PhD-scholarship at the European Organisation of Nuclear Research (CERN). I am grateful to everyone involved in organising the programme – and to the German taxpayers who made it possible.

I would like to thank Patrick van Hees for the opportunity to conduct cone calorimeter experiments on electrical cables at Lund University, as well as Dan, Bjarne and Michael for the support conducting the experiments, cleaning the apparatus and dealing with the ransomware situation.

Silvia, Michael, and I visited a number of pubs in Lund, especially the Inferno. Lars made me aware of the Gentner-Programme, having just gone through it himself. Further, we had extensive conversations about various topics like movies, safety engineering and society, and together with

Michael and John we joined several social events in Geneva. Lunchtime conversations with Michael (and our shared Factorio sessions) helped keep me sane, and he guided me through the ins and outs of life at CERN. With Peter there were further lunchtime discussions, doom-scrolling 9GAG, and even more Factorio: “Go big, or go home!”. Marco, Gunnar, Fabio, Oriol and Art were sharing their expertise and stories on helium spills, cable fires, concrete Jenga and the like.

Together with Corinna, Patrick and Lukas, we created PROPTI and shared our thoughts and knowledge on pyrolysis modelling. Mira helped me navigate the pitfalls of the university’s administration, specifically with the “Bastelamt”. Tàssia and Swathi helped with drilling down on the relevant aspects in modelling pyrolysis, parameter transfer, flame spread and on improving the creation of material parameter sets. Karen shared her experience in experimental work and provided valuable guidance on boundary conditions and expected outcomes – invaluable for a modeller.

Alex, Moe, Jonas and Stefan have always been there to provide distraction, ever since the days when we played in the sandbox together. Justus, Iwie, Henne, Benny, Christian and Malte, who came to visit me in France.

Thank you too, to everyone I forgot to mention.
Overall, there are many stories to tell, but for another place and time.

Kironothil

Kironothil, "Holyweak", a large, serrated zinc disc.

This is a large, serrated zinc disc. All craftdwarfship is of the highest quality. It is encrusted with oval dolomite cabochons, decorated with water buffalo leather and encircled with bands of oval petrified wood cabochons. This object menaces with spikes of zinc.

On the item is an image of Ustuth Tipletter the dwarf and Fene Birthforded the morning of Dominions the roc in schist. Fene Birthforded the morning of Dominions is striking down Ustuth Tipletter. The artwork relates to the killing of the dwarf Ustuth Tipletter by the roc Fene Birthforded the morning of Dominions in Bronzefriend in the Horn of Belts in the early summer of 1 during The Rampage of the roc Fene Birthforded the morning of Dominions in Bronzefriend.

On the item is an image of Sodel Vesselfortresses the dwarf and Fene Birthforded the morning of Dominions the roc in cherry opal. Sodel Vesselfortresses is cringing. Fene Birthforded the morning of Dominions is striking a menacing pose. The artwork relates to the tearing out of the dwarf Sodel Vesselfortresses's right eyelid by the roc Fene Birthforded the morning of Dominions in the early summer of 1 during The Rampage of the roc Fene Birthforded the morning of Dominions in Bronzefriend.

They say that life's a carousel
Spinning fast, you've got to ride it well
The world is full of kings and queens
Who blind your eyes and steal your dreams
It's Heaven and Hell
Oh well

And they'll tell you black is really white
The moon is just the sun at night
And when you walk in golden halls
You get to keep the gold that falls
It's Heaven and Hell
Oh no

Fool, fool
You've got to bleed for the dancer
Fool, fool
Look for the answer
Fool, fool, fool

Heaven and Hell
Black Sabbath

Ronnie James Dio
Tony Iommi
Geezer Butler
Bill Ward
1980

List of Publications

Publication I

Tristan Hehnen, Lukas Arnold, Patrick Van Hees, and Saverio La Mendola.
"Simulation of Fire Propagation in Cable Tray Installations for Particle Accelerator Facility Tunnels".
In: Proceedings from the 8th International Symposium on Tunnel Safety and Security ISTSS 2018. [1]

Publication II

Tristan Hehnen, Lukas Arnold, and Saverio La Mendola.
"Numerical Fire Spread Simulation Based on Material Pyrolysis – An Application to the CHRISTIFIRE Phase 1 Horizontal Cable Tray Tests".
In: Fire 3.3 (2020) [2]

Publication III

Tristan Hehnen and Lukas Arnold.
"PMMA pyrolysis simulation – from micro- to real-scale".
In: Fire Safety Journal 141 (2023) [3]

Contents

1 Introduction **1**
1.1 Motivation 1
1.2 Objectives and Approach 2

2 Methods and Results **4**
2.1 Initial Parameter Estimation Strategy – Publication I 4
2.2 Improved Cone Calorimeter Setup for the IMP – Publication II 6
2.3 Adjustments to the Cable Model 8
2.4 Improved IMP Based on PMMA – Publication III 12
2.5 Role of the Heat of Combustion 14
2.6 Flame Heat Flux 20

3 Discussion and Outlook **24**

4 Appendix **i**
4.1 Publication I: Cable Fires in Particle Accelerator Tunnels i
4.2 Publication II: Numerical Fire Spread Simulation Based on Material Pyrolysis – An Application to the CHRISTIFIRE Phase 1 Horizontal Cable Tray Tests xiii
4.3 Publication III: PMMA Pyrolysis Simulation – from Micro- to Real-Scale l

Chapter 1

Introduction

1.1 Motivation

Uncontrolled fires in buildings pose significant threats to occupants, the environment, property, and the continuity of operations. Fire risk assessments are used to identify hazards, determine the likelihood of their occurrence, assess potential consequences, and propose mitigation measures [4]. From these assessments, fire safety goals are defined in conjunction with the applicable building regulations.

Scenarios, derived from these fire safety goals, can be quantitatively evaluated using either prescriptive or performance-based design approaches, or a combination of both. On the one hand, the prescriptive approach provides specific guidelines from building codes that lead to a presumed safe configuration. On the other hand, these guidelines can limit innovative building designs. They are based on experiment campaigns and only limited extrapolation is possible. Many building codes permit the use of alternative methods or materials, if their performance can be demonstrated to meet, or exceed, the defined goals. Performance-based design offers greater flexibility but also introduces complexity.

Several methods exist for quantitative analysis, ranging from simple hand calculations to advanced computational fluid dynamics (CFD) simulations. CFD simulations are particularly valuable for performance-based designs, enabling detailed analyses of smoke and fire propagation.

Traditionally, the $\alpha \times t^2$ model is used to approximate fire development in design scenarios [5]. While this model is useful, it is rather rigid and cannot easily be adapted to dynamic changes in the fire environment. To address this limitation, more dynamic design fire scenarios are necessary. These scenarios should be able to react to changes in the fire environment, consider the orientation of combustible surfaces and account for the geometry of non-combustible surroundings, such as ceiling heights and room openings [6]. A good example of the interaction between building geometry and combustible surfaces is the fast fire development in the 1987 Kings Cross Underground Station fire [7, 8], where the fire spread rapidly along a wooden escalator and the "trench effect" was discovered.

Dynamic fire scenarios allow for the assessment of very specific situations, such as the release of radioactive materials from combustible sources at different locations within a structure. They also facilitate evaluations of non-regular, or unique structures, such as particle accelerator tunnels and laboratories. Thus, ensuring that fire safety designs are robust and comprehensive for a variety of situations.

In this work, strategies are assessed to create material parameter sets based on data from small-scale experiments, commonly used in fire science. In concert with CFD simulations, the resulting material models can then be used to predict the fire development for performance based design applications, by simulating self-sustained fire propagation.

1.2 Objectives and Approach

The simulation of fire spread is a complex task, as this phenomenon happens over a wide length scale. Gas phase combustion in diffusion flames takes place in a thin reaction zone, in the order of millimetres, separating the fuel from the oxidiser [9]. Especially, during the initial stages of a fire, the heat transfer from the flame front to the sample happens in scales between millimetres to centimetres [10]. Fully developed fires in individual rooms, and smoke spread through buildings, are happening in the order of multiple tens of meters. For practical fire simulations, the fluid cell sizes are comparatively large, in the order of tens of centimetres. This leads to challenges to accurately capture processes of combustion, pyrolysis, energy and mass transfer.

Assumptions are made that combustible materials have some fundamental properties. The assumption is further that these properties can be isolated using specifically designed experiments. Here, micro-scale experiments like differential scanning calorimetry (DSC) [11], microscale-combustion calorimetry (MCC) [12, 13] and thermogravimetric analysis (TGA) [14, 15], as well as bench-scale experiments like the cone calorimeter [16] or CAPA II [17], have been employed to accomplish this separation.

Material models are to be created that capture the thermophysical properties and the thermal decomposition behaviour (pyrolysis). The micro-scale experiments are used in the context of thermal analysis to assess the pyrolysis reactions. The micro-scale experiments, are specifically designed to reduce the influence of energy and mass transport phenomena of a sample material on its decomposition. This allows to tease out the pyrolysis behaviour. For thermal analysis any physical property can be used which changes with time. For example, the mass loss of a heated sample is the physical property of interest to investigate the sample decomposition. The progress of a reaction is called conversion α and ranges from 0, where reaction has not yet started, to 1, where the reaction concluded (equation 1.1). For the mass example, it can be expressed as:

$$\alpha = \frac{m_i - m}{m_i - m_f} \tag{1.1}$$

where m_i, m and m_f are the initial, instantaneous and final sample mass respectively. For a single-step decomposition reaction, pyrolysis can be modelled as presented in equation 1.2,

$$\frac{d\alpha}{dt} = k(T)\ f(\alpha)\ h(P) \tag{1.2}$$

where $d\alpha/dt$ is the conversion rate, $k(T)$ is the rate constant, $f(\alpha)$ the reaction model and $h(P)$ a pressure dependency [4]. The rate constant is commonly described using the classic Arrhenius equation 1.3,

$$k(T) = A\ exp\left(-\frac{E}{R\,T}\right) \tag{1.3}$$

with A being the pre-exponential factor, E the activation energy, R the universal gas constant and T the thermodynamic temperature of the sample. Various formulations exist for the reaction model $f(\alpha)$. In the field of fire safety engineering, the nth-order model is commonly used, as presented in equation 1.4:

$$f(\alpha) = (1\ -\ \alpha)^n \tag{1.4}$$

The pressure component is of importance, if the released gases react with the remaining sample material. This can be mitigated with a sufficiently large purge gas flow rate, to remove the evolved gases. It can then be neglected, as it is in this work. Combining the above equations leads to:

$$\frac{d\alpha}{dt} = A\ \exp\left(-\frac{E}{R\,T}\right)\ (1-\alpha)^n. \tag{1.5}$$

This formulation is used throughout the work presented here, to model the decomposition of the sample materials. Their total decomposition behaviour is computed as the sum over multiple, parallel single-step reactions.

For each reaction step, a set of reaction kinetics parameters A, E and n is needed. They can be determined from the micro-scale experiments, yet cannot be measured directly. Different curve fitting strategies can be employed to derive the reaction kinetics parameters [4]. In recent years, the use of optimisation algorithms has gained traction in the field [18–22]. Different researchers have implemented evolutionary algorithms to perform the parameter estimation, for example Matala [23] or Lautenberger [24]. Throughout this work, a flexible inverse modelling framework, called PROPTI [25, 26], was developed. It is publicly available via Zenodo [27]. PROPTI does not provide optimisation algorithms, but rather uses existing implementations. Its goal is to facilitate the communication between a simulation software and some optimisation algorithm. It further manages the data flow on high performance computing clusters.

The thermophysical parameters are deduced from cone calorimeter data. The involved procedures are described in the following sections.

No experiments were conducted for this work. Respective data is taken from the CHRISTIFIRE campaign [28, 29] and from the MaCFP repositories [30, 31]. Data sets from the experiments are used as target for inverse modelling processes (IMP). PROPTI is used to feed a shuffled complex evolutionary algorithm [32–35] with the target data and initiate simulations with the parameter sets generated from the algorithm. These parameter sets are used in simulations that are conducted with the Fire Dynamics Simulator (FDS) [36–39]. During the course of this work, FDS was developed further so that each of the publications presented here [1–3] uses a different version.

FDS uses an implementation of the decomposition reaction formulation presented in equation 1.5 and is focused on the nth-order reaction model. With the "`TGA_ANALYSIS`" method, FDS provides a convenience functionality to determine the parameter values of the Arrhenius equation 1.3. This method is further limited to first-order reactions, i.e. $n = 1$, as will be further discussed below.

The first two publications focus on fire propagation in horizontal cable tray installations. Material models with decomposition reactions are built for the individual plastic components of the cables. They are mapped into a layered boundary condition, to create a cable model that can be used in simulations where the cable diameters are far smaller than the fluid cell size. Thermophysical parameters are determined from simplified cone calorimeter simulations. The third publication moves away from the cables with their complex internal structure to a pure plastic: poly (methyl metharcylate) (PMMA). These publications are summarised on the following pages. Information that extents beyond the work presented in the publications is discussed around them. It is assessed how well the material parameter sets, determined with information from small-scale experiments, translate to real-scale simulations.

Chapter 2

Methods and Results

2.1 Initial Parameter Estimation Strategy – Publication I

The first publication [1] deals with the simulation of cable fires in FDS 6.3.2 [40]. The goal is to simulate fire propagation in a horizontal cable tray arrangement, driven by the pyrolysis of the plastic insulation material. This publication describes the initial strategy to determine the material parameter sets. It is based on the work of Anna Matala [18] and Chris Lautenberger [19, 24, 41] for the parameter estimation strategy and the CHRISTIFIRE project [28, 29] for the experimental data.

The fundamental idea is, to use data from micro-scale experiments to describe the thermal decomposition of the plastic cable components. Their thermophysical and optical parameters are to be determined from bench-scale experiments. Here, the parameters are determined through inverse modelling, by utilising a shuffled complex evolutionary algorithm. The resulting material parameter sets per cable component are then combined to form the cable model. In a real-scale simulation setup the cable model is then used to predict the fire spread. The cable model is considered as validated, if a real-scale simulation setup can predict the fire development recorded in a respective experiment.

From the cables of CHRISTIFIRE Phase 1 [28], cable 219 was chosen. From all cables studied, it showed the most consistent repeatability during the cone calorimeter experiments. Additionally, the studied cables during CHRISTIFIRE were surplus from different experiment campaigns. This was limiting the amount of cables that could be used in the real-scale experiments. For many experiments, different cables were mixed together within individual trays. Cable 219 is one of the few cables that was placed in trays without adding others in. This allowed to limit the effort in generating material models to a single cable.

The cable model itself is realised as a layered boundary condition to the fluid cells. This is necessary because in practical fire simulations the fluid cell sizes are typically rather large, with an edge length of about 15 cm. The cables have a diameter of about 1.5 cm, and the individual components are even smaller. The layered model is a common approach, when the cables cannot be resolved [21, 42]. Here three layers are utilised, the top and bottom layers consist of the jacket material, with a layer of insulator material in between.

In her work, Matala determined the decomposition reaction kinetics of the combustible cable components based on DSC and TGA data [23]. With CHRISTIFIRE Phase 1, only MCC data is available and is therefore used for publication I. Under the assumption that the heat of combustion of the released gaseous species is constant, the mass loss rate from the TGA and the heat release rate from the MCC can be related by a proportionality factor – the effective heat of combustion (HOC).

In the CHRISTIFIRE report some basic information is provided for the individual cable components, jacket and insulator. These are the HRR profiles from MCC experiments, the fraction of the

sample mass that is left over as inert residue after the MCC experiment and values for the reaction kinetics. Using this information, together with literature values for the thermophysical parameters, did not lead to good performance in the simplified cone calorimeter and cable tray setups (see figures 6, 7 and 8 in publication I [1]). On this basis, it was decided to determine the material parameters completely in the simplified cone calorimeter, utilising an IMP. The MCC data was solely used to determine the amount of decomposition reactions, based on the visible peaks in the MCC HRR plots.

After conclusion of the MCC experiments, a significant amount of inert residue was observed. Depending on the component, between 46 % to 49 % of the initial sample mass was left over [28]. No further information is available about this residue, thus its parameter values are purely guessed during the IMP.

A simplified cone calorimeter simulation setup was created and improved multiple times as outlined below. This setup consists of a domain with a minimal number of fluid cells for computational efficiency. They have an edge length of 10 cm. At first, the simulations were conducted with suppressed gas phase combustion reactions, to reduce the computational cost during the IMP. An external heat flux was prescribed to the sample surface to match the nominal value from the cone calorimeter experiment, i.e. $50\,\mathrm{kW/m^2}$. To capture the contribution from the flame, some extra heat flux was added to the prescribed nominal value. The extra amount was determined from a high resolution simulation. However, this leads to a static impact from a virtual flame. This was realised to be limiting to the overall IMP. The changing material parameters during the IMP, would lead to varying amounts in combustible gases being released. In turn, this leads to variations in flame size, and therefore impact the heat flux contribution to the sample. The gas phase reactions were enabled again, such that at least some of the flame heat flux could be determined dynamically, and consistent with the model. Thus, the same conclusion was reached, as reported by Matala [42], that the flame should be modelled explicitly.

In total, values for 34 individual parameters were determined for the complete cable model. The initial parameter set that used the literature values was used as starting point. Around each value a sampling range was defined, in which the algorithm could search for a better fit during the IMP. The adjusted parameters comprise the reaction kinetics and thermophysical parameters for the cable jacket and the insulator, thermophysical parameters of the residues for both cable components, as well as the thicknesses of the cable jacket, the insulator and the copper layers. The copper layer thickness was consistently pushed to its lower limit during the IMP, to the point where barely any copper was left. Therefore, the copper layer was excluded from the IMP. Similar behaviour was reported by Matala [42].

As IMP target, the HRR of a cone calorimeter experiment at $50\,\mathrm{kW/m^2}$ was used. The HRR could be reproduced well. The resulting parameter set was then used to predict the HRR profile of the remaining two external fluxes, i.e. $25\,\mathrm{kW/m^2}$ and $75\,\mathrm{kW/m^2}$. The $75\,\mathrm{kW/m^2}$ profile was reproduced less well than the $50\,\mathrm{kW/m^2}$ condition, where the peak values were not reached. Significant differences were observed for the $25\,\mathrm{kW/m^2}$ case. The long delay to ignition, about 11 min, could not be reproduced and only a quarter of the peak HRR was reached.

MCC simulations with the best parameter sets were conducted after the IMP. They have been intended to assess the performance of the derived pyrolysis reaction kinetics, since the IMP was focused on the cone calorimeter setup. The HRR profiles recorded during the MCC experiments did not emerge from the IMP. This emphasises the effective nature of the generated parameter sets.

Finally, the best parameter sets were used to predict the fire development in a real-scale setup. The horizontal cable tray arrangement Multiple Tray Test 3 (MT-3) [28] was chosen. It consists of three trays solely filled with cable 219. A propane gas burner was located 0.2 m below the lowest tray, used to ignite cables. The burner released 40 kW for the first 600 s of the experiment. In the simulation, the cable trays are represented by obstructions with a width of 0.4 m, a length of 3.1 m and a vertical separation of 0.3 m. The cable model is applied as boundary condition to these obstructions. With an edge length of 5 cm, the fluid cell resolution is higher than during the IMP.

It turned out to be difficult to achieve self-sustained fire propagation in the MT-3 setup. The parameter set with decomposition reaction kinetics from the report and thermophysical parameters from literature extinguished shortly after the burner was shut off (figure 8 in publication I [1]). The parameter sets determined from the IMP lead to some initial fire propagation but extinguished after the burner shut-off, (figure 8 in publication I [1]). Similar behaviour was observed, when comparing the performance of the material model in simulations conducted with FDS 6.5.3 [43], which was newly released around this time.

It was assumed that the heat transfer from the flame to the cable model was the primary issue for the poor performance. FDS contains a number of prescribed gaseous species, with values defining their combustion behaviour and radiative fractions. During the IMP, the gas phase combustion was modelled with methane as surrogate fuel. In the MT-3 setup the surrogate fuel was changed to toluene, increasing the radiative fraction of the flame from 0.2 to 0.45 and also the radiative heat transfer to the cable. Furthermore, a surface temperature of 410 °C was prescribed to the gas burner, as an estimate for the heated up sand filling. Initially, the default `INERT` boundary conditions was used for burner, which is maintained at room temperature. This would act as a heat sink, specifically once the burner is shut off.

These adjustments led to self-sustained fire spread and the main features of the HRR profile could be reproduced. Specifically, the burner temperature had a larger impact than expected. After the burner is shut off, the total HRR drops noticeably. After a few minutes, the fire is able to recover and propagate to the other trays. It nearly reaches the peak HRR, but a few minutes earlier than in the experiment. The overall fire development is faster than in the experiment.

It could be demonstrated, that FDS is capable to predict self-sustained fire propagation within a horizontal cable tray arrangement. Major stages of the fire could be reproduced, like the brief decay after burner shut off, the following recovery and the propagation to another tray. However, the overall development in the simulation is faster compared to the experiment. Material parameters, determined from bench-scale experiments by inverse modelling, can be used to simulate self-sustained fire propagation in FDS.

Shortcomings of the presented work are:

- creating a material parameter set of only a single cable,
- using only a single heat flux of the cone calorimeter as IMP target,
- the poor resolution in the simplified cone calorimeter setup due to the computational cost,
- changing of the surrogate fuel after the IMP had already concluded,
- the HRR profiles of the MCC experiments diverge significantly compared to profiles determined during the IMP and
- only a single real-scale experiment was assessed.

Some of these aspects are addressed in publication II [2].

2.2 Improved Cone Calorimeter Setup for the IMP – Publication II

The second publication [2] seeks to improve some of the identified shortcomings from the earlier work. Its focus is still on cable 219 from CHRISTIFIRE Phase 1 [28]. Again, the horizontal cable tray MT-3 is used as validation for the parameter sets. New Parameter sets are generated with IMP, to improve on the previous work. The simulations are conducted with FDS 6.5.3 [43] right from the start.

Here, the cable model utilises three layers for the combustible cable components (jacket – insulator – jacket, see figure 2.4). Again, an IMP with a simplified cone calorimeter setup is used. The adjusted parameters are the kinetics of the pyrolysis reactions, as well as the thermophysical parameters of the two cable components and their respective residues. The surrogate fuel is set to toluene already throughout the IMP runs and not changed afterwards.

For the IMP, the fluid cell resolution of the simplified cone calorimeter setup was increased (figure 2.1). Instead of 10 cm, the fluid cells now have an edge length of 4.7 cm. Thus, four cells cover the sample surface, instead of a single cell as before. This also leads to a better resolution of the flow field, the flame and the radiative heat feedback. The new cell resolution is based on the edge length of the window that is cut into the top of the retainer frame of 9.4 cm. It is closer to the target fluid cell size of 5.0 cm, used in the cable tray simulation setup.

During the IMP runs of the previous study [1], it was recognised that parameters can get stuck at their sampling limits during the search. This is actively mitigated here, by conducting multiple staggered IMP runs of the same case. For each new run, the sampling limits of individual stuck parameters are expanded. This leads to overall improved fitness.

Different IMP runs were conducted, with different combinations of cone heat fluxes as targets. Some IMP runs used individual heat fluxes, either $25\,\mathrm{kW/m^2}$ or $50\,\mathrm{kW/m^2}$. Furthermore, IMP runs were conducted with all three heat fluxes, including $75\,\mathrm{kW/m^2}$. These results are presented in figure 6 in [2], and discussed below.

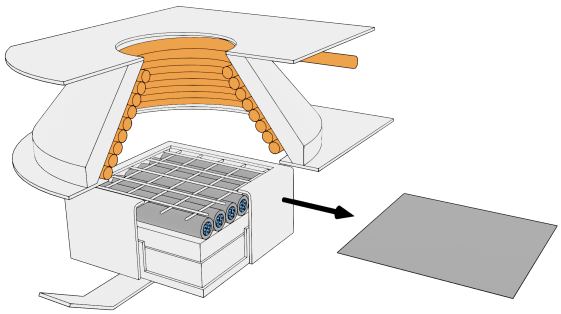

Figure 2.1: Simplifications of the complex cable cross sections into a layered boundary.

The parameter set from the IMP with this explicit target, is able to reproduce the $25\,\mathrm{kW/m^2}$ HRR development, including most of the delay in the beginning. However, for the two other cases the HRR is than significantly over-predicted. All the remaining parameter sets struggle to reproduce the $25\,\mathrm{kW/m^2}$ HRR development, especially the delay to ignition. For them, the ignition starts much earlier. This is a consequence of the combustion model, where mixture between air and fuel leads always to combustion and therefore heat release [43].

The $50\,\mathrm{kW/m^2}$ target, is reproduced well. This parameter set slightly over-predicts the $75\,\mathrm{kW/m^2}$ case. In the $25\,\mathrm{kW/m^2}$ setup, the HRR in the beginning is significantly over-predicted, the delay is not captured at all. Further, the HRR is significantly under-predicted during the main reaction.

The best performance overall is achieved when all three heat flux conditions are used as target simultaneously. Still, the most difficulties are observable in the $25\,\mathrm{kW/m^2}$ case. The delay is not captured well, but better than all cases that are not using the $25\,\mathrm{kW/m^2}$ as the sole target. The main section of the HRR profile is under-predicted, but still only second to the $25\,\mathrm{kW/m^2}$ setup.

The worst performance of the setups studied here, is displayed by the parameter set directly using the decomposition reaction kinetics provided with the report [28]. The IMP is unable to find thermophysical parameters that can compensate the model shortcomings.

With the MT-3 simulations, the performance of the best parameter sets of the different IMP setups was assessed. The simulation setups are essentially the same as in publication I [1]. Directly from the start, they are using a burner surface temperature of 410 °C and a slow decay after burner shut-off.

In these real-scale simulations, the performance of the parameter sets is notably different, compared to the cone calorimeter setups (figure 7 in [2]). Only the one using the $50\,\mathrm{kW/m^2}$ target is able to reproduce the features of the experiment with propagation from one tray to another. It over-predicts the HRR profile, but its total heat release is only slightly larger than determined from the experiment. Compared to publication I [1] the HRR profile is over-predicted, leading to higher peak heat release and an earlier conclusion. Despite the good performance in the simplified cone calorimeter simulation, the parameter set using all three cases as target extinguishes basically immediately once the burner is shut off. Similarly, the parameter set with the fixed Arrhenius parameters starts its decay already before the burner is switched off. The parameter set using $25\,\mathrm{kW/m^2}$ leads to rapid fire spread, over-predicting the peak HRR by more than a factor of four.

The HRR from the MCC experiments is still used only to determine the number of decomposition reactions. Again, MCC simulations are performed with the best parameter sets from the IMPs, for comparison. For these simulations, the then recently introduced FDS functionality `TGA_ANALYSIS` is used. Like reported in publication I [1], the HRR profile from the MCC experiment cannot be reproduced as an emergent property. The shift of the reaction peaks for the best parameter sets is similar as observed in publication I.

Overall, the procedure of generating parameter sets based on cone calorimeter setups during the IMP makes them model dependent. This is further amplified from the observation, that different FDS versions lead to different results for the same material model.

2.3 Adjustments to the Cable Model

Even though fire propagation could be achieved in the works presented above [1, 2], the overall performance is not considered satisfactory. The fundamental commonality of publications I and II is that the material parameters are determined solely in a very simplified cone calorimeter setup. The increased fluid cell resolution in publication II allowed to reproduce the HRR profile better. It should also facilitate the transfer of the parameter set to the real-scale simulation. Yet, the HRR develops faster in the tray setup. Furthermore, the HRR profiles from the MCC experiments of the cable components did not emerge during the IMP. Thus, different aspects were considered between publications II and III, to better understand the model behaviour, which are:

- Performance assessment of parameter estimation strategy with more cables.
- Heat and gas transport through the tray setup.
- Uniformity of the heat flux distribution from the cone heater to the sample top face.
- Higher fluid cell resolution in simplified cone calorimeter setup.
- The modelling approach of the cables as multiple layers.
- Increased accuracy reproducing of the MCC HRR profile.

To assess the parameter estimation strategy, a broader set of cable samples from CHRISTIFIRE Phase 1 [28] is selected. They were chosen under the conditions, that only a single cable type was placed within a given tray and at least two trays were used. Thus, cables 219, 220 and 701 were selected. Following the procedure described in publication II [2], the parameters are estimated. The number of decomposition reactions is determined from MCC experiments. Cone calorimeter results at an external flux of $50\,\mathrm{kW/m^2}$ are used during the IMP. Again, the HRR development in the

cone calorimeter could be reproduced well, see figure 2.2a with cable 701 as example. In the tray setup the performance is overall very poor (figure 2.2b). Some parameter sets lead to very fast fire development, while others do not show meaningful propagation (figure 2.2b).

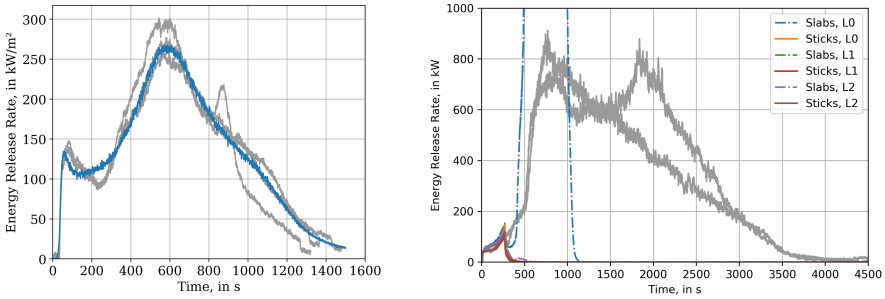

(a) Cone calorimeter at 50 kW/m^2.

(b) Multiple tray setup MT 8.

Figure 2.2: Comparison of HRR profiles of cable 701 [28] between simulation and experiment in bench- and real-scale setups. Experimental data drawn in gray.

The cable tray models as slabs (figure 2.3a) do not lead to fire propagation. During the experiments, hot gases and flames can flow through loosely packed cables in the trays. It is assumed that the continuous obstructions in the simulation interfere too much with the flow field and the heat transfer to the cable model. Due to the coarse fluid cell resolution, individual cables could not be represented in the model. Thus an attempt was made to approximate the loose cable arrangement by long obstructions with a cross section of a single fluid cell (sticks, figure 2.3b), similar to work by Beji and Merci [44]. This change in the geometry of the cable trays did not yield notable changes in the predicted HRR profiles (figure 2.2).

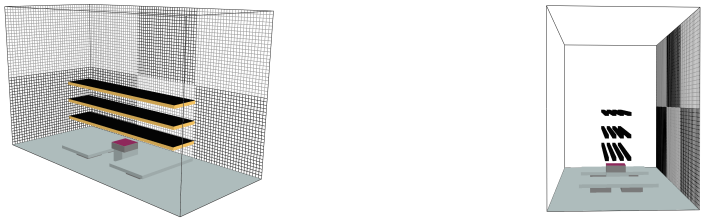

(a) Cable trays as slabs.

(b) Cable trays as sticks.

Figure 2.3: Different attempts to represent the cable tray geometries in the model.

With the poor performance in the tray setups, focus is shifted to more fundamental aspects of the models. They encompass the cone calorimeter setup, the cable model as well as the pyrolysis scheme.

For the simplified cone calorimeter simulation setups in publications I and II, the heat flux component from the heater was prescribed homogeneously across the sample top surface. Experiments and high resolution simulations show that the heat flux from the heater is not uniform [45–47]. It is higher towards the centre and much lower towards the corners, see figure 9 in publication III [3].

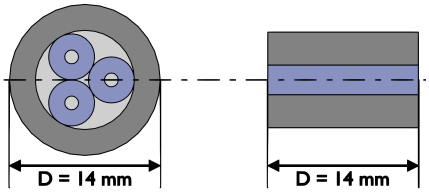

Figure 2.4: Projecting the cross sectional areas of the cable components into layers. The layers maintain the total cross sectional areas of the components. Using fixed densities, the component mass is maintained as well.

With the chosen fluid cell resolutions presented above, either 1 or 2 by 2 cells cover the sample surface. These setups only allow to prescribe an average heat flux to the whole top face of the sample model. To account for the inhomogeneous heat flux, at least 3 by 3 cells are needed. Different fluid cell resolutions during the IMP are investigated further in publication III [3].

The overall strategy to derive the layered cable model is revisited. In the earlier works both, layer thickness and component density, were adjusted by the optimiser in the beginning. Here, both are fixed to values deduced from the experiment report [28]. More care is taken to map the components into rectangular shapes. Diameters and masses are reported for the cable components of each cable. From this, the total cross sectional areas of the individual components (conductor, insulator, jacket) are estimated. They are projected into layers with the width of the cable diameter, maintaining the cross sectional areas to determine the thickness, or height, of the layers (figure 2.4). Issues arise if the cable pieces do not completely fill the cone calorimeter sample holder. For example, with a cable of 14 mm diameter (e.g. cable 219), 7 cable pieces could be placed in a sample holder with 100 mm edge length. This leaves a 2 mm wide space unoccupied, indicated by the red area in figure 2.5a. In context of the IMP, the sample holder edge length seems therefore to be a better reference value instead of the cable diameter. Yet, this gets further complicated if a retainer frame is used. This frame will cover parts of the sample at the outer edge, reducing the direct radiative heat flux received from flame and heater. The blue area in figure 2.5b indicates the surface area of the cable sample that can receive radiative flux from flame and heater through the retainer frame window. For now it is unclear how to deal with this situation. Furthermore, the cable model is mapped into the fluid cell size of the simplified cone calorimeter simulation setup. It is unclear how this model can account for situations where multiple cables are stacked on top of each other, e.g. in Viitanen et al. [21]. This is especially difficult if less cables end up in a cell than were considered during the IMP.

With fixed densities and layer thicknesses, the combustible mass is maintained as well. As added benefit this reduces the number of adjustable parameters, reducing the computational demand of the IMP. Due to fixing the combustible mass, the focus shifts further towards the pyrolysis and combustion reactions. Comparing data from experiment and model, there are deviations between both profiles observable. This is specifically pronounced with the jacket material of cable 701. It shows deformed reaction rate peaks that are not easily captured with a single-step pyrolysis reaction (figure 2.6a). To improve fitness, a simple modelling approach is explored. Employing multiple parallel single-step decomposition reactions, their superposition is able to reproduce the overall MCC HRR profile well (figure 2.6b).

Similar strategies were used by other researchers, for example [18, 20, 48]. In these works, efforts were made to link individual decomposition reactions to known material components, for example different types of cellulose. The isolated components were procured and individually studied in the TGA [48]. It was determined however, that a pyrolysis model built on isolated components is

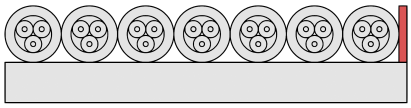

(a) Cable diameter does not allow to fill sample holder completely (red box indicates free space).

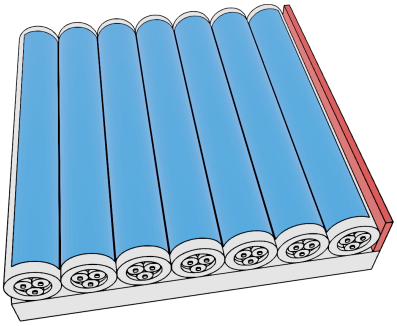

(b) Blue area indicates surface area that can receive radiative heat flux through the retainer frame window.

Figure 2.5: Schematics of cable pieces placed into a cone calorimeter sample holder, on top of an insulation layer. This highlights challenges when modelling the cone calorimeter setup.

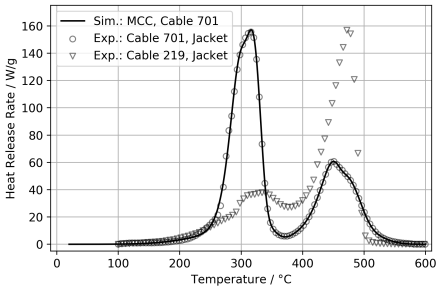

(a) Comparing experiment data with multi-pyrolysis model response.

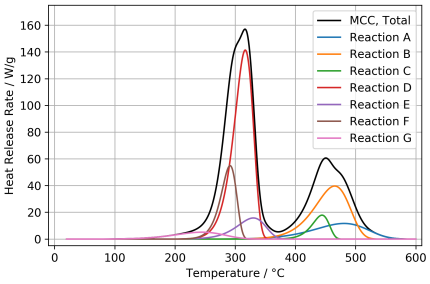

(b) Multi-pyrolysis model components.

Figure 2.6: HRR development for the jacket of cable 701. Comparison of MCC experimental data and simulation response for a heating rate of 60 K/min. Cable 219 jacket added for shape comparison of the HRR profile.

not necessarily able to reproduce the behaviour of the sample material in question. For the work presented here, no attempts are made to link decomposition reactions to known material components. Additionally to the point above, determining all components of all materials one would encounter for practical fire protection/safety engineering simulations is not feasible. In these cases, surrogate models are designed that match mass loss and heat release without focus on involved chemical species [49]. Thus, the focus is here on effective parameter sets, with decomposition reactions and released gaseous species being surrogate models.

All the decomposition reactions used here, release the same combustible gas species and inert solid residue. This leads to a constant, effective heat of combustion. If this model assumption is correct cannot be determined from MCC data alone. The MCC is limited to detect the heat released as a function of the sample temperature, by design [13]. The cables have fire retardant properties, releasing for example hydrogen chloride (HCl) [28]. Other fire retardant agents could be mixed into the plastics that release non-combustible gaseous species, for example aluminium hydroxide (ATH) [50]. ATH releases water vapour around 180 °C and 200 °C. This water vapour would dilute the simultaneously released combustible gases, directly affecting fire propagation. However, detailed information of the chemical composition of the plastics is not available from the report [28], only yields of HCl. Comparing HRR with mass loss profiles from micro-scale experiments could allow to assess possible mass release that leads to no, or little, heat release. PVC is an example where a notable difference is observable between the TGA and MCC profiles [51].

For the CHRISTIFIRE cables this assessment is not possible, due to the limited experimental data. Overall it is difficult to find studies that cover a wide range of experiments with the same sample material. This is a distinguished feature of CHRISTIFIRE, yet still it is not comprehensive enough. Recent international efforts led to the formation of the "Measurement & Computation of Fire Phenomena Working Group" (MaCFP), with the Condensed Phase Phenomena subgroup [52]. This subgroup started out, focused on poly(methyl methacrylate) (PMMA). Different experiments have been conducted, by various research institutes worldwide. Care has been taken, that the participating institutes used the same sample material. Common laboratory-scale experiments were conducted, like MCC, TGA, cone calorimeter and gasification. The results are publicly available via an open-source repository on GitHub – the MaCFP materials database [31]. In a second repository, data from large-scale fire growth experiments is also available in the main MaCFP database [30].

With the wider variety of publicly available data, PMMA is chosen for further studies discussed here. PMMA is known for its behaviour to decompose primarily into its monomer MMA when heated [53, 54]. Thus, a constant effective heat of combustion of the released species can be assumed. Further, it has the added benefit of reducing the sample complexity, since only a single polymer needs to be considered. Parallel panel experiments provide real-scale data to assess the performance of the generated material parameter sets [55, 56]. Publication III [3] details the investigation of the improved IMP procedure, taking mass loss and heat release data from micro-scale experiments into account.

2.4 Improved IMP Based on PMMA – Publication III

The third publication [3], published with the Fire Safety Journal, sets the focus on a simpler sample material: a slab of PMMA. The experimental data is taken from the publicly available MaCFP databases [30, 31]. Data from micro- and bench-scale experiments, specifically TGA, MCC and the cone calorimeter, are taken from the MaCFP materials database [31]. As validation case, data from a parallel panel experiment is used from the fire growth cases of the MaCFP database [30]. A two-step IMP is designed, to generate a sample material parameter set. The then recent version FDS 6.7.6 [36–39] is used.

In the first IMP step, the pyrolysis kinetics and the surrogate fuel are determined. The pyrolysis scheme is modified, compared to the previous work. Multiple, effective decomposition reactions are

introduced. These reactions are not assumed to accurately represent the chemistry, but are used to reproduce the HRR profile of the MCC. Simultaneously, mass loss data from the TGA, at a different heating rate than the MCC, is used as target. Thus, a wider range of heating rates can be taken into account. Slight adjustments during the IMP led to an improved fit to the data of both experiments. Two different IMP runs are conducted during the first step, one with a low heating rate in the TGA of $10\,\mathrm{K\,min^{-1}}$ and one with a high heating rate of $50\,\mathrm{K\,min^{-1}}$. In addition, both used the same MCC data of $60\,\mathrm{K\,min^{-1}}$, simultaneously to the TGA data.

The surrogate fuel is designed to be a gas mixture of carbon dioxide, ethylene and methane. They are common, primitive species, that have been recorded as intermediate species in the reaction scheme of MMA combustion [54]. During the IMP the fraction of the individual components are adjusted. Using MCC and TGA data as target, this leads to an average effective heat of combustion of the gas mixture that fits the experiment. In previous works, the effective heat of combustion was controlled from the material definitions in FDS [1, 2]. This decouples the mass loss in the solid domain of the simulation from the mass released into the gas domain. FDS uses this distinction to maintain the heat release, since the HRR is "the single most important variable in fire hazard" [57]. This procedure assumes, that the HOC of the released gases is constant over the course of the experiment, i.e. each reaction releases the same gas mixture. This seems a reasonable assumption, since PMMA is regarded to primarily decompose into its monomer MMA [53, 54].

The surrogate fuel mixture of publication III [3] assumes, that the released species are unknown, even though it is established that PMMA mostly decomposes into its monomer MMA. For materials concerned in practical fire simulations however, this knowledge is mostly not available. The goal is to create a surrogate that shows an effective heat of combustion as determined from the experiments. Thus, this strategy could be used for materials where the decomposition products are not known with high detail, like the cables investigated earlier for example.

In the second IMP step, the thermophysical parameters are estimated. This includes determining the specific heat capacity. The pyrolysis kinetics and the surrogate fuel are used from the previous step. The thermophysical parameters are estimated, based on data from cone calorimeter experiments. Similar to the previous work, a simplified cone calorimeter simulation setup is used. Different fluid cell resolutions are investigated where the sample top face is covered with 2 by 2, 3 by 3 or 5 by 5 cells. Since these fluid cell resolutions are too coarse to accurately incorporate a heater model, its impact is prescribed to the sample surface. To capture the non-homogeneous heat flux from the heater, a simulation with a high fluid cell resolution was conducted. Heat flux data recorded during the steady-state, was recorded and mapped to the much coarser simulations for the IMP. Different definitions of the temperature dependent specific heat capacity and thermal conductivity are investigated. As further variations, different data sets are used as IMP targets. Most use the sample back face temperature and the HRR as target, with one case using only the HRR. In total, 8 different IMP runs are conducted, which all lead to a good fit of the HRR, with very little variation. This is emphasised in figure 11 in publication III, by plotting all results in the same colour [3].

Data of a real-scale parallel panel experiment [55, 56] is used as validation of the parameter sets determined from the IMP. This experiment consists of two vertical panels 0.6 m wide and 2.4 m tall, that are facing each other with a separation of 0.3 m. A propane gas burner between the panels at the bottom ignites the panels. The parallel panel simulations are conducted with different fluid cell sizes that match the resolutions used during the second IMP step. All best parameter sets are assessed across all these fluid cell resolutions, regardless of the IMP setup. The performance in the real-scale setup varies significantly for the different parameter sets. Their relative performance is very similar across the different fluid cell sizes, yet at higher resolutions the fire develops faster.

It is concluded, that from the parameter set's performance in the cone calorimeter setup alone one cannot predict the performance in the real-scale setup. It is further observed that the heat transfer from the gas phase / flame to the sample surface is still of concern. Experiments were conducted to capture the interaction between the gas burner flame and empty panels [55, 56]. Comparing the

flame heat flux between experiment and simulation at the vertical centre line of one panel, seems to present a good fit (figure 19, in [3]). However, looking at the heat flux across the surface of a panel, significant differences are observable (figure 20, in [3]). Furthermore, for the fluid cell resolutions used for the parallel panel simulations, the fire extinguishes shortly after the burner is shut off. The flames vanish, beginning from the bottom of the panels. Thus, for all the parallel panel simulations the burner had to be running continuously throughout the simulations.

2.5 Role of the Heat of Combustion

It is noteworthy, that the mass loss rates in the TGA simulations diverge from the target for lower heating rates (figure 4 in publication III). They are diverging similarly, regardless if the high or low heating rate data is used as target. This indicates a fundamental cause present in both IMP setups. In publication III, it is discussed that the constant heat of combustion could be the reason for the discrepancy. Given that PMMA is known to release mostly MMA, the assumption of a constant HOC seems reasonable. However, it is releasing mostly MMA but also up to 10 % other species, like methane (CH_4) or carbon dioxide (CO_2) [54]. Assuming a constant HOC may be fine from the point of view of a larger experiment, like the cone calorimeter. There, the combustion products are analysed, by sampling from the gas stream in the exhaust duct. Since this happens after the combustion reaction concluded, only their combined effect is captured. Thus, HOC values determined are an effective HOC [58] of the solid sample material overall. Contributions of individual species, released at different sample temperatures cannot be determined. From the point of view of micro-scale experiments, it may be necessary to tease apart if different gaseous components are released at different sample temperatures. Assuming that TGA and MCC devices are operated under the same conditions with the same sample material, their respective reaction rate curves should overlap. However, synthesising methods, impurities and different decomposition mechanisms depending on the sample temperature have an impact on the released gaseous species [53, 54, 59, 60]. Specifically, methane, methanol, formaldehyde and acetylene combustion reactions have been reported to be part of the burning of PMMA [54]. This could lead to some "variable" effective HOC, due to the changing composition of released gases as a function of sample temperature.

To investigate the impact of a variable effective HOC of PMMA, a simple model is designed. Per primary reaction rate peak (~190 °C and ~380 °C), a pair of parallel decomposition reactions is defined, releasing either CH_4 or CO_2. The pyrolysis reactions are modelled with first-order single-step equations, with their parameters adjusted during the IMP. These reactions are chosen such that their individual contributions yield the reaction rate developments observed in the micro-scale experiments, i.e TGA and MCC. These parallel reactions allow the dynamic creation of the gas mixture, directly from primitive species, i.e. CH_4 and CO_2. This provides more flexibility, compared to reactions that release a static gas mixture, like in publication III [3]. It enables further to shift the reactions against each other, to capture situations of mass loss but without heat release with fewer reactions. With releasing two gaseous species, the computational effort necessary to track various species is reduced. The result is a variation in the effective heat of combustion of the mixture, depending on the material temperature. The focus is the instantaneous mass and heat release, not the gaseous species themselves. This model is therefore a surrogate model. Similar procedures have been used in the past, with some known species like hydrogen chloride (HCl) released from PVC [18], known components in wood [20, 48] or for floor covering with hydrocarbons with one to up to eight carbon atoms [49].

The behaviour of this simple model is shown in figure 2.7. Compared are the performance of the variable effective HOC parameter set ("BUWFZJ-C" [31]) with the reference parameter set defined by the MaCFP working group ("MaCFP Ref." [31, 53]). The variable effective HOC for BUWFZJ-C is computed by the total heat released per time step, divided by the total mass loss per time step. Computing an effective HOC over the complete simulation, i.e. total heat released

divided by the total mass loss, leads to about $23.8\,\mathrm{MJ\,kg^{-1}}$. The MaCFP Ref. parameter set releases a single gaseous species, MMA. Thus, its heat of combustion stays constant throughout the simulation and is in agreement with the effective heat of combustion of PMMA from the literature of about $24.2\,\mathrm{MJ\,kg^{-1}}$ [58]. Noticeable is that the heat release and mass loss peaks overlap for MaCFP Ref., but they are separated for BUWFZJ-C.

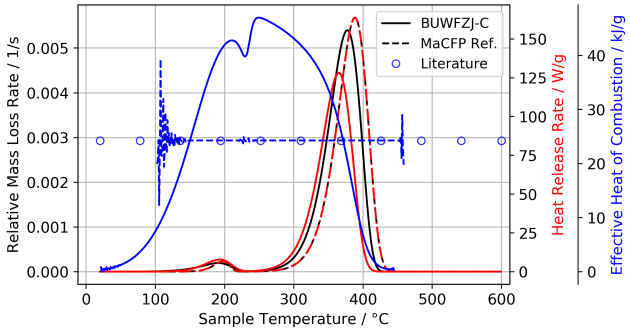

Figure 2.7: A variable effective heat of combustion allows to match mass loss (TGA) and and heat release (MCC) rates. This is achieved by dynamically mixing methane and carbon dioxide ("BUWFZJ-C" [31]) from parallel decomposition reactions. Compared to the MaCFP PMMA reference parameter set ("MaCFP Ref." [31, 53]). Plot reproduced from the poster contribution to the MaCFP-3 workshop [61].

This separation provides some freedom during the IMP. As a test, an IMP run is conducted with multiple simultaneous targets [31] (figure 2.8): five heating rates for the TGA ($2.5\,\mathrm{K\,min^{-1}}$, $5.0\,\mathrm{K\,min^{-1}}$, $10.0\,\mathrm{K\,min^{-1}}$, $15.0\,\mathrm{K\,min^{-1}}$ and $20.0\,\mathrm{K\,min^{-1}}$), a single heating rate for the MCC ($60.0\,\mathrm{K\,min^{-1}}$) and two heating rates for the DSC ($10.0\,\mathrm{K\,min^{-1}}$ and $20.0\,\mathrm{K\,min^{-1}}$). The optimiser is now able to adjust the release of individual species, reaching a better fit across a wider set of micro-scale experiment conditions. Specifically, TGA at low and MCC at high heating rates. For comparison with BUWFZJ-C, additionally the responses of the best performing parameter set of publication III "Cone_04" [3], as well as the MaCFP Ref. parameter set are provided in figure 2.8. The performance is notably improved, BUWFZJ-C matches the mass loss at a heating rate at $10.0\,\mathrm{K\,min^{-1}}$ and the heat flow at $10.0\,\mathrm{K\,min^{-1}}$ and $20.0\,\mathrm{K\,min^{-1}}$ better than Cone_04. It is also able to match the heat release rate at $60.0\,\mathrm{K\,min^{-1}}$ better than the MaCFP reference.

It should be noted however, that there is disagreement in the literature as to the question if MCC and TGA data are directly comparable in the way it is suggested here (figure 2.8). On the one hand, Ding et al. [62] and McKinnon and Stoliarov [49] could detect heat release at lower temperatures than mass loss. It is assumed that heat flux from the combustion chamber reaches the sample from the top and is artificially increasing the real heating rate of the sample. The thermocouple below the sample holder may not be able to capture the resulting temperature change fast enough, due to thermal inertia of the system. They account for this, by shifting the HRR experiment data to slightly higher temperatures, between 4 K to 20 K depending on the material. On the other hand, Snegirev reports variations of mass loss and heat release depending on sample temperature for polyvinyl chloride (PVC) [51]. Without shifting the data, the HRR is recorded at slightly higher temperatures than mass loss. The presented data series in said article behave like one would naively expect for a situation where TGA and MCC results are directly comparable. For now the cause of the difference in the observed behaviour is unclear. It may be the result if the device was not calibrated carefully, or may depend on the design of any given apparatus used. With respect to

TGA devices, De Lannoye et al. [63] reported that there are significant differences in the mass loss data, depending on the apparatus design and calibration. They demonstrated that the reactions may be shifted by up to 30 K for black cast PMMA (figures 9 and 10, in [63]). Thus, differences in design between a given TGA and MCC apparatus could also explain why some researchers report shifted data series and others do not. This needs further investigation.

For BUWFZJ-C the added DCS experiment target data improved the predicted specific heat capacity of the PMMA (figure 2.9a). Its values are determined close to the values from the MaCFP reference. The strategy employed in publication III could not estimate the specific heat capacity during the second IMP step – compare Cone_04 and BUWFZJ-C in figures 2.8g and 2.8h. Moving the estimation of the specific heat capacity into the first IMP step provides further benefits. Since less parameters need to be estimated, less simulations need to be conducted in the computationally more expensive second IMP step. Furthermore, the thermal conductivity is predicted closer to the MaCFP reference as well (figure 2.9b).

A noticeable difference between BUWFZJ-C and the MaCFP reference are the values of the heat of reaction (figure 2.10). Overall, they are much higher for BUWFZJ-C.

In the second step of the IMP, the thermophysical parameters have been determined in a simplified cone calorimeter setup. It is the same setup used in publication III. The performance of the best parameter set of BUWFZJ-C is then assessed in cone calorimeter setups with significantly increased fluid cell resolution. These high resolution setups included a geometrical model of the conical heater. This allows to properly simulate the heat transfer from the heater to the sample, instead of prescribing it. It further captures the interaction of the thermal radiation with the gases between heater and sample surface. Even with vastly increased resolution, from 3.33 cm during the IMP to 0.20 cm, the HRR profile is reproduced remarkably well (figure 2.11). Yet, higher fluid cell resolutions eventually become numerically unstable, which may be an artefact of the specific FDS version used, see 0.20 cm in figure 2.11.

The MaCFP reference parameter set, used in the same configuration, shows diverging behaviour with increasing resolution (figure 2.12a). Compared to the work presented here, Fiola et al. [53] determined the thermal conductivity and optical parameters differently. The optical parameters were determined experimentally. The thermal conductivity was determined from back face temperature, recorded in the CAPA II device [17]. Assuming the reaction kinetics are well determined (figure 2.8), here a new IMP was conducted to adjust the thermal conductivity and optical parameters. Like before [3], the simplified cone calorimeter setup of the second IMP step was employed.

This adjustment leads to a better fit in the simplified cone calorimeter setup. Still, diverging behaviour with increasing fluid cell resolution is observed (figure 2.12b). There are three notable differences between BUWFZJ-C and the MaCFP reference. The heats of reaction for BUWFZJ-C are higher than for the MaCFP reference (figure 2.10). Secondly, the radiative fractions of the gas phase combustion reactions are different. For BUWFZJ-C the combustible species is methane with a radiative fraction of 0.20, while it is 0.31 for the MMA released by the MaCFP reference. Furthermore, the MaCFP reference releases only a single gaseous species. For BUWFZJ-C about half of its released mass is methane or carbon dioxide, due to the high heat of combustion of methane. Similar simulations with Cone_04 show behaviour like the MaCFP reference in figure 2.12a. The commonality between Cone_04 and the MaCFP reference is a similar radiative fraction of the surrogate fuel: 0.35 for Cone_04, as well as the release of a single (lumped) gaseous species.

In the real-scale parallel panel simulation setup, BUWFZJ-C does not perform well (figure 2.13). As observed in previous simulations [3], the fire extinguishes when the burner is shut off. This still needs to be mitigated. The burner stays on during the simulation, but ramped down to about 10 % of its maximum power. After some initial fire growth, this leads to a constant HRR until the combustible material is consumed (figure 2.13). Higher fluid cell resolutions lead to faster spread and higher peak HRR, but overall similar behaviour. This behaviour is significantly different compared to Cone_04 and the MaCFP reference. Cone_04 develops about one minute faster, even for a larger fluid cell size [3], and reaches the peak HRR recorded from the experiment. Qualitatively, the shape

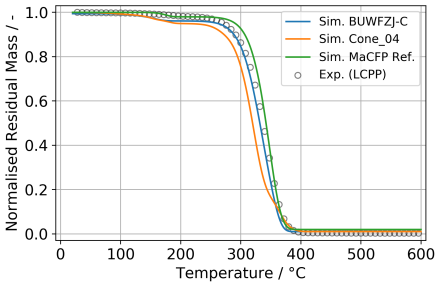

(a) TGA, 2.5 K/min.

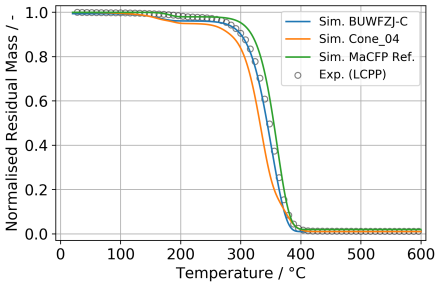

(b) TGA, 5.0 K/min.

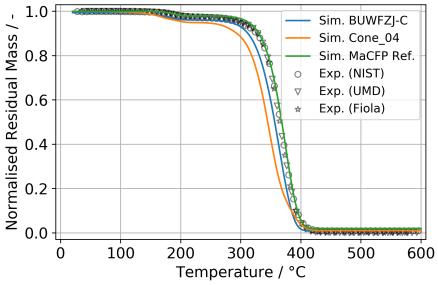

(c) TGA, 10.0 K/min.

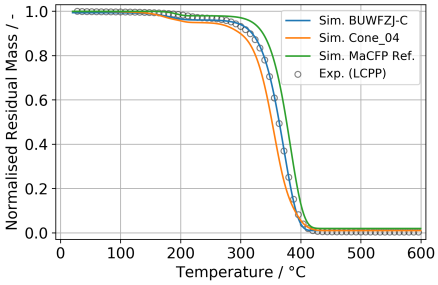

(d) TGA, 15.0 K/min.

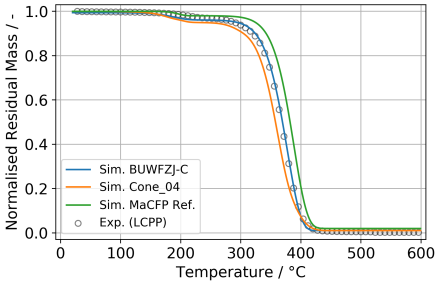

(e) TGA, 20.0 K/min.

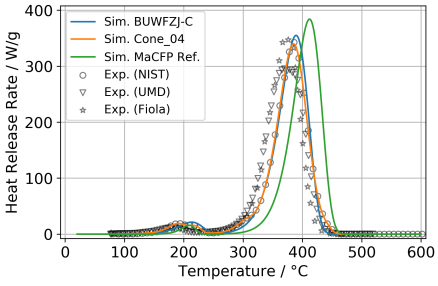

(f) MCC, 60.0 K/min.

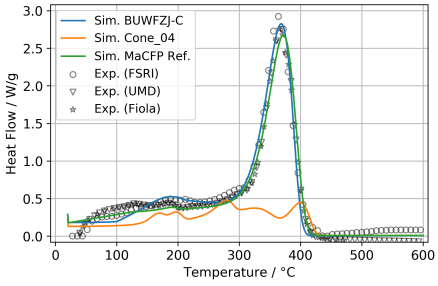

(g) DSC, 10.0 K/min.

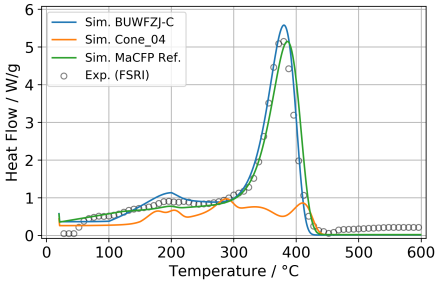

(h) DSC, 20.0 K/min.

Figure 2.8: Micro-scale experiment data [31] used as IMP targets for "BUWFZJ-C". Compared to Cone_04 [3] and the MaCFP reference (UMD) [53], as implemented by NIST.

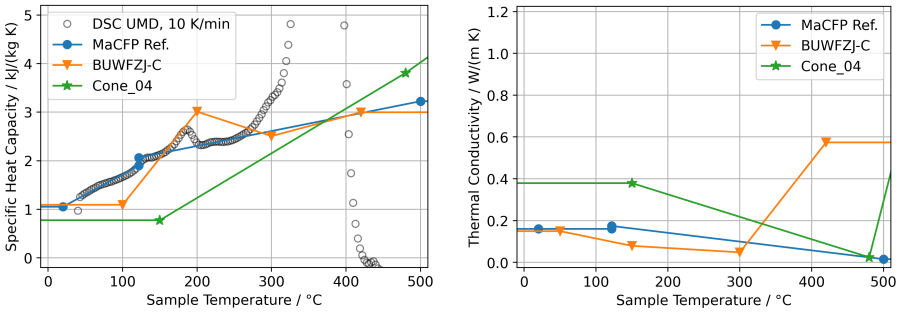

(a) Specific heat capacity of best parameter sets.

(b) Thermal conductivity of best parameter sets.

Figure 2.9: Thermal conductivity and specific heat capacity compared between "BUWFZJ-C", Cone_04 [3] and the MaCFP reference (UMD) [53]. UMD DSC heat flow data ($10\,\mathrm{K\,min^{-1}}$) normalised by instantaneous heating rate, according to Li et al. [64].

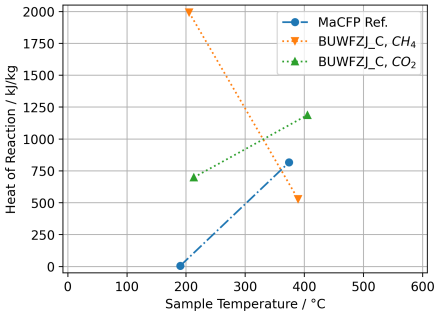

Figure 2.10: For visualisation, the heats of reaction are associated to the peak temperatures of the individual reactions. BUWFZJ-C consists of two reactions releasing carbon dioxide (CO2) and two reactions releasing methane (CH4). MaCFP Ref. consists of two reactions releasing MMA.

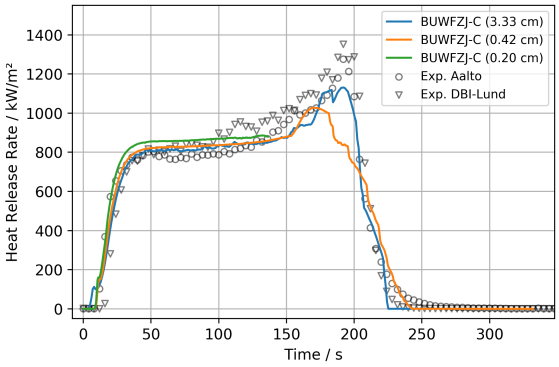

Figure 2.11: Parameter set performance in high resolution cone calorimeter simulation setups, compared to the setup used during the IMP (3.33 cm). Aalto and DBI-Lund data from MaCFP [31].

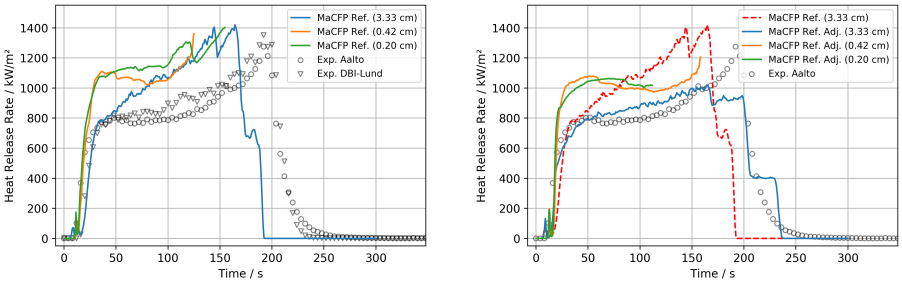

(a) MaCFP reference parameter set as described in Fiola et al. [53].

(b) MaCFP reference parameter set, adjusted using Aalto cone calorimeter data as IMP target.

Figure 2.12: Cone calorimeter simulation at 65 kW/m^2. Adjusted parameter with decomposition reaction kinetics as provided [53] and thermophysical parameters changed in IMP step 2 [3]. HRR data from Aalto and DBI-Lund are taken from the MaCFP data base [31].

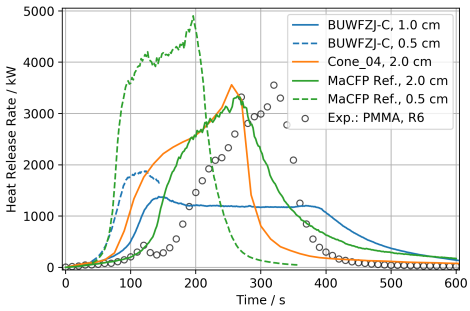

Figure 2.13: Performance of the BUWFZJ-C parameter set in high resolution parallel panel simulations. Data of experiment from MaCFP [31].

of the HRR profile is close to the experiment. The MaCFP reference for low fluid cell resolutions shows a slower decay. For high resolutions, the fire develops faster and reaches a much larger peak HRR.

During the IMP, the solid cell size was set to a low value (`CELL_SIZE_FACTOR = 0.1`) and enforcing a uniform solid grid (`STRETCH_FACTOR = 1`), leading to a solid cell size of 0.0337 mm. This was deemed necessary, because prominent spikes could be observed in the HRR profiles of the simplified cone calorimeter setup. The smaller solid cells lead to a smoother HRR curve. However, during simulations of the parallel panel setup with high fluid cell resolutions, about 1.0 cm and less, this leads to enormous computational demand. Thus, the parallel panel simulation with a fluid cell resolution of 5 mm was not completed.

Numerical instabilities have been observed with the high-resolution cone calorimeter simulations that led to crashes (figures 2.11 and 2.15). The reason is unclear. It may be related to the unstructured geometries (`GEOM`) utilised for the cone heater model. Crashes were not observed with the parallel panel simulations and other flame spread simulations with similarly high fluid resolutions (not discussed here). The unstructured geometries in FDS are still under development.

2.6 Flame Heat Flux

It is interesting to observe how the HRR profiles in the cone calorimeter simulations vary between the different parameter sets, compare figure 2.11 and figure 2.15. In the previous work discussed here, it was observed that heat transfer to the sample is an issue. For all PMMA models presented above, the effective heat of combustion is very similar. With respect to heat transfer, the primary difference is the values of the radiative fraction. This parameter is used in FDS, to ensure that the proper amount of heat is radiated away from a flame [36, 37]. For typical FDS simulation cases, the fluid cell sizes are rather large – in the order of 10 cm to 20 cm. Then the reaction zone cannot be resolved and no accurate flame temperature determined, thus a radiative fraction is prescribed. Further, in the literature there is a lack of consensus with respect to assessing the heat transfer in the cone calorimeter. Many articles have been published, reporting a wide range of convective heat transfer coefficients, between $3.7\,\mathrm{W\,m^{-2}\,K^{-1}}$ to $34\,\mathrm{W\,m^{-2}\,K^{-1}}$ [65, 66]. McCoy et al. conducted experiments with PMMA, among other materials, to capture the heat transfer in the cone calorimeter setup [66]. They observed the flames to be rather thin at the base. Therefore, they hypothesised the radiative heat flux to the sample, from the immediate adjacent flame, to be low. They assume the primary heat transfer mechanism to be convective near the sample edges (figure 2.14d). The FDS simulations

conducted here diverge from the experiment, showing substantial radiative heat flux towards the sample edges (figure 2.14).

The cone calorimeter simulation setups used here are highly resolved (figure 2.11). Prescribing a value for the radiative fraction of about 0.30, used for the MaCFP reference and Cone_04, may over-predict the radiation and lead to a higher heat flux to the sample. The lower radiative fraction of methane (0.20), used for BUWFZJ-C, may act as a correction. The higher fluid cell resolution of in the cone calorimeter simulations, allows to let FDS compute the thermal radiation based on the cell temperature. Different values for the radiative fraction are compared in figure 2.15. A radiative fraction of zero, prompts FDS to compute the radiative heat loss from the actual gas cell temperature. With a resolution of 4 mm the radiative heat flux does not change much compared to methane.

Quaresma et al. could show, that the cone calorimeter simulation setup creates severe conditions [67]. For the high external radiative heat flux of $65\,\mathrm{kW\,m^{-2}}$, the emissivity plays a negligible role. This changes when self-sustained flame spread over a horizontal sample is simulated. Together with figure 2.15, this seems to indicate that the cone calorimeter setup is not sensitive enough to the impact of thermal radiation of the flame. The specific heat capacity of the sample material exhibits a high influence throughout [67].

However, the radiative fraction has a significant impact in the real-scale parallel panel simulation setup (figure 2.16). A radiative fraction of 0.20 leads only to minor flame spread, while a radiative fraction of 0.30 to faster development and a five times larger peak HRR. It should be noted, that the heats of reaction in BUWFZJ-C are much larger compared to the MaCFP reference. This leads to a larger energy consumption during the pyrolysis process. With the low radiative flux a lower amount of energy is available to pyrolyse the sample, which in turn is responsible for the plateau visible in figure 2.13.

During the parallel panel experiments, heat flux to inert panels was also recorded [55, 56]. The heat transfer is strongly influenced by the fluid cell resolution. With smaller cells, the flow field is better resolved, affecting the flame shape. For low fluid cell resolution, a triangular shape in the heat flux map is recorded from the simulation [3]. Hauke simulated the setup with finer fluid cell resolutions [68] than previous work [3]. Fluid cell sizes below 10 mm showed the formation of vortices at the panel edges. They trap parts of the flame and stretch it apart (figure 2.17c), leading to a more rectangular heat flux to the lower end of the panel.

During the third MaCFP workshop at the 14th IAFSS symposium in Tsukuba Japan in 2023, multiple institutes presented parallel panel simulations results (figure 2.18). Two institutes used FDS: NIST and BUWFZJ, and two used FireFOAM: University of Gent and FM Global. Simulation results were provided for different fluid cell resolutions. For both fire modelling codes, the flame spread showed strong dependence on the fluid cell resolution. Smaller cells led to faster HRR development. None of the material models and fire modelling codes could accurately reproduce the behaviour recorded during the experiments, indicating that more research is necessary.

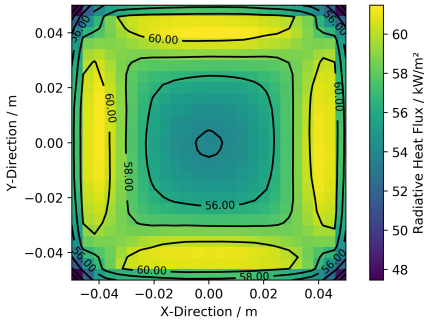

(a) Radiative heat flux map.

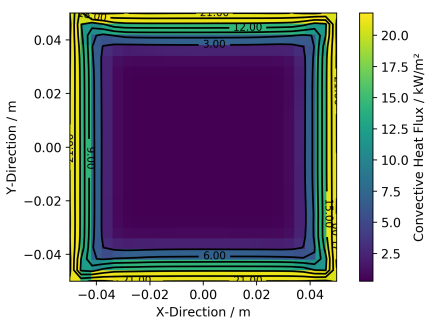

(b) Convective heat flux map.

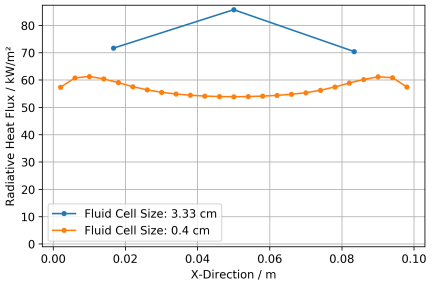

(c) Centre line radiative heat flux.

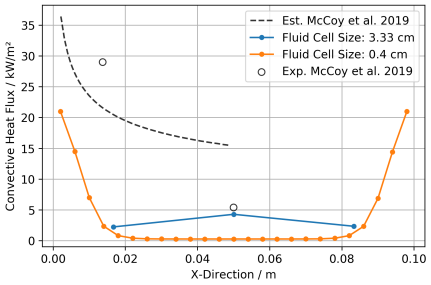

(d) Centre line convective heat flux.

Figure 2.14: Cone_04 simulation with heater geometry, set to 65 kW m^{-2}. Heat flux recorded at 75 s. Dots indicate cell centre locations. Radiative heat flux to hot surface. Convective heat flux data compared to McCoy et al. (51.5 kW m^{-2}) [66].

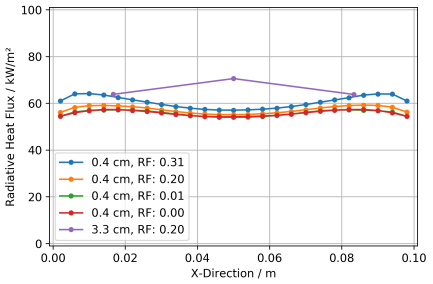

(a) Radiative heat transfer to sample surface during steady-state (BUWFZJ-C).

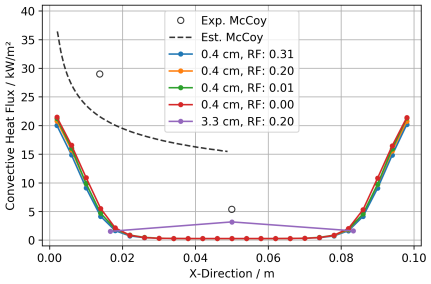

(b) Convective heat transfer to sample surface during steady-state (BUWFZJ-C).

Figure 2.15: Cone calorimeter centre line heat flux at 65 kW m^{-2}, recorded during steady-state and averaged over 4 s. Dots indicate cell centre locations. Radiative heat flux to hot surface. Convective heat flux data compared to McCoy et al. (51.5 kW m^{-2}) [66].

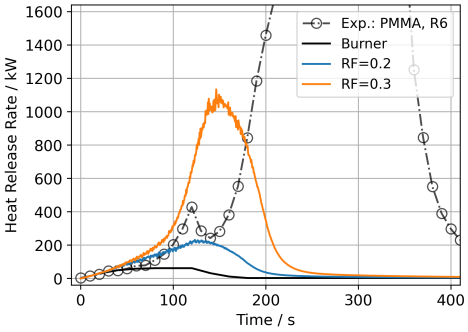

Figure 2.16: Comparison of the impact of the radiative fraction on the fire spread with BUWFZJ-C in the parallel panel setup, fluid cell size 3.33 cm.

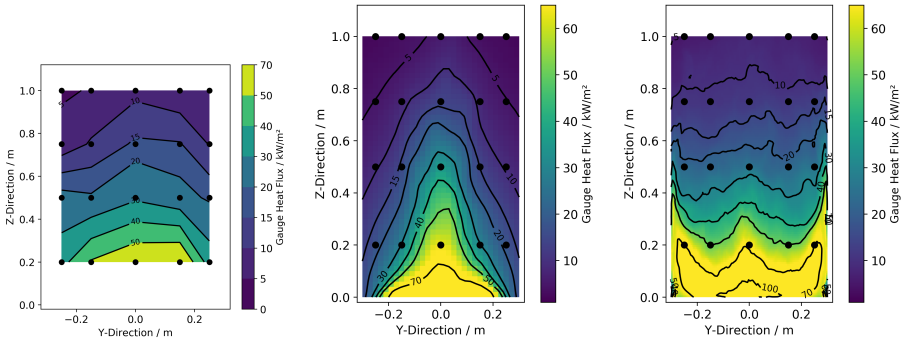

(a) Experiment. (b) Fluid cells: 2.0 cm. (c) Fluid cells: 0.5 cm.

Figure 2.17: Gauge heat flux to empty panels. Smaller fluid cells lead to vortex formation near the panel edges, trapping parts of the flame spreading it out. Experiment data from MaCFP [55], black dots indicating the positions of the heat flux devices during the experiment.

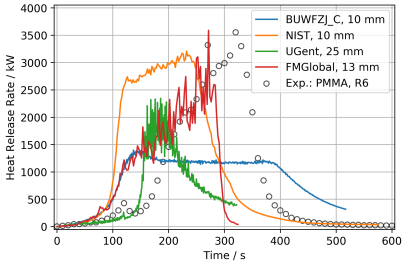

Figure 2.18: Parallel panel HRR development, submitted to the MaCFP-3 workshop [30]. Length values indicate fluid cell size. BUWFZJ and NIST use FDS, FMGlobal and UGent use OpenFOAM.

Chapter 3

Discussion and Outlook

Strategies have been investigated to create material parameter sets that allow the simulation of self-sustained fire propagation. Material models were developed that decompose as function of their temperature and release combustible gas. Fully coupled simulations were conducted, where the heat released from a flame feeds back to a solid sample material, heating it up. With this coupling of gas phase combustion and pyrolysis, self-sustained fire propagation is enabled. Focus was to use common small-scale fire experiments to design the material models and their decomposition schemes. These models are designed here as surrogates, to facilitate usage of the strategies for practical fire safety engineering applications.

The presented procedures require a wide range of experiments conducted for a single sample material. Experiment campaigns that cover these wide ranges are scarce, especially with publicly available data, due to the high amount of effort and resources necessary. Often individual experiments are conducted on selected materials. This forces modelers to piece material models together from multiple sources, if they are not able to conduct targeted experiments. The availability of real-scale experiments is also limited.

It is demonstrated here that, creating material models by combining data from different sources is difficult. The nominally same material is not identical and variations can occur for example during the synthesising of polymers. Furthermore, simulation models like FDS are not monolithic, but a collection of interacting sub-models. Modelling decisions like the choice of fluid cell sizes, definitions of boundary conditions or settings of sub-models affect the simulation result. This requires to calibrate the material and decomposition models to the given situation.

It is necessary to bridge the different length-scales for practical flame spread simulation. Many works focus on small-scale experiments to create material and decomposition models and for their validation, due to the limited availability of real-scale experiments. It is demonstrated here further, that this is not sufficient. Small-scale experiments, like TGA or cone calorimeter, can be captured fairly well, in part because these setups are designed to assess specific behaviour. These simulations are also often simplified, for example neglecting the gas phase in the cone calorimeter. This ultimately leads to difficulties, when the parameter set is transferred to real-scale simulations. The variation in the parallel panel and room corner simulation results, submitted to MaCFP-3 shows this clearly.

Further complexity is introduced from the changes in the model itself. Software updates can essentially be treated as different models altogether. New FDS versions require to rebuild the material parameter set, for the here presented method. This makes comparison of the material model difficult across FDS versions and other models like FireFOAM and Thermakin.

The behaviour of the micro-scale experiments is captured fairly well, as also indicated by the modelling efforts in context of MaCFP. Future research efforts should focus on bench- and medium-scale experiments that involve flame spread, with sizes like used for ISO 5658-2 [69] or ISO 9239-1 [70]. Simulating cone calorimeter and similar setups is not sufficient, since they cannot predict the real-

scale performance [3] and mask the sensitivities of individual parameters that are important for the fire propagation [67]. Experiments should specifically be conducted to involve self-sustained flame spread in setups with different sample orientations [10]. Simplifying these setups and incorporating them into the inverse modelling procedure should help creating more robust parameter sets.

When conducting experiments, a wider set of information of the experiment setups themselves should be recorded. This is particularly evident with the sample deformation observed in cone calorimeter experiments [3, 71] and the flux map of the parallel panel setup without sample [3, 68]. Recording data from the experiment setups without reacting sample should be used to ensure that the behaviour is captured accurately and that the boundary conditions are well characterised. This encompasses also conditions in the laboratory like the ambient temperatures, pressure as well as ventilation conditions and possible drafts, particularly for medium- to real-scale experiments.

The material parameter sets created by the presented procedure lead to effective parameter sets. This is unavoidable, since they are calibrated during the IMP to the environment created by the chosen collection of sub-models and their settings. FDS exhibits difficulties, capturing the delay to ignition in cone calorimeter setups during low heat flux conditions. This raises the question, if not at least some of the sub-model values should be adjusted during the IMP as well. They are, for the most part, set to default values to work well in context of the classical use case of FDS: prescribed heat release rates to assess smoke movement in buildings.

For each material a full IMP needs to be conducted, when the respective material model is needed. Furthermore, for each new version of the simulation software, the material model needs to be rebuilt. This leads to a quite large computational time and effort for the presented parameter estimation strategy. The design of the optimisation algorithm is one of the main reasons for long computing times, since the next parameter set is built on the one that came before. If strategies can be conceived that would allow to run a broad set of simulations that are independent of each other, they would be able to be computed in parallel. There the limiting factor would only be the number of computing cores that are accessible. In the extreme, the full set of simulations could be conducted within the time it takes for the slowest simulation to complete. New strategies like this are necessary to develop, because as it is now the iteration frequency with which improvements can be implemented is very low – in the order of month, if not years.

Chapter 4

Appendix

4.1 Publication I: Cable Fires in Particle Accelerator Tunnels

The first article, "Cable Fires in Particle Accelerator Tunnels", is published in the proceedings of the ISTSS 2018 conference [1].

Table 4.1: CRediT authorship contribution statement of publication I.

Item	T. Hehnen	L. Arnold	P. van Hees	S. La Mendola
Conceptualization	X	X		X
Methodology:	X	X		X
Software:	X	X		
Validation:	X	X	X	X
Formal analysis:	X			
Investigation:	X			
Resources:	X	X	X	X
Data curation:	X			
Writing - original draft:	X			
Writing - review and editing:	X	X	X	X
Visualization:	X			
Supervision:		X		X
Project administration:		X		X
Funding acquisition:	X	X		X

Simulation of Fire Propagation in Cable Tray Installations for Particle Accelerator Facility Tunnels

A Preprint

Tristan Hehnen [a,b], Lukas Arnold [c], Patrick van Hees [d], and Saverio La Mendola [b]

[a]Bergische Universität Wuppertal, Wuppertal, Germany
[b]European Organization for Nuclear Research CERN, Geneva, Switzerland
[c]Institute for Advanced Simulation, Forschungszentrum Jülich, Jülich, Germany
[d]Lund University, Lund, Sweden

Tristan Hehnen: hehnen@uni-wuppertal.de; ORCID: 0000-0002-6123-261X
Lukas Arnold: l.arnold@fz-juelich.de; arnold@uni-wuppertal.de; ORCID: 0000-0002-5939-8995

February 6, 2024

Abstract

In this paper, it is demonstrated that the simulation of fire propagation in cable tray installations, with the Fire Dynamics Simulator (FDS), version 6.3.2, can be achieved. A material parameter set allowing to estimate the fire spread, depending on environmental conditions close to the fire seat, was generated. The parameters are determined by utilisation of an evolutionary algorithm, in an inverse modelling framework, based on experimental data from Cone Calorimeter tests. As a further step, the performance of the parameter set is compared between the FDS versions 6.3.2 and 6.5.3. The foundation of this work are experimental results of the CHRISTIFIRE campaign. The inverse modelling approach is inspired by and based on Anna Matala's and Chris Lautenberger's work. A material parameter set generated by the evolutionary algorithm is then used in a real scale cable tray fire simulation to predict the fire propagation. The total heat release rate (HRR) of the cable tray simulation and the respective experiment are compared and are in good agreement. The major features in the HRR plot of the experimental data are visible in the simulation results, but slightly shifted in time. Thus, predicting the fire propagation in a simulation, based on data of small-scale experiments, seems possible with FDS. However, the parameters used in this work are model specific and very sensitive to changes in the model, like grid resolution and FDS version.

Keywords Fire Dynamics Simulator (FDS) · pyrolysis · CHRISTIFIRE · cone calorimeter · cable tray fire · inverse modelling · evolutionary algorithm · genetic algorithm · SCE-UA · particle accelerator

1 Introduction

The European Organization for Nuclear Research (CERN) is one of the largest particle research laboratories in the world, situated north of Geneva in Switzerland and France. The Organisation's facilities are very divers and encompass a variety of surface buildings, ranging from office buildings, restaurants and hotels to computing centres, large storage facilities, workshops and experimental halls. Furthermore, extensive underground facilities house particle accelerators, which are connected via transfer tunnels between one another, and are directly connected to multi-storey experimental caverns. Combined they have a length of about 76 km [1]. The so-called accelerator chain (Figure 1) starts from a linear accelerator (LINAC 2) where protons are injected into the chain. They are accelerated close to the speed of light, before they are used in various experiments. During this process, the protons travel through different accelerators: the Proton Synchrotron Booster (PSB), the Proton Synchrotron (PS) and the Super Proton Synchrotron (SPS) into the

Large Hadron Collider (LHC). The accelerators LINAC 2, PSB and PS are housed in surface buildings. The facilities of SPS and LHC are deeper underground between 30 m to 150 m. Access is provided via vertical shafts, some of which contain elevators and staircases, whilst others are clear of obstructions to allow for equipment and material transport, using cranes. The tunnel cross section diameters are between 4.5 m to 6.2 m. This allows for the movement of material and personnel. Distances between the access shafts range from 150 m for the PS up to about 3 km for the LHC. Since the accelerators are ring-shaped, the accelerator tunnels are also used as ventilation ducts. Parts of the facilities are relatively old. For example, the PS has been in operation for nearly six decades now. Furthermore, plans for new accelerators are studied. One of which is the Future Circular Collider (FCC) study to design requirements for the FCC. This accelerator is envisioned to be housed in an 80 km to 100 km long, ring-shaped tunnel, up to 400 m below the earth's surface, with a tunnel diameter of about 6.2 m and distances between the access shafts of about 10 km.

During operation of the accelerators, the tunnels and experimental caverns, as well as the equipment installed therein, are subjected to radiation. Over time, this leads to parts of the equipment becoming activated (radioactive). The radiation levels depend on the location along the accelerator, with the highest radiation levels occuring at the beam dumps, the experimental caverns and kicker magnets. Thus, design fires for particle accelerators need to be carefully evaluated, when radiological release in case of fire has to be estimated.

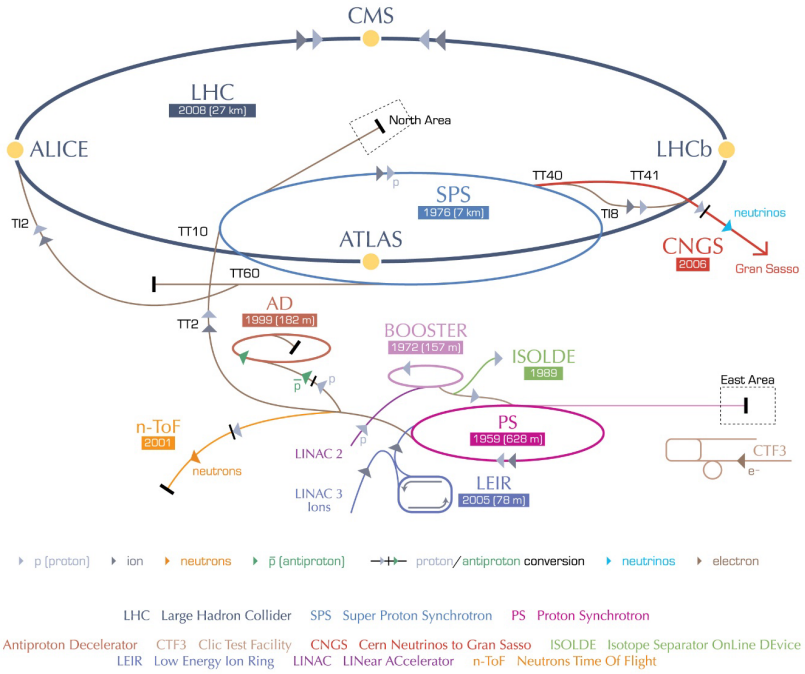

Figure 1: Schematic overview over the particle accelerator facilities at CERN [2].

The accelerator facilities contain a huge amount of electrical cables used for power supply, machine control and data transfer from the experiments to the data centres. Cables constitute one of the major hazards with respect to fire safety inside particle accelerator facilities. A cable fire can lead to the spread of smoke and heat within the facility, jeopardising people and equipment. Due to their unique layout and purpose, statistical data is scarce. Thus, other means to define the design fire need to be established.

Cables are a major fire load not only for CERN, but also in facilities like telecommunication data centres or nuclear power plants. In 2012, the United States Nuclear Regulatory Commission (U.S.NRC) published a report on an extensive cable fire test campaign which had been conducted in the previous years, titled "Cable Heat Release, Ignition, and Spread in Tray Installations During Fire (CHRISTIFIRE)" [3].

Given the rigid nature of design fires, different options are investigated to achieve a more detailed representation of fire and smoke spread simulation. Part of the ongoing research deals with the modelling of the pyrolysis reaction of a material, since it is an important factor when it comes to fire propagation. It determines how much combustible gas will be released based on the solid's temperature, thus determines the fire development. Often pyrolysis models are based on an Arrhenius equation because it allows to describe the results of small scale fire tests, which focus on pyrolysis like micro-combustion calorimetry (MCC), well. On an international level, different groups put effort into understanding pyrolysis and how to simulate this phenomenon properly. For example within the ongoing research, focus has been put on Latin-Hypercube sampling [4, 5], evolutionary algorithms [6, 7] or statistical methods like Bayesian updating [8]. It is of great interest for the fire safety community to have a reliable process which generates material parameter sets based on small scale experiments, that are able to replicate the fire behaviour within a simulation.

In this paper, it is demonstrated that the simulation of fire propagation in cable tray installations, with the Fire Dynamics Simulator (FDS), version 6.3.2 [9], can be achieved if appropriate input data can be obtained in combination with limited experimental testing work. A material parameter set was generated that allows to estimate the fire spread depending on the environmental conditions close to the fire seat. The parameters are determined by utilisation of an evolutionary algorithm, in an inverse modelling setup, based on experimental data from Cone Calorimeter tests.

2 Materials and Methods

In the CHRISTIFIRE program, cable fire tests ranged from small-scale tests of the cable components with MCC, bench-scale tests with tube furnace and Cone Calorimeter to real-scale tests with cable tray arrangements in the open, in mock-up corridors and vertical shafts. This wide variety of tests makes the CHRISTIFIRE campaign a valuable source for the creation of design fires and the validation of simulation results. Out of the tested cables, cable #219 was chosen for this work, because it was one of the cables that was tested in a cable tray arrangement, where all trays were filled with this specific cable. Also, its behaviour during the Cone Calorimeter tests was very similar across all repetitions, while repeatability for other cables was not as good.

Focus was set on three different fire tests: MCC, Cone Calorimeter and cable tray installations in open space. The MCC tests have been performed by using a Pyrolysis Combustion Flow Calorimeter [10]. The MCC was used to determine reaction kinetics parameters of the pyrolysis reaction of the cable components jacket and insulator. Their pyrolysis has been modelled by utilising an Arrhenius equation during the CHRISTIFIRE campaign and the respective parameters are provided in the campaign's report. The results of the MCC tests and the Arrhenius model are reproduced in Figure 5. Furthermore, the heat release rates (HRR), production rates of residue and heat of combustion are provided in the report as well.

Cone Calorimeter tests were performed on cable pieces, which were neatly ordered in one layer in the sample holder. Incident heat fluxes were set to 25 kW/m², 50 kW/m² and 75 kW/m². Three repetitions were performed for each of the first two incident fluxes, one repetition for 75 kW/m². The results of the Cone Calorimeter tests are reproduced in Figures 6 and 7. Since the repeated tests for 25 kW/m² and 50 kW/m² yielded similar results, they are summarised by a grey area in the plots. Cable tray installations (Multiple Tray Tests – MT) were tested in different sizes under a large hood, up to seven trays were stacked upon each other. The width of the trays was 0.45 m, vertical distance between the trays was 0.3 m while the tray length varied. Two different approaches were used to determine the total HRR, by oxygen consumption and mass loss. For the simulation of cable #219, focus was set on the HRR measurement based on oxygen consumption. The chosen test was MT-3, which consisted of three trays.

Within the CHRISTIFIRE framework, a simple fire propagation model for cable trays was developed, called FLASH-CAT (Flame Spread over Horizontal Cable Trays) [3]. It distinguishes between thermoset and thermoplastic cable insulation material, in terms of fire propagation. For CERN the FLASH-CAT approach has been adopted to create design fires to perform assessments of the smoke management within its facilities.

On the simulation side of things, the Fire Dynamics Simulator (FDS) [9] was used. FDS is a threedimensional computational fluid dynamics software, which numerically solves a low mach number specialisation of the Navier-Stokes equation. The computational domain needs to be divided into small rectangular cells creating a mesh. Within this mesh, the transport of fire-driven gas flow and heat transfer is then simulated.

In FDS, objects are defined by their geometry and the material properties. The geometry is built out of box-shaped obstructions (FDS: `OBST`) that influence the flow field. Surfaces (FDS: `SURF`) are then attached to the sides of the obstructions, which contain the respective material information (FDS: `MATL`). `MATL` describes the material properties like density, thermal conductivity or heat of combustion, while the SURF contains information of its application. It does not need to be homogeneous, but can consist of layers of different (homogeneous) materials.

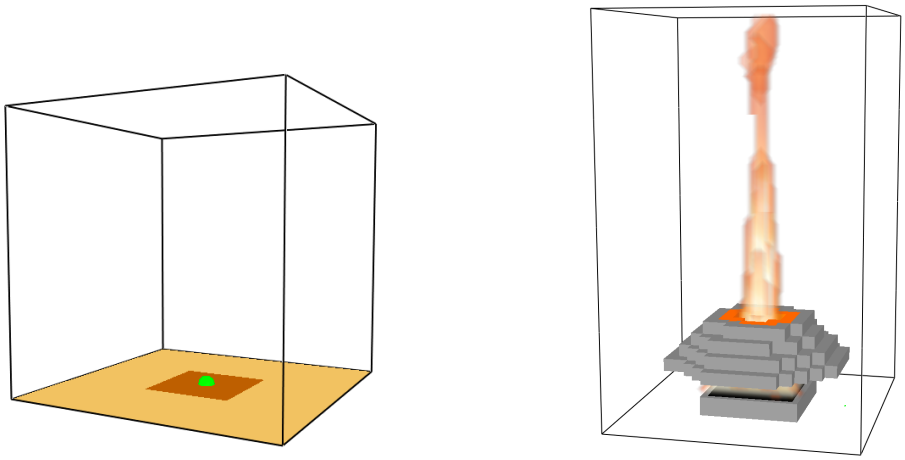

(a) Thermal conductivity of best parameter sets.

(b) Specific heat capacity of best parameter sets.

Figure 2: SmokeView visualisation of different simulation setups: Simple Cone with 10 cm cubeshaped cells (2a), Coarse Cone with 7.5 mm cube-shaped cells (2b).

FDS provides different ways to model fire propagation, e.g. when the surface temperature reaches a specified threshold, a prescribed mass flow is initiated. A more sophisticated method is based on an Arrhenius model for the pyrolysis reaction kinetics of a solid material [9]. Parameters for the Arrhenius model are the activation energy E, the pre-exponential factor A and the reaction order n. The same parameters as provided in the CHRISTIFIRE report. During the pyrolysis process, one or more new gaseous and solid species are generated and the original material is consumed. If a sufficient amount of combustible gas is generated, and combustion is possible, a flame can develop. The temperature of the material is used to control its degradation, which is in turn controlled by the energy transfer to the solid, e.g. by flame radiation, its emissivity and heat transfer within the solid.

Four different simulation setups for FDS were created to simulate the different fire tests: MCC, Simple Cone, Coarse Cone and MT-3. The simulation setups of MCC and Simple Cone are basically the same, where no gas phase reactions are simulated and were based on suggestions in the FDS user's guide [9] and in the work of Anna Matala [6]. The focus was solely on the pyrolysis reactions, with the aim to reduce the demand for computational resources to a minimum. The simulation setup of the MCC consists of four cells in each direction. The temperature of the whole domain was linearly increased over time to simulate the behaviour of the real MCC test. The Simple Cone simulation setup (Figure 2a) was based on [6]. Its computational domain was divided into cube-shaped cells with an edge length of 10 cm and a total extension of 30 x 30 x 40 cm³. The sides and the top of the mesh were given an "open" boundary condition, while the bottom surface was closed. The layered SURF was attached to the bottom boundary of the central cell, to represent the cable sample. Due to the poor resolution in this setup, the incident heat flux to the cable sample was prescribed, using the FDS parameter `EXTERNAL_FLUX` on the `SURF`.

It was later found that suppressing the gas phase reactions (flame) was too much of a simplification. Mainly, because it neglected a significant amount of heat, radiated from the flame to the sample surface [11]. Attempts were made to prescribe an extra amount of heat flux and add it directly to the value for `EXTERNAL_FLUX`. The specific amount was determined by a simulation of higher fidelity (Figure 2b). However, it was realised that the external flux became a limiting factor during the inverse modelling process (IMP), which is covered later.

To assess the sensitivity of the material parameter sets of cable #219, in terms of mesh and flame resolution, a coarse replication of the Cone Calorimeter was created in FDS. The Coarse Cone was set up in a 7.5 mm cube-shaped mesh, where the radiative heat flux is generated by a hot, conical-shaped surface (Figure 2b). Within the Coarse Cone simulation setup, the parameter sets were subjected to heat fluxes as during the CHRISTIFIRE experiments (25 kW/m², 50 kW/m² and 75 kW/m²).

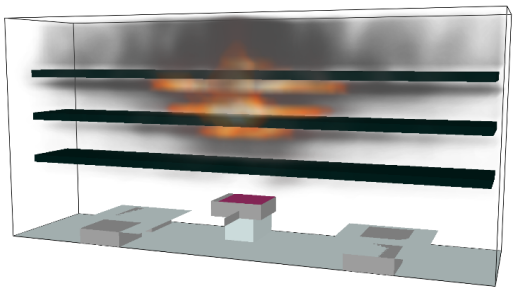

Figure 3: SmokeView visualisation of Multiple Tray Test 3 (MT-3) simulation setup (5 cm cubic cells).

Furthermore, a representation of Multiple Tray Test 3 (MT-3) from CHRISTIFIRE Phase 1 was created in FDS (Figure 3). The simulation setup of MT-3 was based on a mesh with 5 cm cubeshaped cells. Due to the resolution, the geometry of the tray racks themselves has been neglected. The cable layers in each tray were modelled as obstructions of 0.4 m width and a length of 3.1 m. The thickness of each cable layer was of one cell size (5 cm). This enables FDS to calculate the heat transfer in the solid while taking the temperature of the opposite surface into account, due to software limitations. However, this thickness is only of importance for the flow field. For the heat transfer in the cable material a thickness of about 1 cm was prescribed via the SURF, depending on the specific parameter set coming from the IMP. A vertical distance of 0.3 m was kept between the three trays, measured bottom to bottom. Some obstructions were put on the bottom of the simulation domain to mimic the supporting structure of the tray racks, which can be observed on the photographs in the CHRISTIFIRE report. A Propane gas burner, 0.3 m edge length, was located 0.2 m below the lowest tray and provided 40 kW for the first 600 s of the simulation.

Figure 4: Cone Calorimeter experiment.

It was briefly mentioned above, that the Simple Cone simulation setup was used with suppressed gas phase reactions, which was later changed. The reason is, that the amount of combustible gas released determines how large the flames will be, which in turn determines the mass release, as well as the amount of radiation sent back to the sample surface [11]. Therefore, prescribed flame fluxes lead to inaccurate burning behaviour during the IMP. As proposed by Anna Matala [6], gas phase reactions were allowed again, even though the cell resolution in the simplified Cone Calorimeter simulation setup was very coarse (10 cm cube-shaped cells). With higher resolution, tall flames were observed, which are in line with observations of real Cone Calorimeter tests (Figure 2b and Figure 4). This behaviour could not be covered with the coarse grid, but it still allowed to cover parts of the flame's radiation influence. Methane was used as surrogate fuel for the combustion process.

Before the inverse modelling, attempts were made to use reaction kinetics parameters accompanied by the information on residue formation and heats of combustion provided in the CHRISTIFIRE report, directly for the materials in FDS.

Table 1: Overview of which parameters were used during the IMP. The “X" denotes individual parameters that the optimization algorithm had access to.

Parameter	Jacket reaction A	Jacket reaction B	Jacket residue	Insulator reaction A	Insulator reaction B	Insulator residue	Copper conductor
Density	Same for reac. A / B		X	Same for reac. A / B		X	
Emissivity	Same for reac. A / B		X	Same for reac. A / B		X	
Conductivity	Same for reac. A / B		X	Same for reac. A / B		X	
Specific heat	Same for reac. A / B		X	Same for reac. A / B		X	
A	X	X		X	X		
E	X	X		X	X		
n	X	X		X	X		
Heat of combustion	Same for reac. A / B			Same for reac. A / B			
Heat of reaction	Same for reac. A / B			Same for reac. A / B			
Layer thickness	Same for reac. A / B			Same for reac. A / B			X

The remaining thermo-physical parameters were based on the example cases provided with FDS and literature values. However, performance was not satisfactory, except for the simulation of the micro-combustion calorimetry (MCC). Thus, focus was shifted to an inverse modelling approach.

Material and reaction kinetic parameters have been determined by utilising the global optimisation method SCE-UA (short for: shuffled complex evolution method developed at The University of Arizona) [12] in an inverse modelling approach. The IMP was controlled by a self-developed script, utilising the scripting language Python, version 2.7 and the Python package “Statistical Parameter Optimization Tool for Python” (SPOTPY) [13]. This script worked basically as the interface, handling communication between the SCE-UA and FDS.

First an input file for FDS is created and set up as a template. Markers in the template allow the input file to be parsed and the markers to be swapped to the specific parameter values. Another file contains the experimental results that are used as target information. A setup script provides input data for the optimisation process, as defined by SPOTPY. Each parameter was given a lower and an upper value, to limit the search space and to avoid to receive unrealistic values. However, the values are somewhat artificial. The limiting values are basically guess values, loosely based on literature values. For instance, the heat of combustion values got a range of $\pm$ 20% around the CHRISTIFIRE values, and were expanded when the algorithm got “stuck” at one of the limits during the search.

Per generation the number of complexes has been the number of parameters n_{para} plus 1. Each complex contained two times the number of parameters n_{para} plus 1. Thus, the number of individuals (parameter sets) per generation n_{gen} can be described as:

$$n_{gen} = (n_{para} + 1) \times (2 \times n_{para} + 1) \tag{1}$$

Which is the default setup for SPOTPY. After the parameter sets have been created by SPOTPY, they were written into the FDS file, and the simulation was performed. From each simulation only the time and HRR data was kept, the rest was deleted to save hard drive space. The root mean squared error (RMSE), calculated between the experimental and the simulation results, was considered as the fitness value. Parameter sets which had RMSE values closest to zero were rated best. After all parameter sets of a generation had been assessed, they got ranked, shuffled and the new generation was generated. The shuffling is aimed to prevent the optimisation algorithm getting stuck at a local optimum instead of finding the global optimum of the search space. The process was terminated when either a specified number of simulations had been performed, about 100k, or the fitness value did not improve less then $1 \times 10^{6}\%$ over the course of the previous 100 evolution loops (also SPOTPY default).

The SCE-UA was used on the Simple Cone simulation setup, with the experimental results from CHRISTIFIRE as target. Specifically, only one repetition of the 50 kW/m² Cone Calorimeter results was chosen as target for the IMP. The cables were simplified as a `SURF` with three layers (jacket – insulator – jacket), to account for the assembled nature of electrical cables. By using the `EXTERNAL_FLUX` parameter, the conditions of Cone Calorimeter tests could be replicated easily. This approach was regarded to be sufficient for the demonstration purpose, thus reducing the computational costs of the IMP significantly.

In total 34 parameters were used for the optimisation algorithm to work on. Those are the thicknesses of the different layers, reaction kinetics parameters and thermo-physical parameters for each cable component, as well as thermo-

physical parameters of the residues. In the beginning, the copper conductor was implemented as well, but only its layer thickness was accessible for the IMP. During every run of the IMP the thickness of this copper layer was reduced to its lower limit, thus it was removed completely. This behaviour is also in line with findings reported by Anna Matala [6]. An overview of the parameters used during the IMP is provided in Table 1.

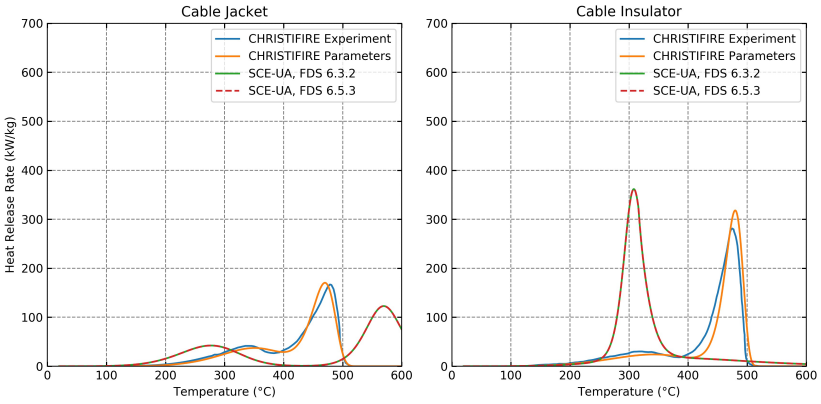

Figure 5: Micro-combustion calorimetry of cable components of cable #219. Comparison between experiment and simulation results of the reaction parameters provided by CHRISTIFIRE Phase 1 and results of the IMP (SCE-UA).

As mentioned above, each cable component was divided into two materials (`MATL`) to cover the two pyrolysis reactions, (reaction A and reaction B). Both `MATL` of a cable component yield surrogate fuel and a residue. The yields were taken from the MCC results of the CHRISTIFIRE report. The IMP was provided with the heat release rate data (HRR) of one repetition of the 50 kW/m² Cone Calorimeter experiment as the target data. The different parameter sets were then used within the MT-3 simulation setup to assess their performance in predicting the fire propagation in a cable tray installation.

3 Results

In Figure 5 the results of MCC tests from CHRISTIFIRE and simulations are shown. The results from the simulations with the parameters provided in the CHRISTIFIRE report match the experimental results very well. The results out of the IMP show significantly different behaviour. Cone Calorimeter data for irradiance levels of 25 kW/m² and 50 kW/m² are provided in Figure 6, for 75 kW/m² in Figure 7. Note that the SCE-UA worked with the Simple Cone simulation setup at 50 kW/m² external heat flux. For this case, experimental and simulation results match relatively well, as expected.

The main features of the experimental results are visible in the simulation results, but slightly off. For 75 kW/m² the results are still similar to the experiment, however at 25 kW/m² the behaviour is significantly different. Increased cell resolution in the Coarse Cone setup improves the results for 25 kW/m² and 75 kW/m² but largely overestimates the results in the 50 kW/m² case. In general, the direct transfer of the CHRISTIFIRE parameters is only able to cover the first peak at 50 kW/m² and 75 kW/m² but shows significantly different behaviour in all other cases.

During the CHRISTIFIRE experiments the HRR of the cable tray arrangements was estimated by the oxygen consumption method, as well as based on the mass loss rate. The results of the oxygen consumption method was chosen to compare them against the simulation results. For simulations of the tray setup it proved to be difficult to achieve fire propagation. In most of the simulations, the fire extinguished on its own, shortly after the burner was switched off. The parameter set based directly on the CHRISTIFIRE results showed only a small contribution to the total HRR of the fire, close to 10 kW.

The parameter set from the IMP showed a contribution of around three times the burner's input. After the burner was switched off, the HRR dropped by 40 kW recovered slightly (10 kW) and then decayed slowly, similar as the FDS 6.5.3 results (Figure 8). Following the assumption that the material and reaction kinetics parameters are determined reasonably well during the IMP, focus was shifted to the heat transfer to the cable.

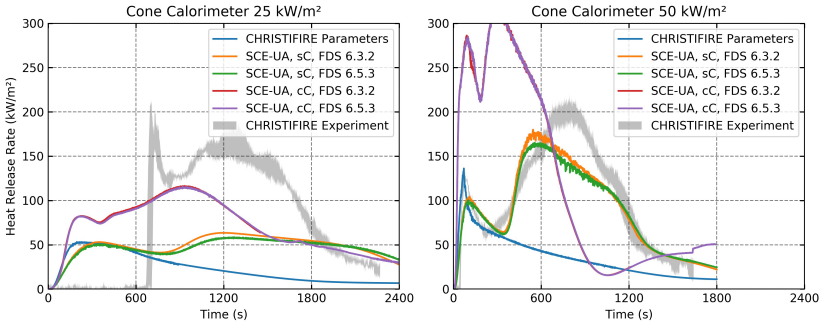

Figure 6: Cone Calorimeter test and simulation results for cable #219, at 25 kW/m² and 50 kW/m² incident flux. Comparison with reaction kinetics parameters provided by CHRISTIFIRE Phase 1 and the best parameter set of the inverse modelling process (SCE-UA). Simple Cone (sC) and Coarse Cone (cC) setups for different FDS versions.

Three parameters were looked at, for the investigation of the influence on the radiative heat transfer: radiative fraction of the flame, soot yield and the surface temperature of the burner. After the investigation, the surrogate fuel was changed from methane to toluene, both are pre-tabulated in FDS. Thus, the radiative fraction of the flame changed from one of the lowest (0.2) to one of the highest (0.45) pre-tabulated values. Soot yield was set to 0.178 g/g based on textbook values for toluene [14]. The surface temperature of the burner was set to 410 °C with a slow decay rate, after the burner was turned off. Specifically the burner temperature was of greater importance as expected at first glance.

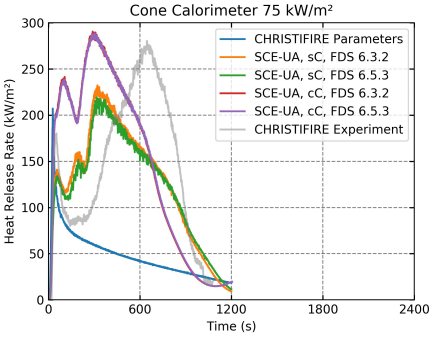

Figure 7: Cone Calorimeter test and simulation results for cable #219, at 75 kW/m² incident flux. Comparison with reaction kinetics parameters provided by CHRISTIFIRE Phase 1 and the best parameter set of the inverse modelling process (SCE-UA). Simple Cone (sC) and Cone (cC) setups for different FDS versions.

Thus, satisfactory fire propagation could be achieved in the simulated cable tray installation.It is important to note that the parameter set was adjusted after the IMP was finished, to achieve fire propagation.Furthermore, comparison of the two FDS versions, 6.3.2 and 6.5.3 shows nearly the same results for the MCC and Cone Calorimeter simulations. When comparing simulation results of the tray arrangement a significant difference is notable after the burner is switched off.

4 Discussion

As a proof of concept, it was demonstrated that the simulation of fire propagation in cable tray arrangements is feasible within FDS. The set up IMP is able to generate parameter sets that are able to predict the general fire behaviour within a real-scale simulation setup, based on small scale experimental data. However, the parameter set performs relatively well only within a tight frame.

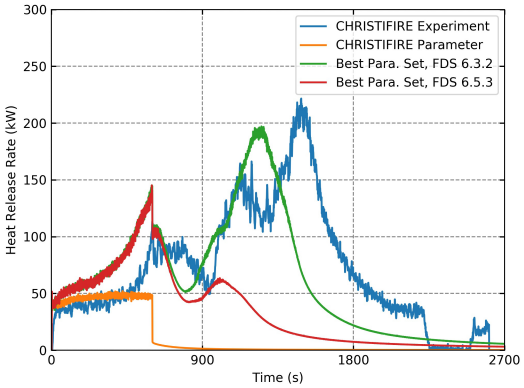

Figure 8: Comparison of Multiple Tray Test 3 from CHRISTIFIRE with simulation results of provided parameters, as well as the best parameter set from the IMP. The gas burner was switched off after 600 s. Highlighting also the influence of different FDS versions.

Furthermore, it is important to note that the user needs to be careful when attempting to transfer the material parameters between different versions of the simulation software. Specifically in the presented case, the parameters are model specific, also depending on the FDS version. Additionally, the demonstrated process, to obtain a material parameter set for fire simulations, could possibly be used for all solid combustible materials. Cables are used as a specific example in this work.

The ability to predict the fire development, based on material parameters and environmental conditions near the fire, enables the user to create better assessments of possible fire and smoke spread, specifically in non-standard facilities. This is of interest, for example, within the (accelerator) tunnel and technical gallery infrastructure at CERN. Cables as a fire load, spread over long distances, from tens of meters up to kilometres. Narrow cross sections may lead to long stretches of cables being pre-heated which will promote the firespread, the extent of which is to be investigated in the future with the outcomes of this work. Obviously, this is not only limited to CERN, but of interest for all cases where cables are installed inside technical galleries, like data centres or power plants. It is also of interest, how much material may be involved and turned into smoke during a fire incident. In the event of a fire in a particle accelerator tunnel, large parts of the accelerators would be contaminated with fire products, which are possibly activated. Soot, mainly carbon, could lead to short circuits. Substances like halogens form corrosive solutions with the humidity of the air and would lead to damage to the sensitive electronics of the accelerators and detectors. Cleaning the accelerators would most likely be performed manually and extremely expensive, also considering the possible long down time of the whole accelerator complex. Furthermore, smoke production and movement is important to assess evacuation strategies in CERN's tunnel network. In some cases, egress routes can become quite long and useful compartementalisation strategies need to be defined.

Currently, the overall process is being revised and improved and some aspects of the envisioned improvements are presented in this paragraph. One severe limitation has been the use of the result of only one experiment as target information. This has been changed to incorporate all repetitions of the Cone Calorimeter experiments with their respective incident heat fluxes as simulation setup for the upcoming optimisation runs. In the beginning, the assumption has been that methane could serve as surrogate fuel, together with the given material parameters. However, after the IMP the surrogate fuel and the soot yield needed to be changed to achieve the desired fire propagation behaviour. For the upcoming runs of the IMP, the surrogate fuel and the soot yield will be set to the values of toluene right from the beginning. The simplified simulation setup of the Cone Calorimeter contains some inaccuracies, like a very coarse mesh, the missing exhaust gas flow and a slightly large edge length. Those points will be addressed for future runs. Specifically smaller mesh cells, despite being costly in terms of computational resources, are desirable in order to better cover the interaction between sample surface and flame.

Furthermore, it can be seen in Figure 5 that the chosen parameters, by the IMP, diverge significantly from the experimental data of the MCC. It is important to emphasis that the IMP was was working with material parameters, that were used in the simplified Cone Calorimeter environment with a model representing assembled cables. This means, in

the MCC tests were performed on a tiny, homogeneous material sample, under conditions that are aimed to specifically test the material behaviour and reduce influences from other sources. Those sources could be, for example, the geometry which could lead to an inhomogeneous heat up, thus an inhomogeneous pyrolysis. By using the configuration of a relatively large furnace with a tiny sample, the main factor for material pyrolysis can assumed to be the samples temperature, while others can be neglected. Due to limitations in FDS however, the representation of the circular cross section of cables is difficult. The chosen model, to represent the cables in the simplified Cone Calorimeter simulation, is inaccurate by using flat layers of material that are stacked upon each other. Therefore, the bumpy structure of the cables, that could be observed when multiple cables lie next to each other, is lost. This should affect the heating up of the cable model in comparison to the real experiment. Furthermore, in the real experiment, the degrading cable material may undergo chemical reactions that are not known here and are not modelled. Thus, it might be necessary to use artificial parameters for reaction kinetics to account for model inaccuracies, and is also expected to some degree. Still, it needs to be investigated if the optimisation algorithm shall have free reign over the reaction kinetics parameters or if it requires some constraints.

With the revised process, more of the CHRISTIFIRE cables will be treated. Followed by non-halogenated cables, which have been tested, within the framework of the FCC Fire Safety Collaboration, at Lund University, Sweden. In addition, the implications of the changes in the radiation and solid heat transfer models between the FDS versions 6.3.2 and 6.5.3 need to be further assessed. Furthermore, the Python scripts are also in an improvement process to set them up in a more general way. This will allow faster changes in the setups to be investigated. A small group of people came together at the University of Wuppertal, Germany, and started the creation of a flexible Python framework to tackle similar inverse modelling problems (working title: propti).

Note: Part of the data used for creating this paper, is publicly available on the Zenodo data base under the following DOI: 10.5281/zenodo.1145947

5 Acknowledgements

The authors want to thank Kevin McGrattan for providing advice, access to the CHRISTIFIRE data and fruitful discussions.

Furthermore, the authors would like to thank their colleagues of HSE at CERN for their valuable input and proof reading.

Part of this work is sponsored by the Wolfgang Gentner Programme of the Federal Ministry of Education and Research of Germany.

Within the study project of the Future Circular Collider, a fire safety engineering collaboration with other particle laboratories was established. Members of this group are some of the major particle accelerator facilities (CERN, DESY, ESS, FNAL and MAX IV) and Lund University. It is aimed towards a better understanding of smoke production and movement in one-of-a-kind underground research facilities, e.g. such as particle accelerators, benefiting life, environment and asset protection. The authors are thankful for all the discussions and advice coming out of this collaboration.

The authors gratefully acknowledge the computing time granted by the JARA-HPC Vergabegremium and VSR commission on the supercomputer JURECA at Forschungszentrum Jülich, Germany.

References

[1] European Organization for Nuclear Research (CERN). *CERN in Numbers [Online, Accessed: 12 October 2017]*. URL https://smb-dep.web.cern.ch/en/content/cernnumbers.

[2] Christiane Lefèvre. *The CERN accelerator complex; Complexe des accélérateurs du CERN [Online, Accessed: 11 October 2017]*, 12 2008. URL https://cds.cern.ch/record/1260465?ln=de.

[3] Kevin B. McGrattan, Andrew J. Lock, Nathan D. Marsh, and Marc R. Nyden. Cable Heat Release, Ignition, and Spread in Tray Installations during Fire (CHRISTIFIRE): Phase 1 - Horizontal Trays. Contractor report, nureg/cr-7010, vol. 1, Office of Nuclear Regulatory Research, 7 2012.

[4] Andreas Meunders, Lukas Arnold, and Benjamin Schröder. Automated Generation and Evaluation of FDS Simulations for Optimizing Parameters with Dakota. Magdeburger Brand- und Explosionsschutztag, 03 2015.

[5] A. Meunders, G. Baker, L. Arnold, B. Schroeder, M. Spearpoint, and D. Pau. Parameter Optimization and Sensitivity Analysis for Fire Spread Modelling with FDS. 10th International Conference on Performance-Based Codes and Fire Safety Design; Brisbane, Australia, 11 2014.

[6] Anna Matala. *Methods and applications of pyrolysis modelling for polymeric materials: Dissertation*. PhD thesis, Aalto University, Finland, 2013.

[7] Christopher William Lautenberger. *A Generalized Pyrolysis Model for Combustible Solids: Dissertation*. PhD thesis, University of California, United States of America, Berkeley, California, 2007.

[8] Marco Andreini, Lukas Arnold, Tristan Hehnen, and Saverio La Mendola. A Probabilistic Model for the Prediction of the Energy Release Rate from the Combustion of Electrical Cables. IFireSS – 2nd International Fire Safety Symposium; Naples, Italy, 2017.

[9] Kevin McGrattan, Simo Hostikka, Randall McDermott, Jason Floyd, Craig Weinschenk, and Kristopher Overholt. *Fire Dynamics Simulator Users Guide, Sixth Edition*. Gaithersburg, Maryland, 11 2015.

[10] Richard E Lyon and Richard N Walters. Pyrolysis combustion flow calorimetry. *Journal of Analytical and Applied Pyrolysis*, 71(1):27–46, 2004. ISSN 0165-2370. doi:https://doi.org/10.1016/S0165-2370(03)00096-2. URL https://www.sciencedirect.com/science/article/pii/S0165237003000962. Practical Applications of Analytical Pyrolysis (special section).

[11] Brian T. Rhodes and James G. Quintiere. Burning rate and flame heat flux for pmma in a cone calorimeter. *Fire Safety Journal*, 26(3):221–240, 1996. ISSN 0379-7112. doi:https://doi.org/10.1016/S0379-7112(96)00025-2. URL https://www.sciencedirect.com/science/article/pii/S0379711296000252.

[12] Q. Y. Duan, V. K. Gupta, and S. Sorooshian. Shuffled complex evolution approach for effective and efficient global minimization. *Journal of Optimization Theory and Applications*, 76:501–521, 1993. ISSN 1573-2878. doi:https://doi.org/10.1007/BF00939380.

[13] Tobias Houska, Philipp Kraft, Alejandro Chamorro-Chavez, and Lutz Breuer. SPOTting Model Parameters Using a Ready-Made Python Package. *PLoS ONE*, 10, 12 2015. doi:https://doi.org/10.1371/journal.pone.0145180.

[14] Morgan J. Hurley, Daniel Gottuk, John R. Hall, Kazunori Harada, Erica Kuligowski, Milosh Puchovsky, José Torero, John M. Watts, and Christopher Wieczorek. *SFPE Handbook of Fire Protection Engineering*. Springer New York, NY, Southern Gate, Chichester, West Sussex PO19 8 Q, England, fifth edition, 10 2015. ISBN 978-1-4939-2564-3. doi:https://doi.org/10.1007/978-1-4939-2565-0.

4.2 Publication II: Numerical Fire Spread Simulation Based on Material Pyrolysis – An Application to the CHRISTIFIRE Phase 1 Horizontal Cable Tray Tests

The second article, "Numerical Fire Spread Simulation Based on Material Pyrolysis – An Application to the CHRISTIFIRE Phase 1 Horizontal Cable Tray Tests", is published in the Fire journal [2].

Table 4.2: CRediT authorship contribution statement of publication II.

Item	T. Hehnen	L. Arnold	S. La Mendola
Conceptualization	X	X	X
Methodology:	X	X	X
Software:	X	X	
Validation:	X		
Formal analysis:	X		
Investigation:	X		
Resources:	X	X	X
Data curation:	X		
Writing - original draft:	X	X	X
Writing - review and editing:	X	X	X
Visualization:	X		
Supervision:		X	X
Project administration:		X	X
Funding acquisition:	X		

NUMERICAL FIRE SPREAD SIMULATION BASED ON MATERIAL PYROLYSIS – AN APPLICATION TO THE CHRISTIFIRE PHASE 1 HORIZONTAL CABLE TRAY TESTS

A PREPRINT

Tristan Hehnen [a,b], Lukas Arnold [c], and Saverio La Mendola [b]

[a]Bergische Universität Wuppertal, Wuppertal, Germany
[b]European Organization for Nuclear Research CERN, Geneva, Switzerland
[c]Institute for Advanced Simulation, Forschungszentrum Jülich, Jülich, Germany

Tristan Hehnen: hehnen@uni-wuppertal.de; ORCID: 0000-0002-6123-261X
Lukas Arnold: l.arnold@fz-juelich.de; arnold@uni-wuppertal.de; ORCID: 0000-0002-5939-8995

February 6, 2024

ABSTRACT

A general procedure is described, to generate material parameter sets to simulate fire propagation in horizontal cable tray installations. Cone Calorimeter test data is processed in an inverse modelling approach. Here, parameter sets are generated procedurally and serve as input for simulations conducted with the Fire Dynamics Simulator (FDS). The simulation responses are compared with the experimental data and ranked based on their fitness. The best fitness was found for a test condition of $50\,\mathrm{kW/m^2}$. Low flux conditions $25\,\mathrm{kW/m^2}$ and less exhibited difficulties to be simulated accurately. As a validation step, the best parameter sets are then utilised to simulate fire propagation within a horizontal cable tray installation and are compared with experimental data. It is important to note, the inverse modelling process is focused on the Cone Calorimeter and not aware of the actual validation step. Despite this handicap, the general features in the fire development can be reproduced, however not exact. The fire in the tray simulation extinguishes earlier and the total energy release is slightly higher as compared to the experiment. The responses of the material parameter sets are briefly compared with a selection of state of the art procedures.

Keywords CHRISTIFIRE · Fire Dynamics Simulator (FDS) · computational fluid dynamics (CFD) · optimisation · pyrolysis modelling · shuffled complex evolution (SCE) · high performance computing (HPC) · fire propagation simulation · cone calorimeter simulation · cable tray fire simulation · radiative heat flux in cable tray fires · SPOTPY · PROPTI

1 Introduction

In the fire safety engineering community, design fires are a frequently used tool when conducting fire risk assessments. The rigidness of the prescribed fire developments, e.g. hydrocarbon curve, is an obvious limitation. Ideally, the fire development could be simulated, based on the material of the objects involved, as well as ventilation conditions and energy distribution near the fire's location. One way to achieve this goal is to simulate material pyrolysis. Laboratory tests are utilised to support these simulation efforts, as in general the explicit measurement of the material properties is not feasible. There is an implicit hierarchy assumed, in which micro-scale combustion tests, like Thermo-Gravimetrical Analysis (TGA) or Micro-Combustion Calorimetry (MCC), can be used to derived basic parameters to describe the pyrolysis reaction rates, for example parameters for an Arrhenius equation. Bench-scale tests, like the Cone Calorimeter, can be utilised to determine the thermo-physical parameters. Afterwards, these parameter sets can be used to simulate the fire development in a real-scale setup.

The fire safety engineering community has conducted quite some research within this field, e.g. [1, 2, 3, 4, 5, 6]. Rogaume provides an overview over some of the challenges when trying to simulate material pyrolysis in [7], also discussing some optimisation strategies for estimating more complex parameter sets. One of the optimisation strategies is the employment of a shuffled complex evolutionary algorithm (SCE) [8], which is relatively common in fire safety engineering [9, 10, 3, 4, 11, 12] due to its performance [13] and is also utilised in the work presented here. For other approaches, as much data is taken from experiments as possible and pyrolysis models are built on it [14].

In this contribution, the focus is set on simulating fire propagation in horizontal tray installations, based on pyrolysis of electrical cables. Fire behaviour of cable tray installations has been studied over previous decades. Specifically, the nuclear industry dedicated resources to investigate cable tray fire development on an international level. Some of the more visible projects have been the "Cable Heat Release, Ignition, and Spread in Tray Installations during Fire" (CHRISTIFIRE) Programme [15, 16] carried out by the United States Nuclear Regulatory Commission (U.S. NRC), "Propagation d'un incendie pour des scénarios multi-locaux élémentaires" (Fire Propagation in Elementary Multi-room Scenarios – PRISME) [17] carried out by the Nuclear Energy Agency (NEA) of the Organisation for Economic Co-operation and Development (OECD) or the "International Collaborative Project to Evaluate Fire Models for Nuclear Power Plant Applications" (ICFMP) [18] carried out by the Gesellschaft für Anlagen- und Reaktorsicherheit (GRS) gGmbH. Research is also conducted in more general terms, like in the "Fire Performance of Electrical Cables" (FIPEC) project [19] initiated by the European Commission. During these projects, different experiments at various scales have been performed, not solely related to cable fires but also fire and smoke propagation in general.

Different strategies have been developed to model the fire development in cable tray installations. Performance of several computational fluid dynamics (CFD) codes, to estimate fire development and propagation in cable tray installations, have been compared in the past [20]. Based on Cone Calorimeter data from the FIPEC project mathematical models for material pyrolysis were created [21]. A relatively simple hand calculation model, "Flame Spread over Horizontal Cable Trays" (FLASH-CAT), was developed primarily from data of the CHRISTIFIRE campaign. The FLASH-CAT model was picked up in the frame of the PRISME programme [22] for trays mounted to a wall, where it was implemented into a CFD code (CALIF3S/ISIS) and some parameters were adjusted, such that the model would better recreate the PRISME data. A very similar setup, also from the PRISME programme, was used where the Cone Calorimeter energy release rate was "painted" on a cable tray model, such that each individual surface cell would follow the development of experimental data [23]. The release starts after a certain material temperature of the cable sample was reached, that could be regarded as an ignition temperature.

The principal inspiration for the work presented here, with respect to pyrolysis modelling with the Fire Dynamics Simulator (FDS), is work conducted by Matala et al. [3] and Lautenberger et al. [24].

In general, a brute force approach is utilised here, for which it is assumed that either only few parameters are known of the studied material, or cannot be transferred directly to the simulation. Thus, all parameters that define a material in FDS, are worked upon during the optimisation process. This is specifically the case for the residues, of which no information is available.

It should be noted that the overall hypothesis for this work is, that parameters are not directly transferable from the experiment to the simulation (yet) and therefore an effective parameter set is to be created, that yields a simulation response close to the data observed in the experiment. The assumed reasons are manifold. An obvious reason in the insufficient spatial resolution of the individual cables, especially in real-scale cases. Additionally, gaps in the understanding of the underlying processes and their complexity may still lead to an incomplete set of models.

The presented work aims to describe a procedure, to create material parameter sets that allow the simulation of fire propagation within FDS. It follows the concept that material behaviour can be studied sufficiently well in the laboratory scale, and thus it allows for extrapolation into real-scale scenarios. The foundation for this work is experimental data obtained by CHRISTIFIRE Phase 1 [15]. Cone Calorimeter tests are chosen as starting point, with a simplified model of the apparatus being utilised in FDS. Employing a numerical optimisation scheme, material parameters are varied in the simplified Cone Calorimeter simulation setup, such as to find the FDS response that is close to the energy release rate data from the experiment. In an inverse modelling process (IMP) the experimental data serves as target, while the material input parameters are adjusted for a simulation response to fit the target. The best parameter set obtained during this process is then utilised in a real-scale cable tray simulation setup. In a validation step, its performance in estimating the fire development is assessed. Furthermore, the results of the presented procedure are compared to selected state of the art prediction approaches.

This work is accompanied by a data repository [25] which contains simulation data like the input files for FDS and PROPTI, data base files with the IMP results and the results of the simulations with the obtained material parameter sets. For a brief description see section 5.

2 Materials and Methods

2.1 Experimental Data

The content of CHRISTIFIRE Phase 1 is briefly summarised below. During that experimental campaign, a relatively large number of different cables has been subjected to fire tests of various scales. Thus, data sets of the same cable, but under different conditions, are available. For the procedure presented here, the focus, of which tests to use, was set on MCC, Cone Calorimetry and horizontal tray installations in the open – the Multiple Tray Tests (MT). As argued below, cable 219 was chosen as the sample, while cables from CHRISTIFIRE Phase 2 have not been considered as of now, however are envisioned to be studied later on.

The choice fell on this specific cable, cable 219, because in contrast to the other cables:

- It showed good repeatability for the different incident heat fluxes during the Cone Calorimeter tests.
- In the multiple tray tests, the individual trays were completely filled with the cable 219.
- In the multiple tray tests, the cables were neatly arranged to rows that extended over nearly the whole tray width. This allowed the tray representation as a single solid slab in the simulation.

During Phase 1 of the experimental campaign, MCC tests had been conducted on the individual cable components (insulator and jacket), using a Pyrolysis Combustion Flow Calorimeter (PCFC) [26]. Samples of about $5\,\mathrm{mg}$ from the plastic components were linearly heated up, to $600\,^{\circ}\mathrm{C}$ at a heating rate of $1\,^{\circ}\mathrm{C/s}$, within a nitrogen atmosphere. Data was determined, like the specific energy release rate per mass, the mass loss, the amount of solid residue produced, heat of combustion, locations of the maxima of the reaction rates, as well as their respective contributions to the overall decomposition process. This also allows to calculate reaction kinetics parameters, modelled by employing an Arrhenius equation per reaction.

Furthermore, the cables had been subjected to Cone Calorimeter tests. Up to three different, constant radiative heat fluxes were imposed on the samples: $25\,\mathrm{kW/m^2}$, $50\,\mathrm{kW/m^2}$ and $75\,\mathrm{kW/m^2}$. The tests at $25\,\mathrm{kW/m^2}$ and $50\,\mathrm{kW/m^2}$ were mostly repeated three times, $75\,\mathrm{kW/m^2}$ was performed just once. Results of these tests are time dependent data series of the energy release rate (ERR) per unit area.

Afterwards, real-scale tests in horizontal tray installations were performed. Tray racks were placed on scales in a relatively large room, under an exhaust hood. Thus, they were considered as burning in the open, with little influence from the surroundings. From one up to seven ladder-backed trays were mounted above each other. The trays had a width of $0.45\,\mathrm{m}$, a length of $2.4\,\mathrm{m}$ or $3.6\,\mathrm{m}$ and were mounted with a vertical distance of $0.3\,\mathrm{m}$. About $0.2\,\mathrm{m}$ below the lowest tray, in the centre, a gas burner was positioned that provided an ignition source of 40 kW $\pm$ 5 kW. Energy release rates were determined by means of oxygen consumption in the exhaust stream and by the mass loss rate.

Results from the Tube Furnace and the Radiant Panel test are neglected during the presented work.

2.2 Inverse Modelling Process

Inverse modelling is used to obtain material parameter sets to describe its behaviour in the simulation. Data obtained from Cone Calorimeter tests serves as target for the inverse modelling process (IMP). An evolutionary, sometimes called genetic, algorithm is utilised to carry out the IMP. Specifically, the Shuffled Complex Evolutionary Algorithm from the University of Arizona (SCE-UA), developed by Duan et al. [8] was chosen. It is implemented in the scripting language Python and part of the framework "Statistical Parameter Optimization Tool for Python" SPOTPY [27]. The SCE-UA is used as provided via SPOTPY, without adjustments to the algorithm. The optimisation is conducted over multiple generations. The size of a generation Φ is determined by equation 1

$$\Phi = (2n_{\text{parameter}} + 1) \cdot n_{\text{complex}} \quad , \tag{1}$$

where $n_{\text{parameter}}$ is the number of parameters to optimise and n_{complex} is the number of complexes within a generation. The number of complexes was chosen to be equal to the number of parameters, which is the default setting of the implementation. In general, it is desirable to reduce the amount of optimisation parameters as the computational complexity, i.e. size of a generation, scales non-linearly with this value.

To assess the fitness of the different parameter sets, the root mean square error (RMSE) is calculated between the simulation response and the target data. An open-source Python framework, PRPOTI, serves as a communication interface between a simulation software, here FDS, and an optimisation algorithm [28, 29, 30].

As stated above, focus was set on cable 219 , in order to streamline the overall process for creating the material parameter sets. In this text, the conducted IMP runs are labelled by indicating the target data (T), the fixed parameters (P), as well as the number of times sampling limits have been adjusted (L). The following labelling options are utilised:

- Indices for experimental conditions of the target data (T):
  - a: $25\,\mathrm{kW/m^2}$
  - b: $50\,\mathrm{kW/m^2}$
  - c: $75\,\mathrm{kW/m^2}$
- Indices of fixed parameter (P):
  - A: Arrhenius parameters (taken from the report [15])
  - L1: layer thicknesses $2\,\mathrm{mm}$ (insulator and jacket)
  - L2: layer thicknesses $4\,\mathrm{mm}$ (insulator and jacket)
  - HT: heat of combustion from toluene (`FUEL`)
  - HC: heat of combustion from the report [15]
- Indices of adjusted sampling limits (L):
  - Successively numbered, starting by 0.

An example of an IMP run label is provided below:

$$T_{a,b,c}P_{A,L1}L_2, \tag{2}$$

where all three irradiance levels are used simultaneously as a joint IMP target, Arrhenius parameters are set to the data from CHRISTIFIRE, the layer thicknesses are set to $2\,\mathrm{mm}$ and it is the second time the parameter sampling limits are adjusted.

The purpose of the different targets is, to determine how well the resulting parameter sets represent the Cone Calorimeter experiments.

It was expected that the IMP runs which take multiple irradiance levels into account would yield more robust parameter sets over a wider range of external fluxes. In previous simulations [31] it was realised that specifically the heat flux of $25\,\mathrm{kW/m^2}$ was difficult to recreate by FDS. Therefore, some IMP runs contained the $25\,\mathrm{kW/m^2}$ case, while others were conducted without it.

2.3 FDS Modelling

The foundation for the FDS simulations is a cable model, consisting of a layered surface (`SURF`) of different materials (`MATL`) and released combustible gaseous species (`SPEC`). All of this information is combined, to form a simulation setup. In general, the simulation setup can be thought of as being the representation of an experimental setup. In this concept, an experimental setup distinguishes not only between individual apparatuses, like Cone Calorimeter or PCFC, but also their settings, e.g. external heat flux or heating rate. In the following, individual aspects of creating the FDS input are discussed.

2.3.1 Cable Geometry

An electrical cable is an assembly of multiple components, conductors covered by an insulator, wound together and surrounded by a jacket. Each component consists of different materials. In general, the cables themselves cannot be resolved geometrically within the conducted simulations. Therefore, they are represented as a flat obstruction of the flow field (`OBST`). To account for the cable's composition, a layered `SURF` was chosen. Top and bottom layer contain the material model for the jacket, while the insulator is embedded in between. Thus, three layers are used in total to represent the cable. This is considered as necessary trade-off, in an effort to reduce the overall computing times.

In an earlier study [31], a copper layer divided the insulator, which lead to five layers. However, during the inverse modelling process (IMP) the conductor thickness was repeatedly pushed to its lower limit. This behaviour was also described by Matala and Hostikka [32]. Following that example, the conductor material layer was removed, to speed up the IMP by reduction of parameters.

2.3.2 Chemical Reaction and Material Composition

As basic concept, pyrolysis is understood as the thermal degradation and consumption of a solid, while gas(es) and solid residue(s) are produced. Based on the material temperature, the Arrhenius equation describes the reaction rate [33]. This is basically the mass release rate of a gas from a solid, which can be converted to the energy release rate, if the gas is combustible.

Even if a material appears to be homogeneous on a macroscopic level, microscopically it may consist of a mixture of various components. These components are likely to decompose at different temperature ranges. Micro-scale tests like MCC, allow to observe such a behaviour. As an example, the plastic material of the cable 219 jacket is assumed to be homogeneous. The experimental data shows two peaks for the cable jacket. This is interpreted as decomposition reactions of two different components, which are represented as two materials (`MATL`) in FDS.

Even though, slightly more detailed information on the gaseous species are provided with the report, toluene is used as surrogate fuel. Cables were tested in the Tube Furnace and yields of CO, CO_2, HCl and soot are available. However, in previous simulations [31] heat transfer to the cable surface was identified as a problem in the simulation. This was attributed to the poor spatial resolution of the flame, due to the coarse fluid cells. Therefore, of the implemented species (`SPEC`) in FDS, one was chosen that offers a high radiative fraction for the flame heat radiation – toluene. Its soot yield, $0.178\,\mathrm{g/g}$, was taken from the SFPE Handbook [34].

Both cable components (insulator, jacket) are each allowed to from a solid residue in the simulation. From the experiments, only the mass yield per component for the residues is reported. Parameters like the (bulk) density, emissivity, thermal conductivity or specific heat are not available. Therefore, they have been left to be determined by the optimiser and are effective parameters. Additionally, they act as buffer material. This means, that the optimiser can potentially adjust the residue parameters when it reaches limits for the remaining parameters.

2.3.3 Micro-Combustion Calorimetry

The MCC data is not directly part of the inverse modelling. Primarily, it gives an indication of how many pyrolysis reactions are to be expected and are thus modelled. Furthermore, they are used to determine if the Arrhenius parameters, that were found from the experimental data and provided in the report, would emerge out of the IMP. In a further step, the pyrolysis parameters are fixed to the ones obtained from the experiment (called "fixed Arrhenius"), in an attempt to reduce the demand for computational resources.

The simulation setup of the MCC test was conducted by utilising the FDS functionality to run only a TGA analysis with no gas phase simulation, i.e. `TGA_ANALYSIS=.TRUE.`.

2.3.4 Simple Cone Calorimeter

For a simple Cone Calorimeter model (SCC) the mesh size is set to an edge length of $47\,\mathrm{mm}$ (cube-shaped cells), see figure 1. For comparison, in earlier work [3] larger cells were utilised ($0.1\,\mathrm{m}$ edge length). The smaller edge length provides a couple of benefits: it leads to a higher resolution of the gas phase, it fits the size of the retainer frame window which has an edge length of $94\,\mathrm{mm}$ and it is close to the target cell size of $50\,\mathrm{mm}$ envisioned for the later cable tray simulation setup. With the increased resolution of the flow field the flame can be resolved more accurately. This in turn leads to a better resolution of the radiative heat flux to the sample surface. Furthermore, sample and flame are surrounded by two cells until the mesh boundary is reached and one fluid cell below the sample surface level. This facilitates the formation of a more stable flow field.

2.3.5 Multiple Tray Simulation

During CHRISTIFIRE Phase 1 , cable fire behaviour has been tested in horizontal cable tray installations in the open. For this work Multiple Tray Test 3 (MT3) was chosen, because trays in this test were solely filled with cable 219.

For the geometrical representation of the experimental setup of MT3 a uniform mesh is chosen. The cells are cube-shaped, with an edge length of $50\,\mathrm{mm}$, see figures 2a and 2b. This choice was mainly driven by an attempt to provide a relatively high resolution, while not being too computationally demanding. It is not based on a mesh sensitivity study. The computational domain is divided into six meshes, as indicated by the differently grey-shaded boxes in figures 2a and 2b. The $50\,\mathrm{mm}$ cell size is also close to the $47\,\mathrm{mm}$ cell size from the SCC simulations, which makes the material parameter sets better transferable to the MT3 simulations. Furthermore, the $50\,\mathrm{mm}$ cell size allowed to have five fluid cells between the trays and four between the burner and the lowest tray. In FDS 6.5.3 the principal model for heat transfer within solids is one-dimensional heat conduction in the direction of the surface normal. For this model to take the temperature of the opposite surface into account, when calculating the material temperature, obstructions need to be one cell thick. Thus, the cable layer was created with the thickness of one cell.

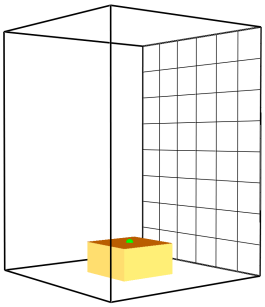

Figure 1: Geometrical representation of the improved Simple Cone Calorimeter (SCC) simulation setup in Smokeview. Darker area represents the model of the cable sample. Was also utilised for the MCC simulations.

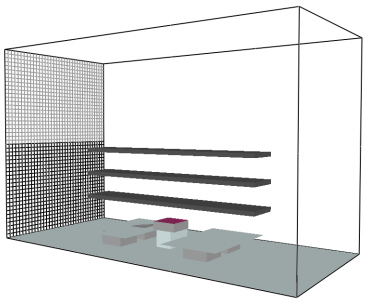

(a) Geometrical representation of the MT3 simulation setup.

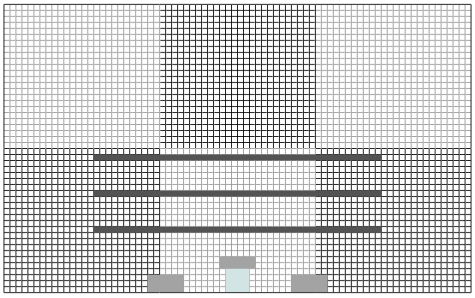

(b) Layout of the computational domain.

Figure 2: Smokeview visualisation of the MT3 setup. Different grey-scales in the background highlight mesh layout.

The metal frame of the trays was neglected during the FDS simulations, because it could not be resolved by the chosen cell size.

In the experiment the cables were neatly arranged to rows that extended over nearly the whole tray width, see figure 3. Therefore, it was assumed, that the representation of the cables as a single, one cell thick, obstruction would be a reasonable geometrical model. In order to maintain a symmetrical flow field, the width of the tray models is reduced to $0.4\,\mathrm{m}$, thus the burner could be positioned at the centre of the tray rack. The length of the slabs is set to $2.4\,\mathrm{m}$, according to the experimental setup.

The gas burner is modelled by using a boundary condition where toluene is introduced into the computing domain (`VENT`). The same gaseous species, toluene, is used for the gas burner, as well as for the cable material. The burner's energy release rate per unit area is matched to its top surface (`VENT`), such that the it releases $40\,\mathrm{kW}$. The burner starts with the beginning of the simulation and is shut down after $600\,\mathrm{s}$.

Also, the `SURF` that describes the top burner face, is assigned a surface temperature that is changed by employing the `TMP_FRONT` parameter and a `RAMP`. Within the first $100\,\mathrm{s}$ of the simulation, after a delay of $1\,\mathrm{s}$, the surface temperature of the burner is linearly increased to $410\,^{\circ}\mathrm{C}$. Afterwards, it is kept constant for $501\,\mathrm{s}$ and ramped down linearly for $2599\,\mathrm{s}$. The decrease starts $1\,\mathrm{s}$ after the burner is shut off, to somewhat account for a decaying flame, due to small amounts of remaining fuel in the piping between the valve and the burner (in the experiment). The prescribed surface temperature is purely guessed. However, it was deemed necessary to provide some model of the hot burner surface to support the gas flow field that would form, as well as the radiative interaction with the surrounding objects, specifically for the bottom face of the lowest cable tray.

Figure 3: Photograph of the cable arrangement in MT3, taken from the CHRISTIFIRE report [15].

2.4 Reference Calculations

To put the results of the IMP in context, three state of the art approaches are followed. This covers an alternative method to determine the model parameters, an approach with prescribed energy release rates, as well as an empirically based model for predicting the fire development within a horizontal cable tray installation.

For the first method the Arrhenius parameters are taken from the MCC results, provided in [15]. This is referred to as "fixed Arrhenius" throughout this text, since they are not touched by the IMP in these specific cases. They are used in the same IMP setups, as discussed in section 2.2, namely the pre-exponential factor A and the activation energy E. The reaction order n was set to 1 (FDS default) and the heat of reaction to $1000\,\mathrm{kJ/kg}$. The remaining parameters are still utilised for the IMP. A further adjustment is to set the layer thicknesses to $2\,\mathrm{mm}$ for each, jacket and insulator. This adjustment is a general improvement to the original setup, since the layer thickness and the density thereof are related and it leads to a reduction of necessary simulations to be conducted.

The second method determines parameters, that allow to map Cone Calorimeter test results to an object's surface, basically a Cone Calorimeter paint. Different approaches for thermally thick samples are summarised and discussed in [35, chapter 7]. In a recently published paper, this concept was utilised in the context of simulating fire spread in cable tray installations [23]. In the work presented here, Janssens' procedure [35] and the "Beji-Merci procedure" [23] are both used to compare the results from the IMP against. Since no ignition times were reported with the Cone Calorimeter tests [15], they are estimated from the energy release rate data, as described in the appendix 7.4.

For the third method, the FLASH-CAT model is utilised. It was developed during the CHRISTIFIRE campaign, based on its experimental data [15]. For all multiple tray tests, a calculation was conducted and the respective results provided with the report. Since the model's results for MT3 were already available, they are extracted from the respective plot provided with the experimental data.

3 Results

3.1 IMP Runs

3.1.1 Development of the Parameter Sets

Due to the large amount of individual simulations performed during the respective IMP runs, in total more than one million, focus was set to the best parameter sets per generation of the SCE-UA. These parameter sets were then used for different simulations, specifically to assess the performance in the tray setup.

At first, the development of the fitness value of the best parameter set per generation for each IMP run is shown in figure 4. It is given by the negative root mean square error (RMSE). Each IMP run starts out with a relatively large distance to the target. Within the first 10 to 15 generations the fitness improves notably and afterwards the rate of improvement decreases.

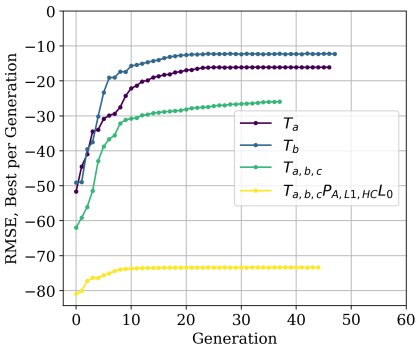

Figure 4: Development of the RMSE values, of the best parameter set per generation, for the IMP runs (T_* and $T_{a,b,c}P_{A,L1,HC}L_0$).

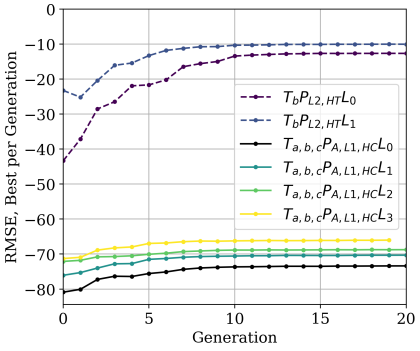

Figure 5: RMSE values for IMP runs with adjusted parameter sampling limits. Successive limit adjustments are marked with L_*.

Appendix 7.1 provides some further information on the development of the individual parameters during the IMP.

3.1.2 Adjusted Parameter Limits

During the IMP runs, some parameters got stuck at their sampling limits. This behaviour is demonstrated in the appendix 7.1.2, where the parameter development is summarised in ribbon plots. To improve on this, a test series is conducted in which the respective limits are shifted.

As general procedure, the sampling limits are adjusted by a percentage of the sampling range. In cases where the parameter is stuck at the upper limit the percentage is added, otherwise it is subtracted. The percentage is chosen arbitrarily, with a value of about 30 %. With these adjusted limits a new IMP run is conducted. The best parameter sets per generation for the adjusted limits are then also run through the whole stack of simulation setups. In general, it can be observed that the shifted sampling limits lead to an improvement of the fitness values. This is demonstrated by groups of the IMP runs $T_bP_{L2,HT}L_*$ and $T_{a,b,c}P_{A,L1,HC}L_*$, see figure 5.

3.2 Cone Calorimetry Simulation Results

As stated above, not all of the IMP runs were utilising all of the different incident heat flux conditions as target. Despite this, after the conclusion of the IMP runs, all best parameter sets were put into simulation setups for all three conditions.

This allows for a comparison of the parameter set's performance under all conditions and specifically compare more rigid (all three tests) to softer (one test) target setups. The following paragraphs describe the results shown in figure 6.

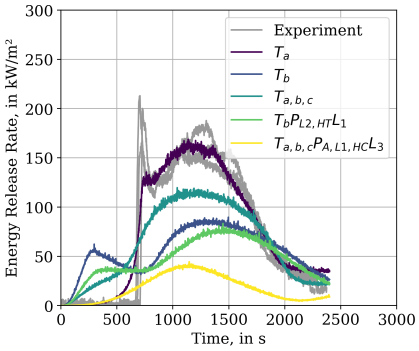

(a) External heat flux of $25\,\mathrm{kW/m^2}$.

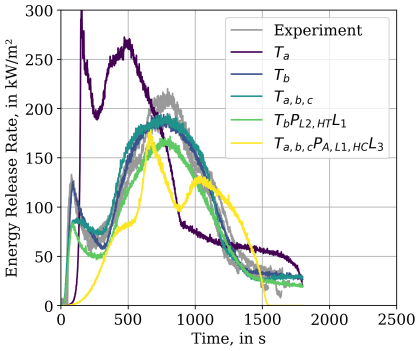

(b) External heat flux of $50\,\mathrm{kW/m^2}$.

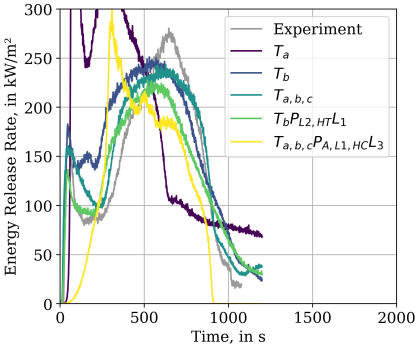

(c) External heat flux of $75\,\mathrm{kW/m^2}$.

Figure 6: Comparison between energy release rates of Cone Calorimeter simulation, across global best parameter sets.

At first, the performance of the IMP results in relation to their respective targets is presented. It can be observed, that for an external radiative flux of $25\,\mathrm{kW/m^2}$ only T_a (target $25\,\mathrm{kW/m^2}$) is able to represent the experimental data reasonably well, except for the first peak, see figure 6a. IMP run T_b is able to reproduce the experimental data well for its target of $50\,\mathrm{kW/m^2}$.

However, comparing the performance of both parameter sets against data that is not used as IMP target shows significant deviation. T_a overestimates the energy release for the other two external flux conditions ($50\,\mathrm{kW/m^2}$, $75\,\mathrm{kW/m^2}$) significantly. Even though, the general features of the experimental data can be reproduced. For T_b, in the $25\,\mathrm{kW/m^2}$ condition, the energy release is over-predicted right from the start, the first peak reaches only a quarter of the energy release as the experiment and happens much earlier. The energy release of the second peak is about a factor of 2 lower as in the experiment. For the $75\,\mathrm{kW/m^2}$ data, the first peak is reproduced, as well as the second, however the intermediate section is over-predicted by a factor of about 1.5.

Visually, $T_{a,b,c}$ shows the best fitness overall three external fluxes, see figure 6. In the $25\,\mathrm{kW/m^2}$ case it is not able to capture the first peak. However, the energy release in the first about 700 seconds is lower, compared to T_b and the second peak is represented better. Under the $50\,\mathrm{kW/m^2}$ condition, the first peak and valley are reproduced, but appear

smoothed. The second peak is represented about as well as in T_b. With an external flux of $75\,\mathrm{kW/m^2}$, both peaks are reproduced and the valley is captured better as compared to T_b.

The parameter set of $T_bP_{L2,HT}L_1$ shows slightly better performance in the Cone Calorimeter simulations compared to T_b. Under an external flux of $25\,\mathrm{kW/m^2}$ the first peak is less pronounced than that of T_b, however the long delay visible in the experiment is also not reproduced. For the $50\,\mathrm{kW/m^2}$ case the performance is slightly worse as T_b, specifically the first peak is not captured well. In the $75\,\mathrm{kW/m^2}$ case, the first peak is still not resolved well, yet the valley is captured more closely than by T_b. In all three conditions the peak energy release is less than the the values reported from the experiments.

The state-of-the-art approach, with pre-determined Arrhenius parameters (here based on MCC data), layer thickness and heat of combustion, is represented by the $T_{a,b,c}P_{A,L1,HC}L_3$ IMP run. Here, all three experiments were used as target. The experimental data of the $25\,\mathrm{kW/m^2}$ case could not be reproduced. It shows none of the distinct features and the peak energy release is a factor of about 4 lower than observed in the experiment. A slightly better reproduction of the experiments could be achieved for $50\,\mathrm{kW/m^2}$ and $75\,\mathrm{kW/m^2}$, however the energy release rate development diverges significantly.

All IMP runs show difficulties to reproduce the $25\,\mathrm{kW/m^2}$ condition. While some show a two-peak-structure, none are able to reproduce the long delay to ignition, that can be seen in the experimental data.

For an overview of the performance of the best parameter sets per generation the reader is directed to the appendix 7.3, where T_b is provided as an example.

3.3 Multiple Tray Simulation Results

For each best parameter set per generation of the IMP runs, a simulation in a MT3 setup was performed. The respective simulation results of the energy release rate are plotted and compared to the experimental data provided by the report [15].

Of the IMP runs, only T_b is able to reproduce the features of the ERR development, see figure 7. The first peak, around the time where the burner is switched off at $600\,\mathrm{s}$, is over-predicted by a factor of about 2. After the burner is switched off, the ERR decreases by about $40\,\mathrm{kW}$, which is similar to what is observable in the experimental data. In the simulation, the decrease is followed by a peak that overshoots the first peak by about $80\,\mathrm{kW}$, which is again similar to the experimental data, however less pronounced there with about $60\,\mathrm{kW}$. The last peak in the simulation response is a bit lower than the previous peak, while in the experiment the final peak is again about $50\,\mathrm{kW}$ larger that the one before. The last two peaks from the simulation overestimate the ERR of the experiment by a third, i.e. about $90\,\mathrm{kW}$. The progression in the simulation is faster compared to the experiment. At the time the experiment reaches the second peak, the simulation has reached the third peak and starts to decrease. The different peaks are associated with the propagation of the flame to the next cable layer within the tray installation.

The parameter set of IMP run T_a leads to a massive over-prediction of the ERR and the features could not be reproduced. In contrast to that, IMP run $T_{a,b,c}$ is not able to cause any significant fire development and does not recover after the burner is switched off. Similar behaviour could be observed for the $T_{a,b,c}P_{A,L1,HC}L*$ set, here only the last run, $*L_3$ is shown as example. With the given limits, the parameter sets are not able to achieve fire propagation after the gas burner is shut off.

$T_bP_{L2,HT}L_1$ is able to recover briefly after the burner is shut off, but does not show meaningful fire development. It is notable that $T_bP_{L2,HT}L_1$ starts from the same trajectory as T_b, but looses a lot of its ERR after the burner is cut. Interestingly, an early parameter set of this run is able to reproduce the experimental data in the MT3 setup better, as the best parameter set of the IMP (not shown here).

For the parameter sets that lead to a propagation it seems that an energy release of about $200\,\mathrm{kW}$ needs to be reached to get a sustainable position, able to cope with the burner shut-off. Yet, it may not be sufficient in all cases ($T_bP_{L2,HT}L_1$).

3.4 Reference Calculation

At first, the results of the FLASH-CAT model are briefly outlined. The model results follow the experimental data, however it over-predicts the energy release rate, see figure 8. FLASH-CAT is also not able to resolve the features (peaks) of the experimental data. In contrast to the experiments, where the combustion is sustained up to about $2500\,\mathrm{s}$, the FLASH-CAT model shows a duration of $5400\,\mathrm{s}$. This leads to a higher total energy release than observed during the experiment, a factor of about 2.8. More details on this are provided in section 3.5.

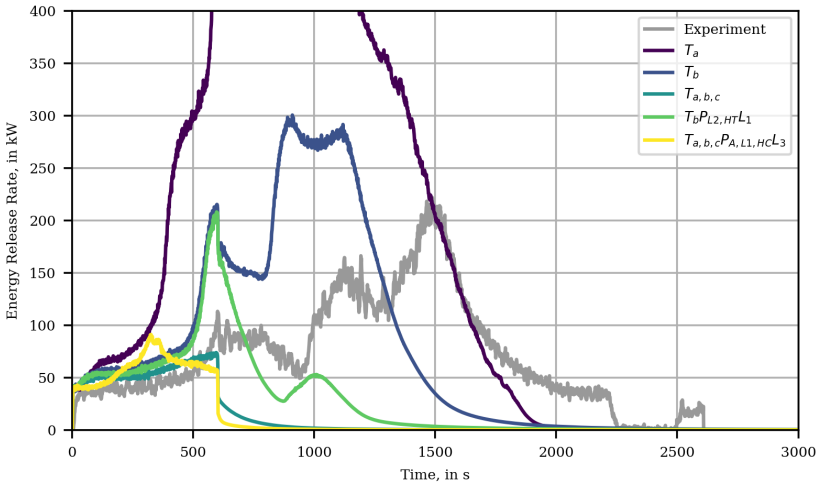

Figure 7: MT3 simulation results for a selection of the best parameter sets per IMP run, compared to experimental data. Peak for T_a at about (829.0 s, 856.2 kW)

Simulation responses for the different approaches of the Cone Calorimeter paint methodology are provided in figure 8. Across the different variations to the procedures, two clusters of results were generated one with high ERR and one with a low ERR. Due to their similarities, the figure shows only one representative for each cluster. For the low ERR cluster, after the burner is switched off the fire decays until extinction near 2200 s. Only the high ERR cluster shows a significant fire propagation and energy release, where the plot resembles the development of the $50\,\mathrm{kW/m^2}$ Cone Calorimeter test that served as input for the `RAMP`. See appendix 7.4 for more details.

3.5 Total Energy Release in MT3 Setup

The total energy release (TER) for each best parameter set per generation was determined and compared to the experimental value, see figure 9. Furthermore, data from the FLASH-CAT model (extracted from [15]) and the reference calculations for the MT3 setup are added to the plot. The TER for the experiment is calculated to be about 0.2 GJ, i.e. by integrating over the experimental data series. The FLASH-CAT model shows a significantly higher TER of about 0.5 GJ. Both values are provided as constant dashed lines in figure 9, to allow a comparison for the different model responses.

For the best parameter set of T_a the TER is slightly higher than the value from the FLASH-CAT model. T_b shows a TER which is slightly higher than the value from the experiment. The remaining IMP runs did not perform well during the MT3 simulation, which is indicated by TER values between 0.05 GJ up to 1.2 GJ. For the reference calculations the lowest TER is about 1.0 GJ for the "Beji-Merci" procedure and the highest over 1.2 GJ for Janssens' procedure, overpredicting the TER by a factor of 2 with respect to FLASH-CAT.

3.6 Micro-Combustion Calorimetry Simulations

Even though, the results of the MCC experiments were not directly used during the optimisation process, the obtained parameter sets are compared to this data. For each best parameter set two FDS input files are generated, which contained either the jacket or the insulator material. Utilising the `TGA_ANALYSIS=.TRUE.` functionality of FDS, a MCC simulation is conducted for the best parameter sets per IMP run. The results of the jacket material are presented in figure 10a, the data of the insulator in figure 10b. The simulation results are compared to the experimental and model data provided by the report [15]. For the given parameter sampling limits, none of the IMP runs is able to reproduce the experimental data as an emergent phenomenon. Simulations with fixed Arrhenius parameters are not shown here, since they, by construction, produce nearly the same result as the model parameters from the report [15].

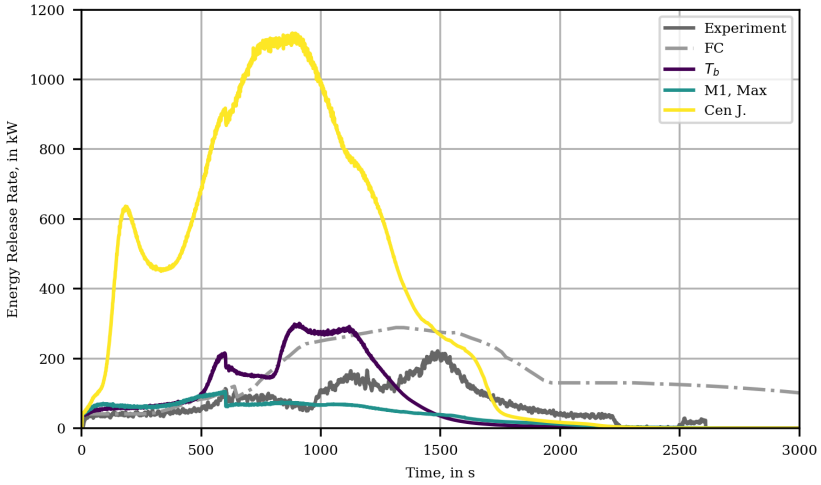

Figure 8: MT3 simulation results for different Cone Calorimeter paint methods and T_b results are provided for comparison. Label "M1" refers to a specific method of the "Beji-Merci" procedure [23], "J." refers to the Janssens' procedure [35].

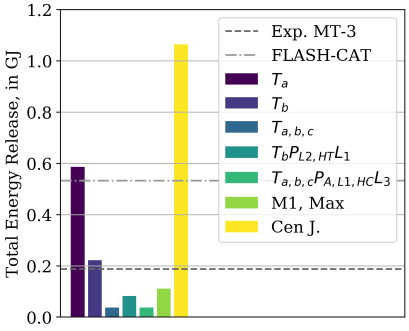

Figure 9: Total energy release of the MT3 simulations, compared with the experimental values and results form the FLASH-CAT (FC) model.

Appendix 7.3 provides an exemplary overview over the performance of the best parameter sets per generation for IMP run T_b in the MCC simulation setup.

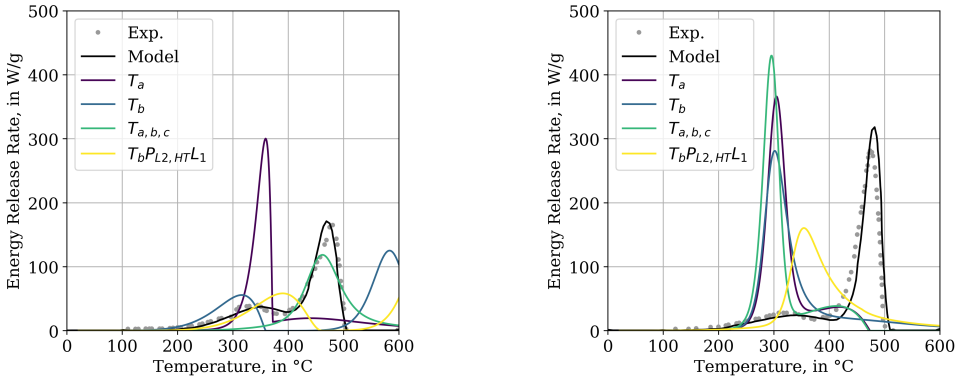

(a) MCC simulation response of the jacket material.

(b) MCC simulation response of the insulator material.

Figure 10: Comparison of energy release rates of MCC simulation (`TGA_ANALYSIS=.TRUE.`) of cable 219, across best parameter sets of different IMP runs, against experimental (Exp.) and model data [15].

4 Discussion

It is obvious, that the IMP results presented here do not fit perfectly to the experimental data. Other models, which are strongly based on empirical data, can achieve a better fit, eventually by construction. Yet, their ability to forecast other scenarios is potentially limited. The work presented here is intended to provide a reference to a methodology for finding parameters that reasonably represent the fire behaviour of cable materials. In future work, the parameter transferability and limits of the methodology have to be investigated further.

Still, to the authors knowledge, the here presented work is the first time a successful material parameter based fire propagation simulation in a cable tray arrangement was achieved.

An important observation is the performance of IMP run $T_{a,b,c}$. Qualitatively, it performs best in the Cone Calorimeter simulations across all external flux conditions, see figure 6. Though, its fitness values show notably worse performance as for example T_b, see figure 4. On the other hand, the fitness assessment is different due to different target functions. Thus, it is not reasonable to compare fitness values across different IMP. In the cable tray simulations, however, no sustained fire development could be achieved after the burner was switched off. As of yet, we have no explanation for this behaviour. Especially, since the jacket material response in the MCC setup, it is relatively close to the experimental data.

It should be pointed out, that the here generated parameter sets are subject to different dependencies. For one, it can be shown that the performance is dependent on the fluid cell size and the solution only converges for higher resolutions, as discussed below. Furthermore, parameter set performance is also sensitive to computer architecture, software versions and operating systems, see appendix 7.6.

It is curious that the Cone Calorimeter experiments can be reproduced relatively well, after optimisation. However, the extrapolation to the trays seems difficult. Similar behaviour can be observed when trying to extrapolate from the micro scale to the Cone Calorimeter.

Essential new aspects that have been considered for the overall process, i.e. parameter generation and cable tray simulations, are summarised below:

- The mesh resolution was increased in the optimisation step significantly, when compared with Matala's work [12].

- A wider array of material parameters was taken into account during the optimisation step, including the residues' parameters, and not only the reaction kinetics.
- With toluene a gas species was chosen, that produces more soot as compared to propane, which leads to a higher radiative fraction of the flame.
- The gas burner was assigned a (highly speculative) surface temperature profile with a slow decay to account for the heat up and feedback during the experiments.

As mentioned above, in order to become a reference for further investigations, an extensive appendix is provided. It contains all the considered approaches, and summarises the data sets and analysis methods provided in an online repository [25].

4.1 IMP

As a general conclusion, it can be demonstrated that the presented approach, using the SCE algorithm and the here formulated constrains, is able to find material parameter sets that are able to reproduce the Cone Calorimeter test responses within FDS 6.5.3, see figure 6. This is in agreement with findings reported by other researchers, e.g. [10, 32, 4]. The resulting parameter sets are shown to produce simulation responses that match their individual targets relatively well.

This outcome is not a general statement, as it is the result of the constrains set by the used model (FDS) and the chosen parameter sampling limits. Brief tests conducted to adjust the parameter limits seem to be beneficial to improve the overall fitness, as demonstrated in figure 5. Despite changes to the sampling ranges, not all parameters could be directed away from the limit they were stuck at, see appendix 7.1.2. This may be improved by more aggressive changes to the sampling ranges, but also by taking the improved FDS input (e.g. layer thickness of $4\,\mathrm{mm}$, no `HEAT_OF_COMBUSTION` from the cable material) into account.

The generated parameter sets are to be regarded as effective parameters, in that they are not necessarily realistic values. However, the sampling limits have been chosen to not allow values that are too far away from what could be regarded realistic. Since no information was available for the thermo-physical parameters of the residues of the cable components, they were basically used as buffer material. Due to their parameters being part of the optimisation parameters, the algorithm is able to indirectly influence the material decomposition, by changing e.g. the thermal inertia and the emissivity of the sample.

One could imagine to follow a similar concept with the gaseous species, by introducing a "gaseous buffer". On a simple level it could mean to mix an inert `SPEC` to the `FUEL`, like nitrogen, and have the algorithm be able to adjust the fraction. However, to cover the initial delay for low flux conditions better, it may be useful to introduce more gas mixtures, e.g. for each cable component, that are associated to the pyrolysis reactions, as discussed by Matala [3, publication 4]. This requires that more detailed information on the composition of the released gas mixture is available. Otherwise this model would only be as arbitrary as any other. The CHRISTIFIRE Phase 1 report [15] provides information on yields of selected gaseous components from tube furnace tests. Even though this information was not used in the study presented here, to maintain consistency with the selected surrogate fuel of toluene, the argument can certainly be made that the yields alone are not sufficient. Primarily, because they represent the average value during steady-state conditions. This makes it difficult to connect them with the changing temperature profiles present in the other setups, like MCC or Cone Calorimeter. More detailed data-time series would be specifically necessary, when it is to be attempted to connect the mass loss of the sample to the release of gaseous species and the resulting formation of a flame. This is in contrast to the approach followed here, where only the energy release of the flame was considered and the path to the formation of the flame was mostly ignored.

As stated above, the IMP yields good parameter sets for reproducing the Cone Calorimeter results. Thus, it seems that the interaction/relationship of the heat transfer with the pyrolysis processes can be reproduced sufficiently well. In order to individually check the validity of the pyrolysis process, the MCC test data is utilised. Yet, the Arrhenius parameters gained deviate from the ones reported from the experiment, despite expected otherwise. To represent the pyrolysis better, one could attempt to use the Arrhenius parameters directly, as obtained from the experiments, i.e. not considered during the optimisation. However, with the fixed Arrhenius parameters the simulations of the Cone Calorimeter and the multiple tray tests do not yield a reasonable response. This could only be achieved when the IMP was given access to the whole ensemble of the material parameters, therefore controlling the interaction globally. Additionally, it is known, that the oxygen concentration in the gas phase around the sample can not be neglected and might significantly influence the material decomposition behaviour [36]. Thus, MCC tests where the sample is heated in a nitrogen atmosphere might not be representative to the conditions during Cone Calorimeter tests. This could also be a cause as to why the generated material parameters are not transferable from the Cone Calorimeter simulations to the MCC simulations.

This leads to the conclusion that these processes and their interactions are not sufficiently well reproduced. It might be caused by incomplete modelling approaches, e.g. formation of bubbles or cracks, the crude geometrical representation of the cables, i.e. layered, or a combination thereof. This drawback is compensated by producing effective parameters, including the Arrhenius parameters.

Having said the above, it should be pointed out that the `HEAT_OF_COMBUSTION` parameter for the `MATL` was misunderstood, thus it ended up being part of the pool of optimised parameters, originally. The project had progressed too far when this was realised and due to the computational demand it was decided to not re-run all IMPs. Thus, the mass fluxes, leaving the solid and entering the gas phase, are not consistent. Yet, the energy release is consistent. Since the optimisation target has been the ERR, this misunderstanding has no direct consequences downstream, i.e. Cone Calorimeter and tray setup, as long as gained parameter values for the Arrhenius parameter and the `HEAT_OF_COMBUSTION` are used together. This may potentially be the reason why the individual values of the Arrhenius parameters alone are not representing the MCC results.

4.2 Gas Phase in Cone Calorimeter Simulations

Compared to previous work [31, 3], where the sample surface was resolved with only a single fluid cell, the resolution is increased here. The simplified Cone Calorimeter model has four fluid cells, two by two, to resolve the sample surface instead. This leads to smoother energy release profile, as well as a higher resolution of the flame. Even though the energy release rates seem to converge for higher resolutions, significant grid-dependence can be observed, specifically for the determined heat fluxes towards the sample. The heat flux profiles exhibit a more pronounced development, which follow the profile of the energy release. This is attributed to a higher resolution of the flame and thus the improved calculation of the radiative and convective heat fluxes. It highlights the need, to take the flame already into account during the IMP as an emergent phenomenon, as opposed to a static prescribed radiative flux. Further information on the grid sensitivity is available in appendix 7.2 and appendix 7.5.1.

4.3 Multiple Tray Setup

In general, the observed grid-dependence in the SCC simulations is not expected to have a significantly negative impact on this study. Mainly, because the cell size during the optimisation step is close to the cell size in the MT3 validation setup.

It is further interesting to note, that the highest heat fluxes in the tray simulation setups are occasionally about a factor of 2 higher than the imposed conditions in the Cone Calorimeter tests, see figure 21b. It is not quite clear if this is an "artefact" out of the simulation, or actually observable in real tests, since no data was available to compare this observation to. It also raises the question, if higher external fluxes in the Cone Calorimeter tests might be necessary to be added to the existing stack of tests. Future (cable) tests could look into this kind of behaviour.

4.4 Low Heat Flux Condition

This section discusses the impact of the low heat flux condition, i.e. about $25\,\mathrm{kW/m^2}$ and less, in the Cone Calorimeter and cable tray simulation setups. With the given FDS simulation setup, it is very difficult to reproduce the $25\,\mathrm{kW/m^2}$ Cone Calorimeter tests, see figure 6 for example. This is due to the ignition delay observed during the experiments. In IMP run T_a ($25\,\mathrm{kW/m^2}$ target), the fast increase in the energy release at ignition cannot be reproduced. It is smoothed, i.e. the energy release starts long before the ignition and the first peak is not present.

This primarily seems to be related to how FDS (here version 6.5.3) handles the gas phase combustion. For any given cell, combustion is allowed to occur even if the fuel concentration is very low. In reality however, the concentration of fuel gas might not be sufficient for combustion to ensue and just leave the sample surface. This difference leads to a non-zero energy release very early on in the simulation. Additionally, the radiative heat feedback is increased, which in turn leads to faster increase of sample temperatures and therefore quicker release of more combustible gas. As a result, a smoother transition from the pre- to the post-ignition phase is observed, in contrast to the rapid step-like increase observed in the experiments.

In this simulation campaign, the released species (`SPEC`) was only combustible gas, while it is likely, specifically for cables designed to be fire retardant, that inert gaseous species are released first. Thus, it may make it difficult for FDS to deal with the delay visible in the $25\,\mathrm{kW/m^2}$ test responses. The approach of Matala, publication 4 in [3], of providing a more detailed decomposition model, which may also release inert gaseous components, could be a solution.

Keeping this shortcoming in the modelling in mind, only the parameters of IMP T_a are able to reproduce the low flux case in the Cone Calorimeter simulation reasonably well. However, applying this parameter set to other, higher, flux

conditions in the Cone Calorimeter leads to a significant over-prediction of the energy release rate and fire development. Similar behaviour can be observed in the cable tray simulation setup, where the fire development is significantly more severe, with respect to a faster progression and a higher peak energy release rate that is about 4 times higher as in the experiment, see figure 7.

IMP runs with the remaining experiments as target show difficulties to reproduce the low flux condition. Even though, the parameters of the $50\,\mathrm{kW/m^2}$ are able to reproduce the $75\,\mathrm{kW/m^2}$ behaviour relatively well and vice versa. Under an incident flux of $25\,\mathrm{kW/m^2}$ the energy release starts notably earlier with a larger magnitude, as compared to the $25\,\mathrm{kW/m^2}$ IMP parameters and the experiment.

The importance of the $25\,\mathrm{kW/m^2}$ case is not completely clear. On one hand it seems that it does not matter too much, when the higher fluxes can be represented well, i.e. by using the higher fluxes as IMP targets. Even though, the energy release rate in the MT3 simulations is notably overestimated around the time of the burner cut-off. On the other hand, assuming a fire propagating along a horizontal fuel bed, every surface element in front of the flame needs to "pass through" a low flux regime to be ignited and differences here should influence the overall speed of the fire propagation. The latter part is demonstrated in figure 21b in appendix 7.5.2, where it can be seen that large areas of the cable tray experience low heat flux conditions over the whole course of the simulation.

One way to provide clarification, could be to investigate the actual heat flux levels to be expected in large scale configurations during fire experiments. For one to determine if the observed surface flux levels in FDS are sensible and also to determine if Cone Calorimeter experiments with higher fluxes are necessary in the optimisation process.

4.5 Geometrical Representation of Cables

The one-dimensional heat conduction model utilised in the presented simulations could influence the fire development. Specifically, when considering the absence/presence of the copper conductor. This conductor may serve as a heat sink near the fire seat and pre-heating the insulation material further away from the fire [21]. In the Cone Calorimeter simulation setups this might not be of too much importance, due to the small cable pieces and the relatively uniform heat up of the exposed surface. In that case, it may mainly behave as a heat sink and should be covered by the effective parameter set derived from the IMP. It should be more influential for the cable tray simulations. However, in the given setups it was not possible to resolve the necessary length scales. Investigations of this behaviour may become possible in the near future, due to the three-dimensional heat conduction model added to newer FDS versions, as well as new functionalities allowing for unstructured solids (i.e. `GEOM` name list group).

It has been pointed out, e.g. [19, 23], that cables are not necessarily put in a tray such that they form a continuous slab. Often, they are somewhat loosely packed or combined into bundles. These structures may however be in the sub-grid scale. Matala investigated if individual cables could be modelled in the sub-grid scale, by utilising cylindrical particles [23]. It would be interesting to see how the new unstructured solid method (`GEOM`) method is able to actually resolve the cable models geometrically.

4.6 Reference Calculations

As described earlier, the application of both reference methods, Cone Calorimeter paint and FLASH-CAT, did not yield satisfying results in the here investigated setup. In the following paragraphs possible reasons are discussed.

For the Cone Calorimeter paint approach not only the energy release rate data is needed, but also the thermal parameters ($k\rho c_p$), to determine an effective surface ignition temperature. These parameters were not available for the plastic material, thus density and heat capacity were guessed, based on material properties found on a web page for material properties. This may hamper the comparability between this work and [23], but should be representative for an approach a practitioning fire safety engineer might pursue. In the work presented here, the cables have been modelled as continuous slabs, instead of "poles", which may be one reason why Beji and Merci could obtain more convincing results in some of the *a posteriori* simulations in [23].

The predicted duration of the fire in the FLASH-CAT approach is based on the combustible mass per tray and a flame front propagation speed [15]. Ignition of the individual trays is controlled as a timed sequence, based on the experimental findings. In contrast to the observation in the experiments and also the simulations presented here (T_b), eventually all trays get involved and are consumed completely. This seems to be the main cause for the much longer duration (figure 8), as well as the larger magnitude of the total energy release (figures 9).

4.7 Robustness of the Model Parameter Sets

Cable 219 was deliberately chosen to be investigated, because it (a) showed the best reproducibility of the repeated Cone Calorimeter tests, (b) the cable was used in trays containing the same cable and (c) the individual cables were arranged in rows which made it easier to represent in the simulation.

Other cable tray tests in the campaign showed a more severe fire development, but contained a mixture of various cables per tray and between trays. Having gained confidence that the proposed procedure can generate useful material parameter sets, more cables are to be investigated in future work, e.g. cables 220 and 701.

These two show similar behaviour in the Cone Calorimeter. Furthermore, they were used in tray experiments with mixed cables, where individual trays were filled with a single cable type of 220 or 701, but no mixture of cables within a tray. Thus, it might be easier to reproduce, than cable mixtures within trays. It would also make MT8 and MT11 accessible, that showed a much severe fire development, with peak energy release rates of about 800 kW. In the long run, larger scale simulations need to be performed, like the corridors and the vertical shaft setups, from phase 2 of the experimental campaign [16].

With the investigation of further cables, the robustness of the method presented here can be evaluated. More robust material parameter sets allow investigation of the influence of parameters like distances, number of trays and burner energy release rates and times, cable tray arrangements in corridors can be investigated. This would also set goals for future cable testing campaigns, to validate the simulation results.

4.8 Design Proposals for Future Experiments

For further work on parameter optimisation, to simulate fire propagation, it is important to have access to data from bench-scale, as well as well documented large scale fire experiments. The former is needed during the optimisation, while the latter is necessary to validate the parameter set's performance, which is of specific importance. Simulations focusing on micro- and bench-scale alone, as well as neglecting the gas phase reactions seem not to be sufficient to replicate the large scale fire behaviour. To fill gaps within the existing body of experimental data, future test campaigns should start from the CHRISTIFIRE campaign design as a base line. It is suggested by the authors to focus on one single cable to perform all tests with. Tests in the open offer good cases for simulation software, while presenting a rather modest need for computing resources. However, real world installations are often found in confined spaces, close to walls and ceilings. It is therefore necessary to perform similar experiments as the corridor setup presented in phase 2 [16]. Experimental setups with smaller wall sections connected to the trays in the open, similar to FIPEC [19] or like the ones used by Zavaleta et al. [37], could serve as an intermediate step.

Information of peripheral conditions, like material data of surrounding materials, distances to walls (laboratory size/footprint), ventilation conditions, surface temperatures of burner, floor and other surfaces around the test should be recorded as well, to be able to create more comprehensive models.

5 Data Repositories

During the course of the IMP runs, and the following analysis of the results, an extensive amount of data was produced. Aiming to allow other researchers to gain a better insight into to whole work, we provide public access to most of the data. Thus, this paper is accompanied by publicly available online data repositories. A summary repository is hosted via Zenodo [25]. It contains only the data necessary to reproduce the figures shown here, like the `propti_db.csv` or `*_hrr.csv` files, but not the full simulation results. Also, all input files for FDS and PROPTI are provided, as well as the target data.

Furthermore, Jupyter notebooks are provided with the respective repositories. These notebooks are used to process the results from the IMP's and provide an overview by creating various plots. Some are used to guide investigations on the parameter sets, by allowing to create new FDS input files from within the notebooks, as well as presenting the new results within the same notebook afterwards.

From the summary repository at Zenodo, a link will lead to a more comprehensive repository, hosted by the Forschungszentrum Jülich. It contains the full FDS simulations that were created during analysing the IMP results, such that they can be loaded into SmokeView for further study.

6 Acknowledgements

The authors gratefully acknowledge the computing time granted (project jjsc27) by the JARA-HPC Vergabegremium and VSR commission on the supercomputer JURECA at Forschungszentrum Jülich [38, 39].

This work has been sponsored by the Wolfgang Gentner Programme of the German Federal Ministry of Education and Research (grant no. 05E15CHA), as part of the CERN Doctoral Student Programme.

The authors would like to thank Kevin McGrattan for fruitful discussions, suggestions and access to experimental data.

Furthermore, thanks goes to the members of FCC Fire Collaboration for discussions and suggestions, as well as CERN's Health, Safety and Environmental Protection unit (HSE), for providing access to computing resources.

Table 1: Overview of the optimisation parameters of the IMP runs for the insulator. Data from the experiment is provided, if available. Layer thickness has been projected from a circular to a rectangular cross section to account for the layered representation in FDS. From the best parameter sets, over all IMP runs, the minimum (IMP Min.) and maximum (IMP Max.) values are provided. The parameter sequence is the same as for the ribbon plots, simply skipping parameters that are not used. (Note: values labelled with "*" are guessed and/or FDS default.)

"Physical" Parameter	Experiment	IMP Min.	IMP Max.	Unit
Insulator Thickness	1.97e-03 *	3.46e-03	4.99e-03	m
Emissivity	unknown	3.24e-01	6.83e-01	-
Density	1.18e+03 *	1.02e+03	1.15e+03	kg/m^3
Conductivity	unknown	2.05e-01	2.30e-01	W/(m K)
Specific Heat	unknown	1.49e+00	1.72e+00	kJ/(kg K)
Heat of Combustion	3.26e+04	3.89e+04	4.15e+04	kJ/kg
Insulator Reaction A				
Pre-exponential factor	3.99e+01	3.62e+01	4.19e+01	1/s
Activation Energy	4.10e+04	4.24e+04	5.00e+04	kJ/kmol
Reaction Order	1.00e+00 *	5.02e-01	2.08e+00	-
Heat of Reaction	1.00e+03 *	2.54e+02	6.08e+02	kJ/kg
Insulator Reaction B				
Pre-exponential factor	4.50e+20	4.26e+20	5.26e+20	1/s
Activation Energy	3.15e+05	2.36e+05	2.60e+05	kJ/kmol
Reaction Order	1.00e+00 *	5.07e-01	3.65e+00	-
Heat of Reaction	1.00e+03 *	4.84e+02	7.62e+02	kJ/kg
Insulator Residue				
Density	unknown	4.46e+02	6.12e+02	kg/m^3
Conductivity	unknown	1.93e-01	2.00e-01	W/(m K)
Specific Heat	unknown	6.90e-02	8.60e-01	kJ/(kg K)
Emissivity	unknown	2.98e-01	6.50e-01	-

7 APPENDIX

7.1 Parameter Limits

An overview over the utilised parameters is provided in tables 1 and 2. These tables also contain experimental data provided, which is limited to the MCC results [15], apart from some guessed values for the reaction orders, heats of reaction, as well as layer thicknesses.

7.1.1 Ribbon Plots

In order to summarise the development of each parameter, over the course of the IMP, ribbon plots were created, see figure 11. As an example, the jacket layer thickness development of T_b was chosen to illustrate how the ribbon plots are produced. On the left side of figure 11, a scatter plot provides an overview of each individual parameter value for each repetition (x-axis), within its sampling range (y-axis). The points are plotted with a slight transparency, to indicate where most of them are accumulated. In the centre plot, a histogram is presented that contains the information over the sampling range. This is further compressed, by creating a heat map ribbon of the histogram, shown on the right hand side. Due to the binning necessary for the histogram, all parameter sampling ranges are immediately normalised. Thus, all parameter ribbon plots of a single IMP run can be stacked together horizontally. Furthermore, *y=0* then shows the lower limit of the respective sampling range, while *y=1* shows the upper limit, as can be seen in the subsequent plots in figure 12.

With the ribbon plots, the effective development of the parameters during the IMP can be observed. Within the given simulation setups and parameter ranges, some parameters are forced to the limits of the respective sampling ranges. As an example, the ribbon plot of IMP run T_b is shown in figure 12b.

7.1.2 Shifted Parameter Sampling Ranges

During the time where the primary IMP runs (T_*) were performed, the layer thickness and the density were independently varied. Later on this was changed, because both are related, thus one of them was set to a fixed value. Similarly,

Table 2: Overview of the optimisation parameters of the IMP runs for the jacket. Data from the experiment is provided, if available. Layer thickness has been projected from a circular to a rectangular cross section to account for the layered representation in FDS. From the best parameter sets, over all IMP runs, the minimum (IMP Min.) and maximum (IMP Max.) values are provided. The parameter sequence is the same as for the ribbon plots, simply skipping parameters that are not used. (Note: values labelled with "*" are guessed and/or FDS default.)

"Physical" Parameter	Experiment	IMP Min.	IMP Max.	Unit
Jacket Thickness	3.12e-03 *	3.80e-03	6.00e-03	m
Emissivity	unknown	3.35e-01	9.80e-01	-
Density	1.32e+03 *	8.55e+02	1.11e+03	kg/m^3
Conductivity	unknown	1.73e-01	2.06e-01	W/(m K)
Specific Heat	unknown	1.29e+00	1.71e+00	kJ/(kg K)
Heat of Combustion	2.53e+04	2.31e+04	2.74e+04	kJ/kg
Jacket Reaction A				
Pre-exponential factor	1.51e+03	1.62e+03	2.27e+03	1/s
Activation Energy	5.86e+04	5.50e+04	6.40e+04	kJ/kmol
Reaction Order	1.00e+00 *	5.16e-01	2.99e+00	-
Heat of Reaction	1.00e+03 *	2.52e+02	7.28e+02	kJ/kg
Jacket Reaction B				
Pre-exponential factor	4.92e+14	3.70e+14	4.79e+14	1/s
Activation Energy	2.28e+05	1.94e+05	2.64e+05	kJ/kmol
Reaction Order	1.00e+00 *	5.15e-01	2.20e+00	-
Heat of Reaction	1.00e+03 *	9.20e+02	1.71e+03	kJ/kg
Jacket Residue				
Density	unknown	4.81e+02	5.99e+02	kg/m^3
Conductivity	unknown	1.69e-01	2.29e-01	W/(m K)
Specific Heat	unknown	6.95e-01	1.03e+00	kJ/(kg K)
Emissivity	unknown	3.65e-01	9.89e-01	-

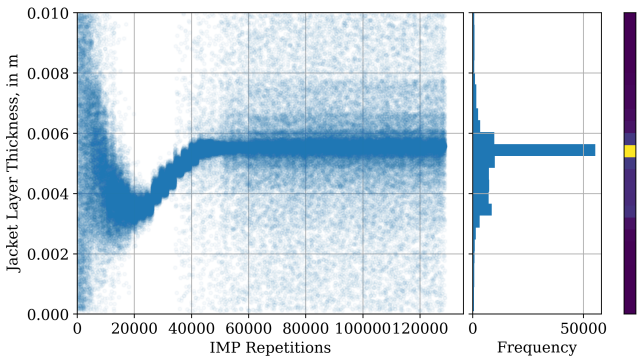

Figure 11: Demonstration of how parameter information is condensed. Left side shows the parameter development for the jacket layer thickness during T_b. The centre plot shows the frequency of the sampled parameters, distributed over 25 bins. The colour bar at the right side is a heat map ribbon of the histogram in the centre, with yellow being the highest frequency and blue the lowest.

the HEAT_OF_COMBUSTION was be removed because it is connected to the surrogate fuel concept. For the use case demonstrated in this paper the amount of released fuel is controlled via the Arrhenius model. Therefore, the released energy should correspond to this released fuel and not be scaled by a HEAT_OF_COMBUSTION value of a different material.

A more comprehensive assessment on the outcome of shifting the sampling limits is based on IMP $T_{a,b,c}P_A$. The decision, to use IMP runs with fixed Arrhenius parameters for this assessment, was simply made to reduce the computational demand. It is still sufficient to demonstrate the fitness improvement by shifting the sampling limits, see figure 5.

Figure 13 provides four ribbon plots that demonstrate how the parameter development changes for the adjusted parameter limits. On the left side, figure 13a, the original IMP run with the fixed Arrhenius parameters is shown. To its right are three successively adjusted runs ($T_{a,b,c}P_AL_1$ to $T_{a,b,c}P_AL_3$). It can be seen that for the given sampling ranges some improvement could be achieved, see also figure 5. However three parameters, stuck at the upper limit, were not sufficiently influenced.

The best parameter sets per generation with the adjusted limits are also tested in the SCC setup. The overall behaviour is quite similar to primary IMP runs, T_b and $T_{a,b,c}P_{A,L1,HC}$. The T_b derivatives (T_b*) fit the $50\,\mathrm{kW/m^2}$ quite well, as it is the target, while diverge in similar fashion for the other tests. Responses for the fixed Arrhenius derivatives show similar behaviour as IMP $T_{a,b,c}P_{A,L1,HC}$. Comparisons of the simulation responses with the Cone Calorimeter test data is provided in figure 14.

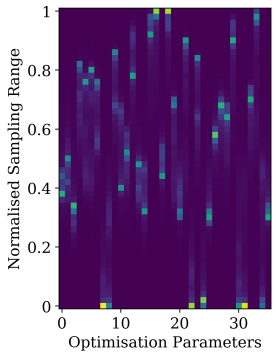

(a) IMP: T_a.

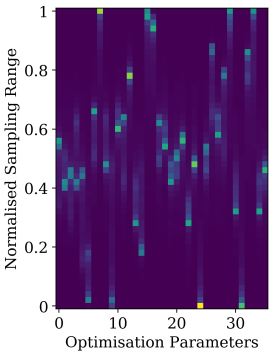

(b) IMP: T_b.

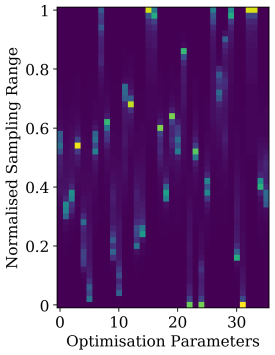

(c) IMP: T_c.

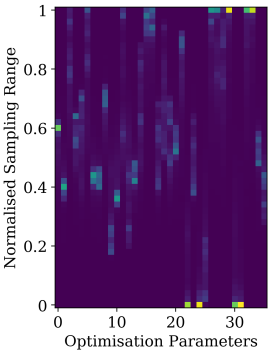

(d) IMP: $T_{a,b,c}$.

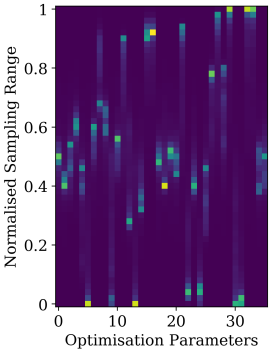

(e) IMP: $T_{b,c}$.

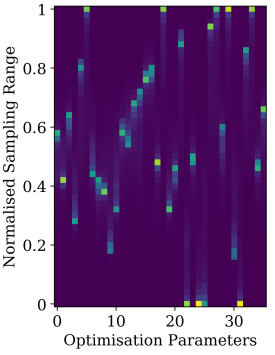

(f) IMP: $T_{a,c}$.

Figure 12: Frequency distribution of the optimisation parameters of the different IMP runs (T_*). The normalised sampling range is distributed over 51 bins.

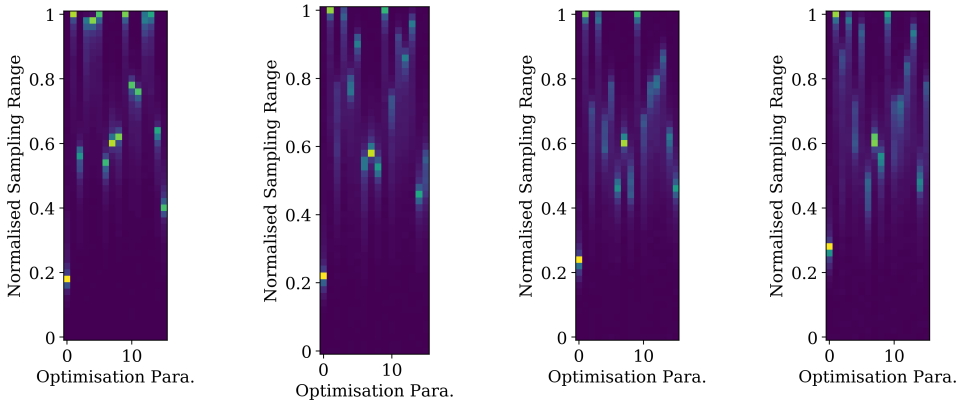

(a) $T_{a,b,c}P_{A,L1,HC}$ (b) $T_{a,b,c}P_{A,L1,HC}L_1$ (c) $T_{a,b,c}P_{A,L1,HC}L_2$ (d) $T_{a,b,c}P_{A,L1,HC}L_3$

Figure 13: Comparison of the parameter distributions for adjusted parameter limits, with fixed Arrhenius parameters. Sampling ranges have individually been shifted upwards for the stuck parameters, in an effort to improve the overall fitness. Original sampling limits are shown in the left most plot, with successive shifts shown to the right.

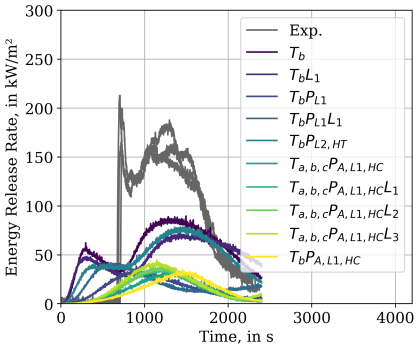

(a) Incident heat flux of $25\,\mathrm{kW/m^2}$.

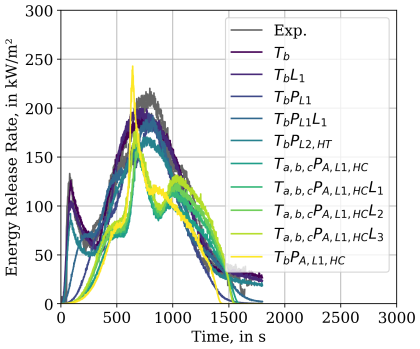

(b) Incident heat flux of $50\,\mathrm{kW/m^2}$.

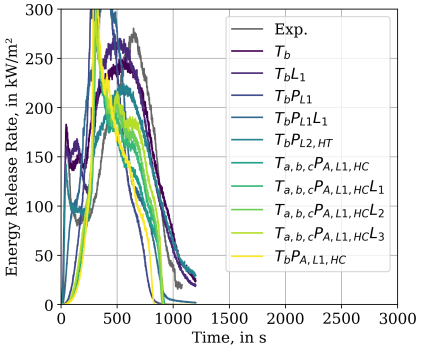

(c) Incident heat flux of $75\,\mathrm{kW/m^2}$.

Figure 14: Energy release rates of the best parameter set for IMPs with adjusted parameter limits (SCC).

7.2 Grid Sensitivity

7.2.1 Cone Calorimeter

To investigate the behaviour of the parameter sets for different cell resolutions, the best parameter set of T_b was chosen. The simplified Cone Calorimeter simulation setup SCC was used as base mesh. Its cell resolution was reduced by a factor of 0.5, thus the sample surface was covered by a single cell. To achieve higher resolutions, the cell size of the base mesh was divided by factors 2 to 5. The results are presented in figure 18 and compared to the experimental data (dashed line). It can be seen that the parameter set does not provide a resolution-independent solution for the energy release rate. For the higher external fluxes it seems to be achievable for a factor of two and higher resolutions. In the $25\,\mathrm{kW/m^2}$ setup the convergence is slower. It can also be noted, that a resolution reduction leads to a much more noisy response.

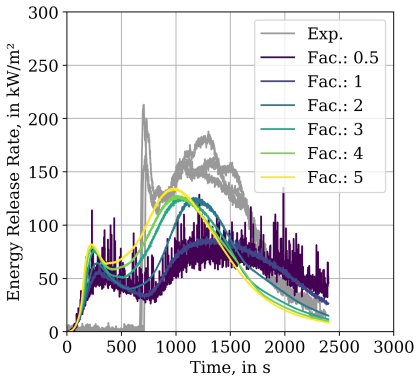

(a) Incident heat flux of $25\,\mathrm{kW/m^2}$.

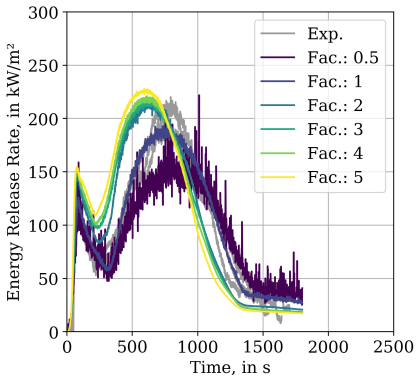

(b) Incident heat flux of $50\,\mathrm{kW/m^2}$.

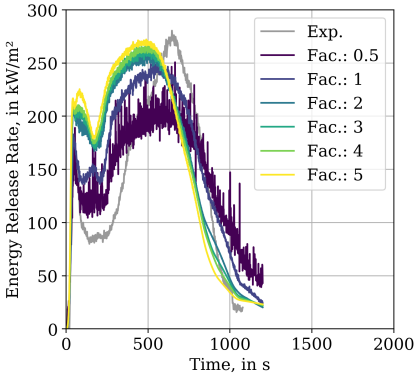

(c) Incident heat flux of $75\,\mathrm{kW/m^2}$.

Figure 15: Comparison between energy release rates of Cone Calorimeter data, from simulation and experiment (Exp.). Fluid cell sizes were changed by the noted factor, w.r.t SCC ($47\,\mathrm{mm}$). The used material parameter set is taken from IMP T_b.

Comparison between energy release rates of Cone Calorimeter data, from simulation and experiment (Exp.). Fluid cell sizes were changed by the noted factor, w.r.t SCC ($47\,\mathrm{mm}$). The used material parameter set is taken from IMP T_b

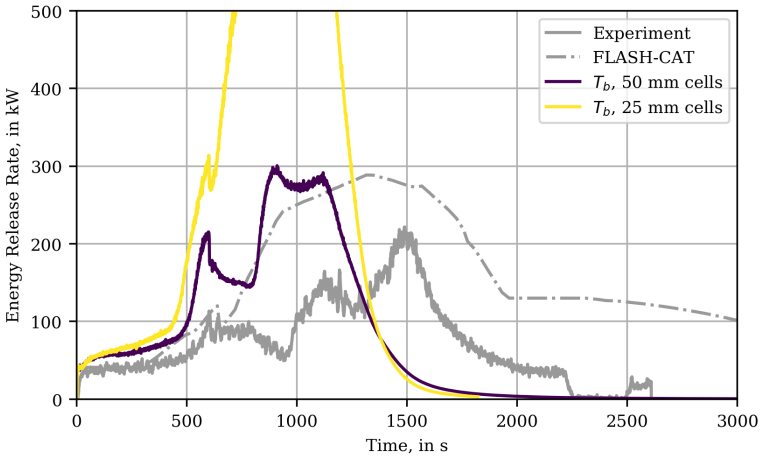

Figure 16: MT3 simulation results for the best parameter set of IMP run T_b for with cell sizes of $50\,\mathrm{mm}$ (original setup) and $25\,\mathrm{mm}$. The peak of the simulation with $25\,\mathrm{mm}$ cells is located at about $(958.0\,\mathrm{s}, 975.3\,\mathrm{kW})$.

7.2.2 MT3

The best parameter set for IMP run T_b was also utilised in a MT3 simulation setup with $25\,\mathrm{mm}$ cells. The results further highlight the strong grid-dependence of the parameter sets, see figure 16. Note that the fire developed so strongly that the flame was cut at the upper boundary of the `MESH` and thus the energy release rate is likely higher than the observed maximum value of $(958.0\,\mathrm{s}, 975.3\,\mathrm{kW})$. In the higher resolution case $25\,\mathrm{mm}$, the fire also propagated over nearly the whole tray length, in contrast to the lower resolution. The fire in the lower trays decayed earlier than the fire on the top tray. This lead to the extinguishing of the fire in the top tray before reaching the end.

7.3 Best Parameter Set per Generation Development

To provide an impression on how the simulation response for the parameter sets change during their development, three plots are provided. They contain the best parameter sets per generation of IMP run T_b, applied in the three simulation setups of the stack: MCC in figure 17a, simple Cone Calorimeter in figure 17b and MT3 in figure 17c. For all three plots, in dark blue the results of the first generation are drawn, while the most recent generation is drawn in yellow. For MCC and SCC, the first ten or so generations show some variation and converge afterwards.

Interestingly, despite using the same sequence of parameter sets, the MT3 simulations show much more variation during the parameter evolution, as compared to the SCC simulations.

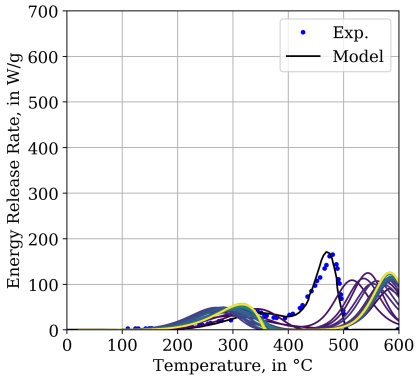

(a) MCC simulation response of the jacket material.

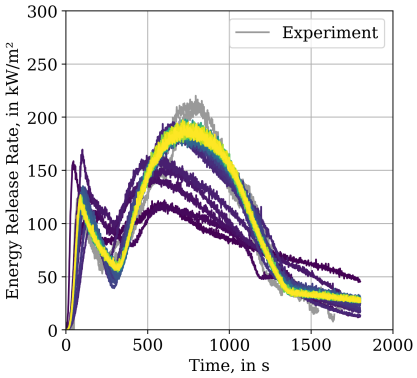

(b) Cone Calorimeter simulation results.

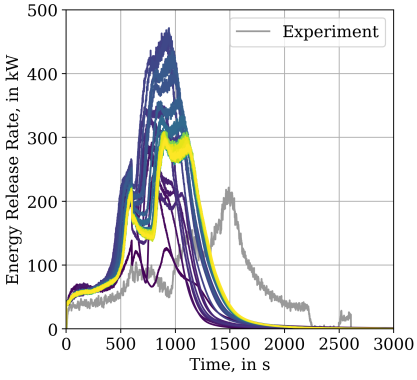

(c) MT3 simulation results.

Figure 17: Development of the response from the best parameter set per generation, for IMP T_b (50 kW/m2), compared to experimental data [15] (Exp.). Dark blue represents generation 0, yellow represents generation 47.

7.4 Cone Calorimeter Paint Methods

Since no ignition times were reported with the Cone Calorimeter tests, they are estimated from the energy release rate data. For each experiment, one ignition time is taken at the beginning of the peak and one roughly in the centre. These times are taken visually from the respective plots. As example see figure 18a of a repetition of the $50\,\mathrm{kW/m^2}$ tests. The blue dot marks the minimum ignition time, while the red dot marks the centre. Furthermore, thermal conductivity ($0.1165\,\mathrm{W/(m\,K)}$) and density ($1175\,\mathrm{kg/m^3}$) for chlorosulfonated polyethene, the jacket material, were unknown and taken from a web page providing material data for designers and engineers [40]. To steer the combustible gas release in FDS, a control function (`RAMP`) is created from the first repetition of the $50\,\mathrm{kW/m^2}$ data series. The beginning of the data, until reaching the estimated ignition time, is neglected in this control function, with respect to the minimum ignition time. Note: The $25\,\mathrm{kW/m^2}$ showed a smoother increase, thus the chosen ignition times are debatable.

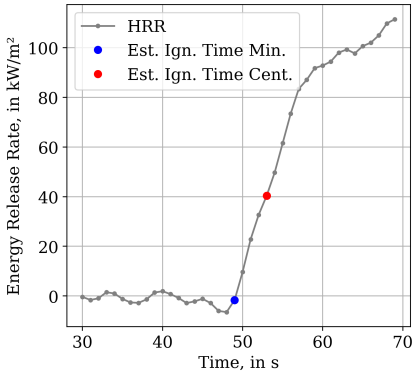

(a) Illustration of how the ignition times were estimated, based on a repetition of 50 kW/m2 Cone Calorimeter test. The blue dot indicates the minimum ignition time, while the centre is marked in red.

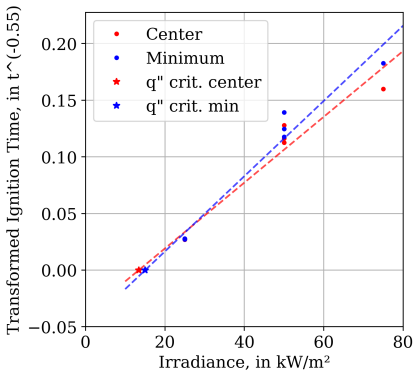

(b) Estimation of the critical heat fluxes, based on the “minimum" and “centre ignition times". Note: At 25 kW/m2 six data points are overlapping, three red, three blue.

Figure 18: Illustration of the procedure to estimate ignition times in the Cone Calorimeter experiments.

For all seven data sets of the experiments, both ignition times, minimum and centre, are determined and are provided in figure 18b. Each group, red and blue, is used to determine the critical heat flux for Janssens' procedure, by finding the intersection point of a linear fit, through the respective group, with the x-axis. The critical fluxes are marked by a star.

In the paper [23] three data points were utilised, one for a higher, and two for a lower radiative flux. This lead to two different linear fits drawn into a plot, of which the x-axis intersections were determined. It is not quite clear if, for more available data points for the lower flux, an average value would be desirable or if the lowest and highest values are to be taken into account regardless. It was decided to mimic the previously described procedure. For the irradiance levels of $25\,\mathrm{kW/m^2}$ and $50\,\mathrm{kW/m^2}$, three data points are available. From each of these clusters the highest and lowest transformed time are taken. From the $75\,\mathrm{kW/m^2}$ data point multiple lines are drawn one through each of the highest/lowest points described before. Due to two guessed ignition times from the experimental data, this process is performed for each group resulting in eight linear fits. Some of the lines produce intersection points on the negative side of the x-axis, leading to negative critical heat fluxes. The negative values are ignored and from the remaining positive values the lowest and highest are chosen, mixing both guessed ignition time groups together. Based on these remaining critical fluxes, thermal inertia parameters are determined following the two methods discussed by Beji and Merci [23]. Thus, four data sets are obtained and MT3 simulations performed.

For the "Beji-Merci procedure", the two methods discussed in their paper [23] followed the basic methodology of Jansssens's procedure. A linear fit is created, taking two data points at different irradiance levels into account. The intersection with the x-axis is used here as critical heat flux as well. Four critical heat fluxes have been determined, one for each estimated ignition temperature and one for heat fluxes. Thus, four data sets are obtained and MT3 simulations performed.

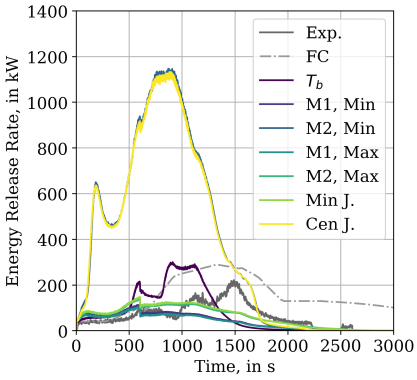

Figure 19: MT3 simulation results for different Cone Calorimeter paint methods. Labels "M1" and "M2" refer to different methods of the Beji-Merci procedure [23], "J." refers to the Janssens' procedure [35].

Better values for Janssens' procedure could be produced when using the minimum heat flux where ignition occurs (q_{min}), instead of the critical heat flux (q_{crit}), as highlighted in the description of said procedure in the Ignition Handbook [35]. However, information about q_{min} was not available in the report [15] and thus only q_{crit} was utilised. A possible approach may be to calculate the mean point between q_{crit} and the lowest irradiance level used in the tests, however this was not attempted here. For more details on the overall procedure, see `ReportConeCalorimeterPaint.ipynb` in [25].

7.5 Heat Flux Assessment

7.5.1 Cone Calorimeter Radiative Flux Assessment

The fluid mesh resolution study is also used to assess the `INCIDENT_HEAT_FLUX` to the sample surface. The results are presented in figure 20. A device is employed that integrates the heat flux over the sample surface (`DEVC` with `STATISTICS='SURFACE INTEGRAL'`). The data is smoothed before plotting, by employing a Savitzky-Golay algorithm. A 2nd order polynomial is utilised, with a window length of about 10 % of the data points, per data series. Each of the three sub-plots contains a dashed horizontal line to indicate the external flux level that represents the test condition. These values were also defined by the `EXTERNAL_FLUX` parameter in the surface lines (`SURF`) during the IMP runs. It can be seen, as a general observation, that the heat flux at the sample surface in the simulation is always larger than the prescribed external flux value. The heat feedback decreases with lower and increases with higher cell resolution. For the base SCC simulation setup (factor 1), the radiative heat flux from the flame is about $3\,\mathrm{kW/m^2}$ higher in the $25\,\mathrm{kW/m^2}$ case to up to $10\,\mathrm{kW/m^2}$ for the $75\,\mathrm{kW/m^2}$ case. For resolutions higher than the base SCC setup, the incident heat flux is significantly higher than the prescribed external flux.

It is interesting to note, that the two peak structure, is mostly not reproduced in the `INCIDENT_HEAT_FLUX` plots for a factor of 0.5. It seems also to smooth out for higher fluxes, see figure 20c.

7.5.2 Multiple Tray Simulation Radiative Flux Assessment

Within the MT simulations, the distribution of the radiative heat flux on the tray surface was tracked, per time step and surface cell. The tracked value in FDS was, among others, the `INCIDENT_HEAT_FLUX`. As an example the `INCIDENT_HEAT_FLUX` distribution for T_b is shown in figure 21a. Shown are the unfolded surfaces of the three obstructions representing the respective trays. The larger areas of the three groups are the top and bottom faces, with the lower one being at the bottom. Blue colours show a `INCIDENT_HEAT_FLUX` of $0\,\mathrm{kW/m^2}$ up to $160\,\mathrm{kW/m^2}$ in yellow.

To assess the general development of the `INCIDENT_HEAT_FLUX` over the whole simulation time and tray surface, a histogram heat map is provided for the best parameter set of T_b see figure 21b. For each individual time step, a histogram was created for the heat fluxes between $0\,\mathrm{kW/m^2}$ to $160\,\mathrm{kW/m^2}$. Three dashed lines show the external heat fluxes that were used during the Cone Calorimeter tests. The heat map colour encodes the surface area receiving a

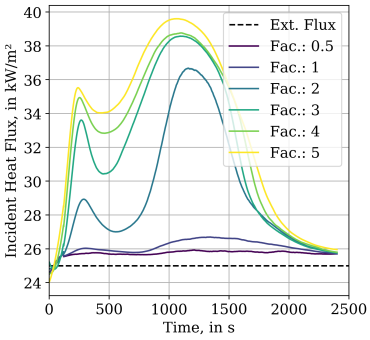

(a) Experimental condition: $25\,\mathrm{kW/m^2}$.

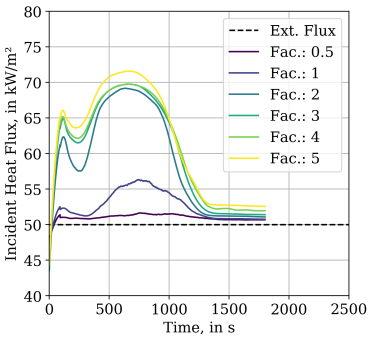

(b) Experimental condition: $50\,\mathrm{kW/m^2}$.

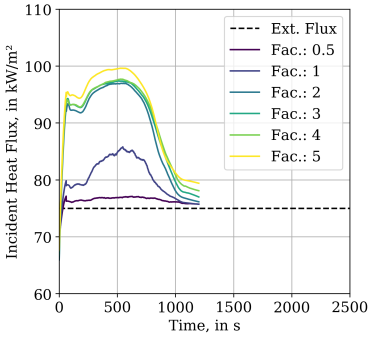

(c) Experimental condition: $75\,\mathrm{kW/m^2}$.

Figure 20: Different `INCIDENT_HEAT_FLUX` responses for material parameter set of T_b in Cone Calorimeter simulations with different cell sizes. Cell sizes based on SCC ($47\,\mathrm{mm}$) and are changed by dividing through the noted factor. Noise reduction by Savitzky-Golay, 2nd order polynomial, window length about 10 % of the amount of data points.

certain radiative flux. During the whole simulation most of the area of the trays only receives low levels of heat radiation, up to about $15\,\mathrm{kW/m^2}$. At about $400\,\mathrm{s}$, the area increases that receives higher radiative fluxes, which coincides with a growing fire and its propagation from the bottom of the lowest tray into the space between the lowest and the middle tray, where the bottom of the tray in the middle gets involved. At around $700\,\mathrm{s}$ some decay, initialised by the burner cut-off $100\,\mathrm{s}$ before, is superimposed by the propagation of the fire into the space between the middle tray and the tray at the top, thereafter reaching the top of the top tray. At about $1000\,\mathrm{s}$ the fire starts to extinguish.

The `INCIDENT_HEAT_FLUX` values are demonstrated to reach much higher flux values, as experimental data was available during the IMP, within the simulation. During the full MT3 simulation, individual cells reached significantly higher flux levels as observed in the Cone Calorimeter simulations. They are nearly twice as high, for the resolution of the IMP simulations under the most severe external flux of $75\,\mathrm{kW/m^2}$, see figure 20. For Cone Calorimeter simulations with higher resolutions the peak heat flux of about $100\,\mathrm{kW/m^2}$ gets closer to maximum in the tray but is still about $40\,\mathrm{kW/m^2}$ short. For now it is not quite clear, if the high flux levels in the trays are an artefact from the simulation or realistic, since no experimental data was available to check it against. The relatively high flux levels in the higher resolutions for the Cone calorimeter seem to point towards higher fluxes are to be expected. They might simply not be able to be reproduced correctly with the low resolution during the optimisation.

Furthermore, as expected, it can be observed that the amount of cells with lower flux levels is relatively large. To visually distinguish areas with trivial heat flux, i.e. zero, the data points are omitted.

An animation of the very similar `GAUGE_HEAT_FLUX` development, as a side-by-side comparison between figures 21b and 21a, can be found in the `Videos/MT3_GaugeHeatFlux` directory within the data repository [25].

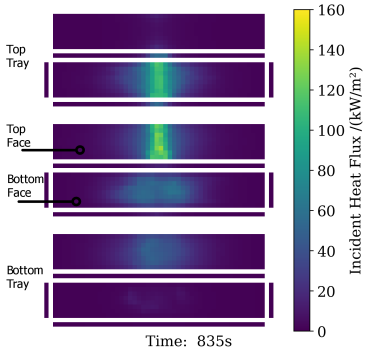

(a) Unfolded tray surface for a single time step, see also figure 2a.

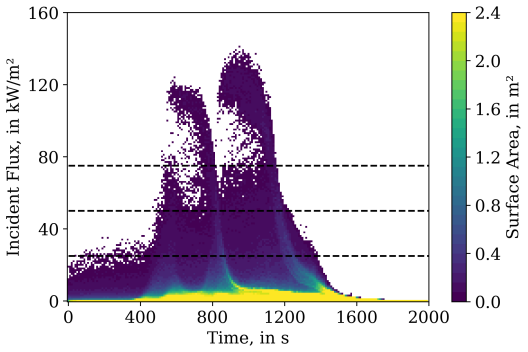

(b) Histogram heat map over the whole tray surface, per time step. External flux for Cone Calorimeter experiments shown as dashed lines. Cells of zero heat flux are omitted (white).

Figure 21: Simulation results showing the development of the `INCIDENT_HEAT_FLUX` on the cable tray surface for the best material parameter set of IMP T_b.

7.6 Computer and Software Versions

A brief assessment of the transfer-ability of the generated parameter sets to different FDS versions, and operating systems, was conducted. Compared are here the FDS versions 6.5.3 [33] and 6.7.0.

Simulations necessary during the IMP were performed on the supercomputer JURECA at the Forschungszentrum Jülich (FZJ) in Germany [38], which utilises an Linux-based operating system. A self-compiled FDS 6.5.3, revision FDS6.5.3-0-gbac6600, was utilised for the IMP, as well as simulations of the best parameter sets per generation after the completion of the respective IMP. This comprised different simulation setups, the MCC, simplified Cone Calorimeter and MT. Thus, consistency between the different setups was ensured. Also on JURECA, FDS 6.7.0, with the revision `FDS6.7.0-0-g5ccea76-HEAD`, was used for comparison with FDS 6.5.3. Both FDS versions are self-compiled against the software libraries available on JURECA. A pre-compiled version of FDS 6.5.3, revision `FDS6.5.3-598-geb56ed1` as provided by NIST via the respective web page, was used on a desktop workstation with a Windows 10 operating system. The FDS input files were the same for all cases, Cone Calorimeter setup and MT3 setup.

The best parameter set of T_b was used as an example for the transferability assessment. Thus, in the subsequent plots FDS 6.5.3 on JURECA is marked with T_b. FDS 6.7.0 on JURECA is marked with JU and FDS 6.5.3 on the workstation is marked with WS.

Results of the MCC simulations across the different FDS versions and operating systems show no difference, see figure 22. For the Cone Calorimeter simulations it can be seen that the peak energy release rates are slightly higher with FDS 6.7.0 (JU) than for both FDS 6.5.3 versions (WS, T_b), see figure 23. The same procedure was followed with the MT3 simulation setup, see figure 24. In this plot, differences are visible between all FDS versions. Both FDS versions on JURECA show a relatively similar behaviour, with FDS 6.5.3 showing a bit higher peak energy release rate, while the version of the workstation over-predicts the peak energy release by a factor of nearly 2.

This adds a further aspect of dependencies for the model, and highlights that parameter set performance is also sensitive to computer architecture, software versions and operating systems.

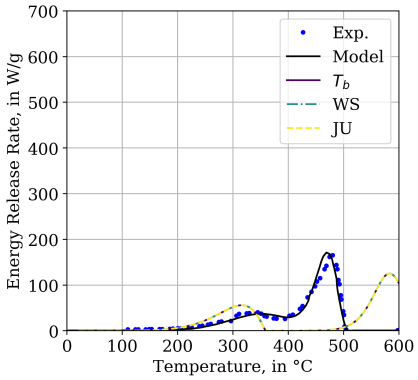

(a) MCC simulation response of the jacket material.

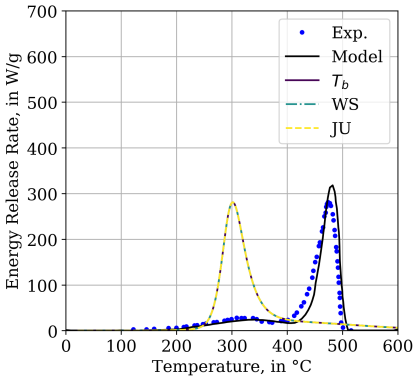

(b) MCC simulation response of the insulator material.

Figure 22: Comparison between energy release rates of MCC simulation of the best parameter set of IMP T_b (`TGA_ANALYSIS=.TRUE.`). T_b: JURECA, Linux, FDS 6.5.3; WS: Workstation, Windows 10, FDS 6.5.3; JU: JURECA, Linux, FDS 6.7.0.

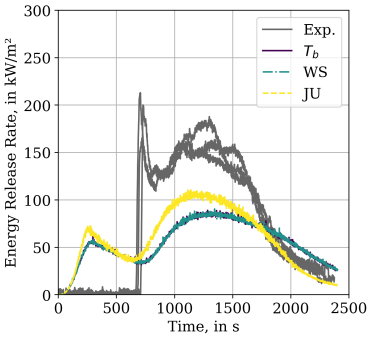

(a) Experimental condition: $25\,\mathrm{kW/m^2}$.

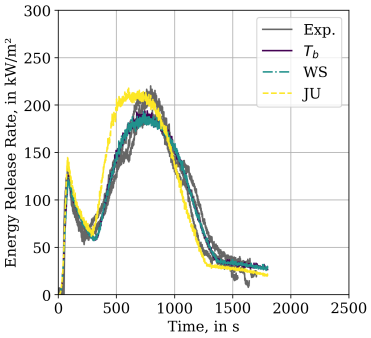

(b) Experimental condition: $50\,\mathrm{kW/m^2}$.

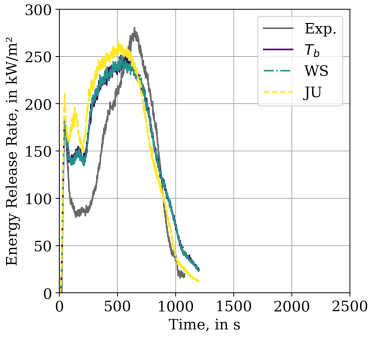

(c) Experimental condition: $75\,\mathrm{kW/m^2}$.

Figure 23: Comparison between energy release rates of Cone Calorimeter simulation of the best parameter set of IMP T_b. T_b: JURECA, Linux, FDS 6.5.3; WS: Workstation, Windows 10, FDS 6.5.3; JU: JURECA, Linux, FDS 6.7.0.

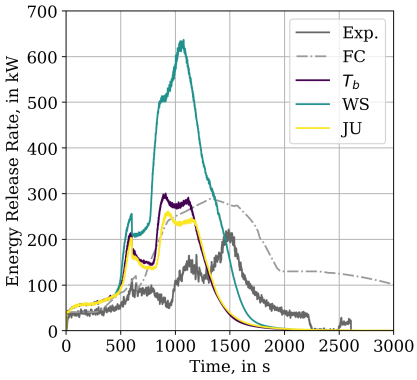

Figure 24: Comparison between energy release rates of MT3 simulation of the best parameter set of IMP T_b. T_b: JURECA, Linux, FDS 6.5.3; WS: Workstation, Windows 10, FDS 6.5.3; JU: JURECA, Linux, FDS 6.7.0.

References

[1] Jukka Hietaniemi, Simo Hostikka, and Jukka Vaari. Fds simulation of fire spread – comparison of model results with experimental data. Technical report, VTT Building and Transport, 6 2004. URL https://www.vtt.fi/inf/pdf/workingpapers/2004/W4.pdf.

[2] Xiaoyun Wang. *Fire Dynamics Simulator (FDS) Pyrolysis Model Analysis of Heavy Goods Vehicle Fires in Road Tunnels*. PhD thesis, University of Canterbury, Private Bag 4800, Christchurch, New Zealand, 2017.

[3] Anna Matala. *Methods and applications of pyrolysis modelling for polymeric materials*. PhD thesis, 2013. URL http://urn.fi/URN:ISBN:978-951-38-8102-3.

[4] Fengchang Yang, Christian Rippe, Jonathan Hodges, and Brian Lattimer. Methodology for material property determination. *Fire and Materials*, 05 2019. doi:10.1002/fam.2721.

[5] Johan Mangs and Simo Hostikka. Experiments and numerical simulations of vertical flame spread on charring materials at different ambient temperatures. *Fire Safety Science*, 10:499–512, 01 2011.

[6] Boon Hui. Chiam. Numerical simulation of a metro train fire. Master's thesis, Department of Civil Engineering, University of Canterbury, 2005.

[7] Thomas Rogaume. Thermal decomposition and pyrolysis of solid fuels: Objectives, challenges and modelling. *Fire Safety Journal*, 106:177 – 188, 05 2019. doi:10.1016/j.firesaf.2019.04.016.

[8] Qingyun Duan, Vijai K. Gupta, and Soroosh Sorooshian. Shuffled complex evolution approach for effective and efficient global minimization. *Journal of optimization theory and applications*, 76(3):501–521, 1993.

[9] Chris Lautenberger. Gpyro3d: A three dimensional generalized pyrolysis model. In *Fire Safety Science-Proceedings of the Eleventh International Symposium*, pages 193–207. International Association for Fire Safety Science, 2014.

[10] Chris Lautenberger, Guillermo Rein, and Carlos Fernandez-Pello. The application of a genetic algorithm to estimate material properties for fire modeling from bench-scale fire test data. *Fire Safety Journal*, 41(3):204 – 214, 2006. ISSN 0379-7112. doi:https://doi.org/10.1016/j.firesaf.2005.12.004. URL http://www.sciencedirect.com/science/article/pii/S0379711205001372.

[11] Simo Hostikka and Anna Matala. Pyrolysis model for predicting the heat release rate of birch wood. *Combustion Science and Technology*, 189(8):1373–1393, 8 2017. ISSN 0010-2202. doi:10.1080/00102202.2017.1295959.

[12] Anna Matala, Simo Hostikka, and J Mangs. Estimation of pyrolysis model parameters for solid materials using thermogravimetric data. *Fire Safety Science*, 9:1213–1223, 01 2009. doi:10.3801/IAFSS.FSS.9-1213.

[13] Patrick Lauer, Corinna Trettin, Friedrich-Wilhelm Wittbecker, and Lukas Arnold. Performance of optimization algorithms for deriving material data from bench scale tests. *Fire and Evacuation Modelling Technical Conference 2016*, 2016.

[14] Mark McKinnon, Stanislav I. Stoliarov, and Artur Witkowski. Development of a pyrolysis model for corrugated cardboard. *Combustion and Flame*, 160:2595–2607, 11 2013. doi:10.1016/j.combustflame.2013.06.001.

[15] Kevin B. McGrattan, Andrew J. Lock, Nathan D. Marsh, and Marc R. Nyden. Cable heat release, ignition, and spread in tray installations during fire (christifire): Phase 1 - horizontal trays. Contractor report, nureg/cr-7010, Office of Nuclear Regulatory Research, 7 2012.

[16] Kevin B. McGrattan and Scott D. Bareham. Cable heat release, ignition, and spread in tray installations during fire (christifire) phase 2: Vertical shafts and corridors. Contractor report, nureg/cr-7010, vol. 2, Office of Nuclear Regulatory Research, 9 2013.

[17] Laurence Rigollet. Investigating heat and smoke propagation mechanisms in multi-compartment fire scenarios – final report of the prisme project. Final report, nea/csni/r(2017)14, OECD Nuclear Energy Agency (NEA), 1 2018. URL https://www.oecd-nea.org/nsd/docs/2017/csni-r2017-14.pdf.

[18] Marina Röwekamp, Jason Dreisbach, Walter Klein-Heßling, Kevin McGrattan, Stewart Miles, Martin Plys, and Olaf Riese. International collaborative fire modeling project (icfmp). Summary of benchmark exercises 1 - 5, grs - 227, Gesellschaft für Anlagen- und Reaktorsicherheit (GRS) mbH, 9 2008. URL https://www.grs.de/sites/default/files/pdf/grs-227.pdf.

[19] Stephen J. Grayson, Patrick Van Hees, Uberto Vercellotti, Hervé Breulet, and Andrew Green. *Fire Performance of Electrical Cables – FIPEC Final Report on the European Commisision SMT Programme SMT4-CT96-2059*. Interscience Communications Limited, 2000. ISBN 0 9532312 5 9. URL https://www.sp.se/en/index/research/eu-project/projectcompleted/fipec/sidor/default.aspx.

[20] Marina Roewekamp, Walter Klein-Hessling, Olaf Riese, and Heinz Berg. Flame spread in cable tray fires and its modeling in fire simulation codes. *Journal of Konbin*, 6:41–56, 01 2008. doi:10.2478/v10040-008-0057-z.

[21] Patrick Van Hees, J Axelsson, A M. Green, and S J. Grayson. Mathematical modelling of fire development in cable installations. *Fire and Materials*, 25:169 – 178, 07 2001. doi:10.1002/fam.767.

[22] Sophie Bascou, Pascal Zavaleta, and Fabrice Babik. Cable tray fire tests simulations in open atmosphere and in confined and mechanically ventilated compartments with the calif3s/isis cfd software. *Fire and Materials*, 43(5): 448–465, 10 2018. doi:10.1002/fam.2680.

[23] Tarek Beji and Bart Merci. Numerical simulations of a full-scale cable tray fire using small-scale test data. *Fire and Materials*, 12 2018. doi:10.1002/fam.2687.

[24] Chris Lautenberger and AC Fernandez-Pello. Optimization algorithms for material pyrolysis property estimation. *Fire Safety Science*, 10:751–764, 2011.

[25] Tristan Hehnen, Lukas Arnold, and Saverio La Mendola. Numerical fire spread simulation based on material pyrolysis - an application to the christifire phase 1 horizontal cable tray tests - data set, 10 2019. URL https://zenodo.org/record/3407091.

[26] Richard Lyon and Richard N Walters. Pyrolysis combustion flow calorimetry. *Journal of Analytical and Applied Pyrolysis*, 71:27–46, 03 2004.

[27] Tobias Houska, Philipp Kraft, Alejandro Chamorro-Chavez, and Lutz Breuer. Spotting model parameters using a ready-made python package. *PLoS ONE*, 10:e0145180, 12 2015. URL doi:10.1371/journal.pone.0145180.

[28] Lukas Arnold, Tristan Hehnen, Patrick Lauer, Corinna Trettin, and Ashish Vinayak. Application cases of inverse modelling with the propti framework. *Fire Safety Journal*, page 102835, 2019. ISSN 0379-7112. doi:https://doi.org/10.1016/j.firesaf.2019.102835. URL http://www.sciencedirect.com/science/article/pii/S0379711219300438.

[29] Lukas Arnold, Tristan Hehnen, Patrick Lauer, Corinna Trettin, and Ashish Vinayak. Propti, 3 2018. URL https://zenodo.org/record/1438349.

[30] Lukas Arnold, Tristan Hehnen, Patrick Lauer, Corinna Trettin, and Ashish Vinayak. Propti – a generalised inverse modelling framework. In *Proceedings from the third European symposium on fire safety sciences ESFSS 2018*, 9 2018.

[31] Tristan Hehnen, Lukas Arnold, Patrick Van Hees, and Saverio La Mendola. Simulation of fire propagation in cable tray installations for particle accelerator facility tunnels. In *Proceedings from the 8th International Symposium on Tunnel Safety and Security ISTSS 2018*, Borås, Sweden, 3 2018. RISE Research Institutes of Sweden.

[32] Anna Matala and Simo Hostikka. Pyrolysis modelling of pvc cable materials. In *Fire Safey Science – Proceedings of the Tenth International Symposium*. doi:10.3801/IAFSS.FSS.10-917.

[33] Kevin McGrattan, Simo Hostikka, Randall McDermott, Jason Floyd, Craig Weinschenk, and Kristopher Overholt. *Fire Dynamics Simulator User's Guide*, 11 2017.

[34] Morgan J. Hurley, Daniel T. Gottuk, John R. Hall Jr., Kazunori Harada, Erica D Kuligowski, Milosh Puchovsky, Jose´ L. Torero, John M. Watts Jr., and Christopher J. Wieczorek. *SFPE Handbook of Fire Protection Engineering, fifth edition*. Springer-Verlag New York, 11 2016. ISBN 978-1-4939-2564-3. doi:10.1007/978-1-4939-2565-0.

[35] Vytenis Babrauskas. *Ignition Handbook*. Fire Science Publishers, Issaquah WA, USA. Co-published by the Society of Fire Protection Engineers, 2003. ISBN 978-0-9728111-3-2.

[36] Takashi Kashiwaci and Thomas J. Ohlemiller. A study of oxygen effects on nonflaming transient gasification of pmma and pe during thermal irradiation. pages 815–823. Proceedings: Nineteenth Symposium (International) on Combustion/The Combustion Institute, 1982.

[37] Pascal Zavaleta, Stéphane Charbaut, Guillaume Basso, and Laurent Audouin. Multiple horizontal cable tray fire in open atmosphere. In *Proceedings of the Fire and Materials 2013 Conference*, pages 57–68, 01 2013.

[38] Jülich Supercomputing Centre. Jureca: General-purpose supercomputer at jülich supercomputing centre. *Journal of large-scale research facilities*, 2, 2016. URL http://dx.doi.org/10.17815/jlsrf-2-121.

[39] Dorian Krause and Philipp Thörnig. JURECA: Modular supercomputer at Jülich Supercomputing Centre. *Journal of large-scale research facilities*, 4:A132, 2018. doi:10.17815/jlsrf-4-121-1.

[40] Chlorosulfonated polyethen material data. URL www.designerdata.nl/plastics/elastomers/CSM.

4.3 Publication III: PMMA Pyrolysis Simulation – from Micro- to Real-Scale

The third article, "PMMA Pyrolysis Simulation – from Micro- to Real-Scale", is published in the Fire Safety Journal [3].

Table 4.3: CRediT authorship contribution statement of publication III.

Item	T. Hehnen	L. Arnold
Conceptualization	X	X
Methodology:	X	X
Software:	X	X
Validation:	X	X
Formal analysis:	X	
Investigation:	X	
Resources:		X
Data curation:	X	
Writing - original draft:	X	
Writing - review and editing:	X	X
Visualization:	X	
Supervision:		X
Project administration:		X
Funding acquisition:		X

PMMA Pyrolysis Simulation – from Micro- to Real-Scale

A Preprint

Tristan Hehnen
ORCID: 0000-0002-6123-261X
Chair of Computational Civil Engineering
University of Wuppertal
Pauluskirchstraße 7
Wuppertal, 42285 Germany
hehnen@uni-wuppertal.de

Lukas Arnold*
ORCID: 0000-0002-5939-8995
Institute for Advanced Simulation
Forschungszentrum Jülich
Wilhelm-Johnen-Straße
Jülich, 52428 Germany
l.arnold@fz-juelich.de
and
Chair of Computational Civil Engineering
University of Wuppertal
Pauluskirchstraße 7
Wuppertal, 42285 Germany
arnold@uni-wuppertal.de

March 30, 2023

Abstract

In fire spread simulations, heat transfer and pyrolysis are processes to describe the thermal degradation of solid material. In general, the necessary material parameters cannot be directly measured. They are implicitly deduced from micro- and bench-scale experiments, i.e. thermogravimetric analysis (TGA), micro-combustion (MCC) and cone calorimetry. Using a complex fire model, an inverse modelling process (IMP) is capable to find parameter sets, which are able to reproduce the experimental results. In the real-scale, however, difficulties arise predicting the fire behaviour using the deduced parameter sets. Here, we show an improved model to fit data of multiple small scale experiment types. Primarily, a gas mixture is used to model an average heat of combustion for the surrogate fuel. The pyrolysis scheme is using multiple reactions to match the mass loss (TGA), as well as the energy release (MCC). Additionally, a radiative heat flux map, based on higher resolution simulations, is used in the cone calorimeter setup. With this method, polymethylmetacrylate (PMMA) micro-scale data can be reproduced well. For the bench-scale, IMP setups are used differing in cell size and targets, which all lead to similar and good results. Yet, they show significantly different performance in the real-scale parallel panel setup.

Keywords Fire Dynamics Simulator (FDS) · Inverse Modelling · Pyrolysis · Arrhenius Equation · Polymethylmetacrylate (PMMA) · Thermogravimetric Analysis (TGA) · Micro-Combustion Calorimetry (MCC) · Cone Calorimeter · Parallel Panel Test · MaCFP Materials Database

1 Introduction

The simulation of fire propagation is of great interest for the fire safety engineering community. It could lead to reduced costs for mitigation measures, since the fire scenario could be less over-predicting and fire protection measures could be better evaluated. It could even make certain types of assessments possible, for instance when the release of (radioactive) combustion products is to be determined, and not prescribed within a design fire. Much research is performed in this direction internationally [1, 2, 3, 4, 5, 6, 7, 8, 9, 10, 11, 12]. This approach requires material parameter sets, which

*Corresponding author.

allow meaningful reaction to changed physical conditions near the fire. For example, reduced oxygen should lead to less energy release from the flame, which in turn reduces the heat transfer to the sample, impacts the release of combustible gas and ultimately leads to a smaller flame. The performance of these parameter sets needs to be assessed over all involved length scales, not only in the micro- and bench-scale. Specifically, the transition from the bench- to the real-scale is important. Assessment of the parameter set's performance is only meaningful in the real-scale, i.e. in terms of validation. Thus, the real-scale should not be part of the estimation of the parameter set itself.

We present here a general strategy to estimate material parameter sets, which is built on existing approaches. These approaches are based on micro- and bench-scale tests, here using cast black PMMA as an example. The parameter sets are applied for fire spread simulations, using the Fire Dynamics Simulator (FDS) [13]. Although the material parameter sets lead to similarly good representation in the micro- and bench-scale, they lead to significantly different results in the real-scale. It is highlighted, that the experiments at this scale introduce further modelling parameters, e.g. the characteristics of the ignition source. Thus, the system is not only dependent on the performance of the material parameters alone.

For the parameter estimation, an optimisation algorithm is employed in an inverse modelling process (IMP). In this work, we deliberately assume no information on pyrolysis and combustion parameters of PMMA. With this, the modelled system gains many degrees of freedom to represent, e.g., the intermediate states and structural changes, which are in general not measurable from the virgin material. Additionally, these parameters may not be available in practical scenarios, and the presented approach aims for a general applicability. As a general strategy, the process presented here is divided into three major steps, in an effort to reduce the otherwise significant computational demand. In the first step, reaction kinetics of the material decomposition (pyrolysis) and the energy release in the gas phase (combustion) are determined. This is based on micro-scale tests, thermogravimetric analysis (TGA) and micro-combustion calorimetry (MCC). A large number of parameters (33) is used to define the PMMA decomposition scheme. By using an extremely simplified micro-scale simulation setup the computational demand can be kept low – in the order of days. In the second step, the thermophysical and optical parameters are determined in the bench-scale. The simplified cone calorimeter setup used in this step is computationally much more expensive. Looking at fewer parameters (15), the computational demand can be kept relatively low as well. Still, the needed computing time is in the order of months on a high performance computing cluster to complete a full IMP, including multiple sampling limit adjustments. Finally, the performance of the parameter sets is assessed in a real-scale simulation setup of a parallel panel test. This is considered here as validation step, since the goal is to determine parameter sets in the small-scale that lead to the appropriate behaviour to predict the fire development in the real-scale.

The here proposed method is built on state-of-the-art strategies of using FDS for pyrolysis simulation, e.g. [8, 9, 10, 14]. The primary changes are the use of multiple superimposed pyrolysis reactions, using a gas mixture as surrogate fuel and conducting simplified cone calorimeter simulations with higher fluid cell resolution during the inverse modelling. The surrogate fuel consists of combustible and non-combustible primitive species. During the IMP, their fractions are adjusted such that the average heat of combustion (HOC) of this mixture fits to the experiment data. With this, FDS can use the mass loss rate from the solid directly as input for the gas phase without the usual scaling.

Furthermore, the radiative flux from the cone heater to the sample surface is not uniform [15, 16], which is taken into account here. A high resolution simulation with a conical heater geometry was conducted and the resulting radiative heat flux determined. This result is then baked into a flux map for a simplified cone calorimeter setup. This setup has a higher fluid cell resolution than is typically used. With the higher resolution and the inhomogeneous heat flux it is possible to capture an uneven sample consumption.

The inverse modelling is conducted with PROPTI [17, 18, 19], an in-house developed publicly available inverse modelling framework. New dependencies were implemented to determine the gas mixtures (Git commit hash: `3a05366`), more recent versions of PROPTI should support this directly. In this work, PROPTI used the shuffled complex evolutionary algorithm from SPOTPY [20], version 1.5.14. With `FDS6.7.6-810-ge59f90f-HEAD` we use a self-compiled FDS version, to incorporate a fix when FDS computes the stoichiometry for gas mixture combustion, see issue "Fuel FORMULA for SIMPLE_CHEMISTRY #9862" in the FDS GitHub repository. Thus, one may encounter errors when trying to reproduce this work with the stable FDS 6.7.6 or earlier versions, in general it should work with newer versions. Throughout this work, FDS is used with default settings if not stated otherwise. The experimental data for the micro- and bench-scale tests are taken from the MaCFP materials database [7] (Git commit hash: `7f89fd8`). The result of the inverse modelling is an effective material parameter set. Its performance is compared against real-scale experiment data of parallel panel tests, taken from the MaCFP database [21] (Git commit hash: `25614bd`). Comparisons with the FDS validation suite are provided as reference [22].

This article is accompanied by a publicly available data repository on Zenodo [23], containing the simulation data and analysis scripts, as well as a video series on YouTube explaining how they are set up [24].

2 Materials and Methods

At first, in this section, a brief introduction to the pyrolysis and combustion basics for PMMA is provided. Then the micro-scale experiment and simulation setups are presented, which are the basis for the pyrolysis parameter estimation. The fuel mixture for the gas phase combustion is introduced afterwards. Then the bench-scale experiment and simulation setups for the estimation of the thermophysical parameters are discussed. Finally, an overview of the inverse modelling process and a description of the real-scale setup are presented.

2.1 Pyrolysis and Combustion Basics

Fire spread on solid materials involves the transformation of the material into a combustible gas. This transformation, controlled by the temperature of the solid, is called pyrolysis. The long molecule chains of a polymer are split into smaller molecules. In the case of PMMA, this is mostly its monomer methylmetacrylate (MMA), more than 90 %, and small amounts of carbon dioxide [14, 25, 26, 27]. However, the MMA is not directly involved in the combustion [27]. It further decomposes into even smaller chemical compounds, among which are methane, acetylene, ethylene, carbon monoxide, carbon dioxide, and hydrogen [27]. These smaller molecules are then taking part in the gas phase combustion (flame). The combustion reaction involves many intermediate species and reactions. Already for simple hydrocarbons like methane, reaction mechanisms are proposed [28, 29, 30] that involve 30 to over 1200 intermediate reactions and over 200 intermediate species. Reaction mechanisms for longer carbon chains contain the reactions of the shorter molecules [31]. Concentrations of the individual species also change across the combustion reaction zone [32]. It seems that the limiting factor to the fidelity of the reaction models is primarily the available computing power [13, 33]. Reaction schemes also differ by which PMMA decomposes, depending on the polymerisation method and molecular weight [26, 27, 34], as well as with different test apparatus designs [private communication with Karen De Lannoye].

The material decomposition and combustion models used within this work using FDS is strongly simplified, yet reflects common practise in scientific and engineering applications. First, using a model based on Arrhenius equations, the sample is transformed into a gas (`NU_SPEC`) and a solid inert residue (`NU_MATL`), see section 2.2. This is solely controlled by the sample temperature. The released gas is directly involved in the combustion reaction, see section 2.3. Intermediate reaction steps of further decomposition of the MMA are neglected here. This is regarded as an intermediate approach, located between a single surrogate or many intermediate chemical reactions and species. It still maintains the benefit of the surrogate: the reduced computational cost, because fewer species and reactions need to be tracked.

2.2 Micro-Scale Setup

The focus of the micro-scale simulations is to determine the temperature-dependent material decomposition reactions (pyrolysis). The experimental data, that is used as target during the parameter estimation, is taken from the open-access MaCFP git repository [7]. Two data sets are used in two different IMP setups. First, TGA data recorded with a heating rate of 10 K/min, and MCC data at 60 K/min, provided by the National Institute of Standards and Technology (NIST). Secondly, TGA data from Sandia National Laboratories (Sandia) recorded at a higher heating rate of 50 K/min. This is used in an effort to get close to matching heating rates for TGA and MCC. As of writing, no 60 K/min TGA data set is available from the MaCFP repository.

All the experimental data series, see figure 1, are averaged within each group, to be used as target during the IMP. The TGA data is normalised to get the normalised residual sample mass over temperature, and the final residue amount is determined (figure 1a). The amount of residue produced is very small, less than one percent of the starting sample mass. This value is used directly as residue production for each decomposition reaction in FDS (`NU_MATL`). From the processed MCC experimental data the average heat of combustion is determined.

Two different IMP setups are designed (table 1), the first uses the TGA with a heating rate of 10 K/min and the MCC at 60 K/min. The second uses the TGA with a heating rate of 50 K/min and the MCC at 60 K/min. With this, the first setup has a relatively large difference in the heating rate and the second setup a smaller one.

Table 1: Overview over the different micro-scale IMP setups.

IMP Setup	Target Details
MCCTGA_01	TGA at 10 K/min, MCC at 60 K/min
MCCTGA_02	TGA at 50 K/min, MCC at 60 K/min

An FDS functionality (`TGA_ANALYSIS`) is used to evaluate an extremely simplified micro-scale simulation setup. The pyrolysis is simulated by employing Arrhenius equations for the decomposition reactions. It is used as provided with

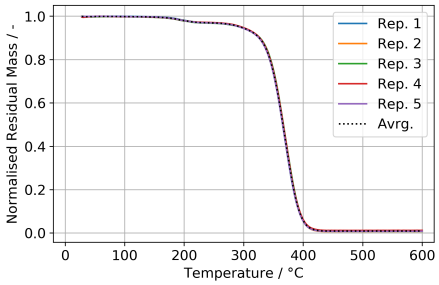

(a) TGA normalised residual mass, for a heating rate of 10 K/min (NIST).

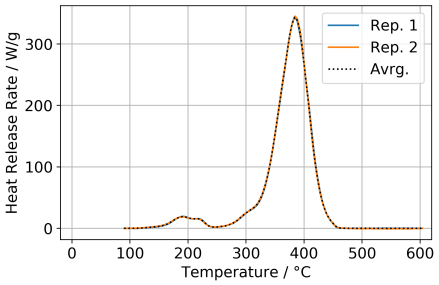

(b) MCC energy release rate, for a heating rate of 60 K/min (NIST).

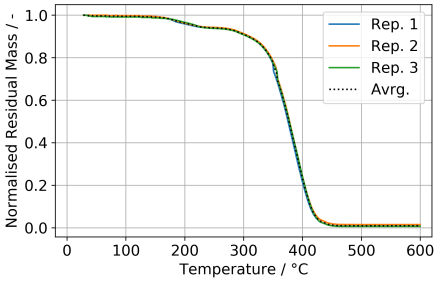

(c) TGA normalised residual mass, for a heating rate of 50 K/min (Sandia).

Figure 1: Data from different repetitions (Rep.) of micro-scale experiments, MaCFP [7]. Average (Avrg.) used as IMP target.

FDS. The goal is to use as few reactions as possible, yet approximate the experiment to a high precision. The overall process starts out from the MCC experiment data. Multiple pyrolysis reactions, eight in total, are manually positioned, such that they roughly approximate the experiment data and form the first guess for the parameter set. The fine-tuning of the reaction parameters using an IMP concludes the first step of the procedure.

In FDS, the decomposition reactions are associated with the material definitions (`MATL`). A sample can consist of multiple material components. These are combined into a boundary condition (`SURF`). The materials defined here get mostly the same parameters and only differ with respect to the parameters of the Arrhenius equations. This leads to a homogeneous material which decomposes differently depending on its temperature. The reference values, `REFERENCE_TEMPERATURE` and `PYROLYSIS_RANGE`, are chosen for being more human-readable, compared to the pre-exponential factor and activation energy. They assume the reaction order to be unity. The reaction order essentially skews the peak, which can be reproduced by multiple peaks/reactions in superposition. The reference values define the shape of the peak, its area is controlled by the fraction of the sample mass associated to this reaction in the surface definition (`MATL_MASS_FRACTION`). Thus, the energy release is controlled by the mass fractions. This allows to create a uniform gas mixture to be used for all decomposition reactions. It also means that each reaction has access to a predefined amount of sample mass. Each of the reactions releases the same fractions of residue and gas mixture. Furthermore, each Arrhenius reaction is assigned a heat of reaction (HOR), which is also determined during the IMP. In total, four parameters describe a single reaction and are determined: the two reference values, the sample mass fraction per reaction and the respective HOR.

2.3 Gas Phase Combustion

In the here proposed method, the complete energy release is assumed to take place as a gas phase reaction in the flame – no oxidation at the solid surface. Furthermore, it is assumed that the involved materials, the combustible gases and

the polymer, are hydrocarbons. Thus, for different materials the strategy might need to be adjusted, but should be transferable in principle.

Since PMMA mostly decomposes into its monomer MMA when heated [14, 25, 26, 27], it could be considered as the gaseous fuel. This is also commonly done in practice, see for example the "NIST/NRC Parallel Panel Experiments" validation case for FDS [22]. Due to neglecting all intermediate reaction steps and species, this fuel is considered a surrogate, i.e. a surrogate fuel. In FDS, the surrogate is often chosen to be a pure, primitive species, like propane or the aforementioned MMA. This might lead to difficulties connecting it to the gas released in an experiment, of which the heat of combustion is likely different. FDS deals with this situation, by scaling the mass of combustible species introduced into the gas domain based on the energy release [13]. Appendix section C provides an exemplary description of this concept. In the proposed method here, a simple gas mixture is used with the goal to get an average HOC so that the mass loss rates match for the solid and gas phase. With "simple" meaning only a few primitive components. It is built, using the lumped species concept in FDS. Here, components are chosen that are already implemented in FDS and are also part of the overall combustion reaction mechanism [27]. They differ in their respective molecular weight and heat of combustion. No specific emphasis is given to the radiative fraction (`RADIATIVE_FRACTION`), thus it uses the default of 0.35 for unknown species [13]. The chosen species are: methane, ethylene and carbon dioxide, see section 2.1. The fractions of methane and ethylene are directly adjusted during the IMP. Carbon dioxide is used to account the remaining difference. Using three adjustable components, the degrees of freedom for the mixture and therefore the computational demand is kept low. They are also part of a computationally inexpensive simulation setup, compare table 3, but still connect to the simulations with gas phase combustion. Since the combustible species are hydrocarbons, the "simple chemistry" approach of FDS 6.7.6 can be used, with a soot yield of 0.022 g/g taken from [35], table 8.1.

During the real-scale validation simulations, two different gas phase reaction definitions are used: the gas burner (propane) and the fuel mixture for PMMA. This requires the "complex chemistry" approach in FDS 6.7.6 and individual gas phase reactions. The stoichiometry of the gas mixture is extracted from the best parameter set of the first IMP step, for details see appendix B. Two different gas phase reactions enable, for example, the assignment of different values for the radiative fraction and soot yield.

2.4 Bench-Scale Setup

The cone calorimeter experiment data is taken from MaCFP [7], provided by Aalto University. The experiments have been conducted at a radiative heat flux of 65 kW/m², without a retainer frame. Square samples of cast black PMMA with an edge length of 10 cm and a thickness of 0.6 cm were used. Heat release rates and back side temperatures, are processed similarly as described in section 2.2. The experiments show good repeatability, as demonstrated by the energy release in figure 2a. It is assumed here that the back side temperature is measured at the sample centre. However, it is reported that in the experiment the temperature was measured at three points: the centre (Temp_1) and 1.5 cm to the sides (Temp_2/3). With a cell size of 3.3 cm, which is the main grid resolution as explained below, and a cell at the sample centre, all of these locations fall into this centre cell. Regardless of their location, most thermocouples show very similar temperature development, see figure 2b. Few diverge and are rejected here.

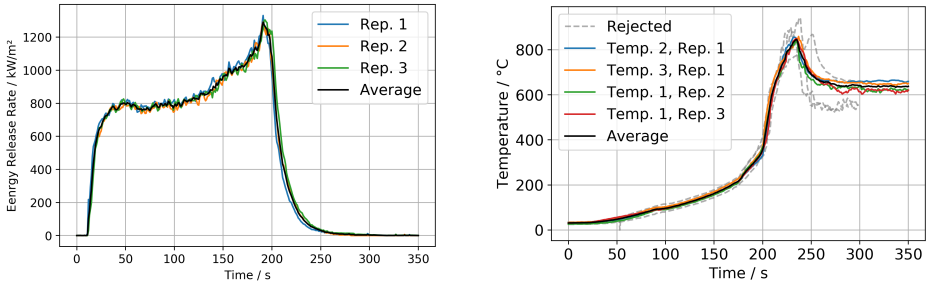

(a) Energy release.

(b) Back side temperature.

Figure 2: Cone calorimeter experiment results, for 65 kW/m² radiative flux condition (MaCFP [7], Aalto). "Temp_1" values are recorded at centre, "Temp_2/3" are recorded 1.5 cm to the sides. Averages are used as IMP target.

In the bench-scale, the cone calorimeter apparatus is simulated in a simplified way. The simulation mode in FDS is set to Large Eddy Simulation (`LES`) to facilitate the transfer to the real-scale setup. The computational domain is a single

mesh and computed by a single computing core. The fluid cell sizes are based on the sample dimensions. It is assumed to be a square with an edge length of 10 cm. The domain extents 30 cm in the x- and y-directions, with the sample centred. From the top of the sample, the domain extents 60 cm in the positive and two cells in the negative z-direction. Throughout this document, the fluid mesh resolutions are referred to by the number of fluid cells dividing a sample edge. For example, consider that each edge is divided by 3, thus 3×3 cells cover the sample surface. This is referred to as "C3". It results in an edge length for the cells of 3.33 cm. Consequently, for C5 the cell edge length is 2.0 cm and 5×5 cells are covering the sample surface.

Different IMP setups are used to determine the material parameter sets. They vary with respect to the temperature-dependent specific heat and thermal conductivity definitions, IMP targets, as well as fluid cell sizes. The material parameter set is built on a base case, labelled "Cone_01" (table 2). For it, the PMMA density is computed to about 1201.72 kg/m^3, based on the reported sample mass and dimensions. The remaining thermophysical and optical parameters are: emissivity, absorption coefficient, refractive index, specific heat and thermal conductivity. They are solely determined during the IMP. Their initial sampling ranges are guessed and changed with successive limit adjustments. Parameters for the pyrolysis and combustion are taken from the micro-scale IMP (MCCTGA_02), see section 3.1. Thermal conductivity and specific heat for the sample material are represented as temperature dependent values (`RAMP`). The parameter values are adjusted during the IMP, while the temperature points are fixed. In Cone_01 and Cone_03 to 05 the three temperature points are arbitrarily chosen to be 150 °C, 480 °C and 800 °C. Cone_02 uses the definitions from the NIST parallel panel validation case (dashed lines in figure 31 and figure 32), which are physically informed. In Cone_06 and Cone_07 the temperature values are determined based on the significant temperature interval of the MCC measurement, see stars in figure 3. The chosen values are 150 °C, 300 °C and 450 °C to represent this interval. They are also used for Cone_08, but here the conductivity for PMMA and the backing material are in addition using the low temperature data reported by DBI/Lund from the MaCFP materials database [7].

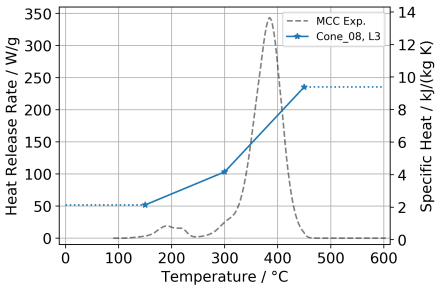

Figure 3: Example of a temperature dependence of the specific heat, realised as a ramp in FDS (Cone_06 and 07). The chosen temperature values are based on the significant temperature interval in the MCC experiment. The same temperature references are used for the heat conductivity.

In general, the backing material and the residue are treated as unknown. The density of the backing material is set to 65 kg/m³, taken from the Aalto contribution [7]. The density of the residue is chosen arbitrarily to be 2500 kg/m³. For backing and residue, their individual emissivity, thermal conductivity and specific heat are adjusted during the IMP. The respective sampling ranges are guessed. This is intended to provide some freedom, in an attempt to separate the sample behaviour from the boundary conditions of the experiment. The back face temperature is used as IMP target to achieve this separation. For one IMP setup (Cone_04) only the energy release is used as target to serve as comparison. With respect to fluid cell sizes, the default is C3. However, Cone_05 uses the C5 and Cone_07 the C2 setup. An overview of all investigated setups is outlined in table 2.

In the boundary definition of the PMMA layer, the solid mesh is set to be uniform with a stretch factor of 1. The number of solid cells was increased by a factor of 10 (cell size factor of 0.1).

The radiative heat flux of the heater is imprinted to the sample surface in the low resolution setups, such that a heater model can be neglected. This radiative heat flux is determined by employing a high resolution simulation (C12) containing a geometrical model of the heater, see appendix section A. The model is designed based on information in the literature [36, 37]. The resulting heat flux distribution on the sample surface is recorded (`GAUGE HEAT FLUX`), see figure 4. It is observable, that the radiative flux is not uniform across the sample surface, as was also reported earlier [15, 16, 38]. Based on the fluid cell size of the respective the IMP (C2, C3 and C5), low resolution maps are

Table 2: Overview over the different simplified cone calorimeter IMP setups. Density is 1201.72 kg/m^3 for all cases. Fluid cell size is C3, if not stated otherwise.

IMP Setup	Details
Cone_01	Base case
Cone_02	Temperatures for the specific heat and conductivity RAMPs based on FDS parallel panel validation case
Cone_03	PMMA slab thickness set to 6.1 mm
Cone_04	Only HRR as IMP target
Cone_05	With 2 cm fluid cell resolution (C5)
Cone_06	Temperatures of conductivity and spec. heat RAMPs based on MCC plot (figure 3)
Cone_07	Like Cone_06, with 5 cm fluid cell resolution (C2)
Cone_08	Like Cone_06, lower temperature data added to RAMPs for conductivity of PMMA and backing, from DBI [7]

computed, see figure 5. These maps are implemented, using multiple surface definitions with different heat flux values (EXTERNAL_FLUX) for the individual sample surface cells.

The low fluid cell resolutions allow to conduct the IMP in a manageable time frame (table 3) and still incorporate gas phase combustion. Just adding the flame heat flux to the imposed flux from the virtual heater is not sufficient. The flame formation is based on the combustible mass released from the sample, which in turn is based on the heat flux to the sample. If the contribution of a flame to the radiative flux is prescribed, it effectively defines a static imaginary flame with no connection to the gas phase model and should therefore be avoided.

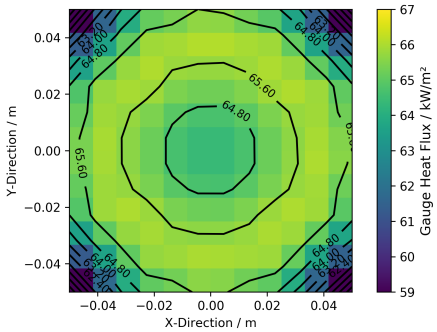

Figure 4: Gauge heat flux from simulation with geometrical heater model (GEOM) for a target of 65 kW/m². Sample with an edge length of 0.1 m (C12).

2.5 Inverse Modelling Process

The inverse modelling is controlled using the framework PROPTI [17, 18, 19]. It uses a shuffled complex evolutionary (SCE) algorithm [39], implemented in Python in the SPOTPY package [20].

The initial sampling limits of the individual parameters are chosen as best guess. If during the IMP parameters get stuck at one of their limits, their sampling space is expanded in the respective direction. Thus, the sampling space gets only larger and the same parameter combinations of the previous runs can still be reached. Typically, after a couple generations it is clear which parameter approaches a limit and a new IMP run can be set up. These changes in sampling limits are denoted with a capital "L" followed by a number, for example "L0" is the original sampling space, "L1" would be the first expansion and so on. See appendix D for an example. This leads to a staggering of the IMP runs.

The overall parameter estimation is divided into two steps. In the first IMP step, the reaction kinetics parameters for the material pyrolysis are determined. In the second step, the thermophysical and optical parameters are estimated using the reaction kinetics of the first step. The goal is to distribute the workload for the parameter estimation over two different simulation setups. This allows to move a large amount of parameters to a simulation that can be conducted quite fast –

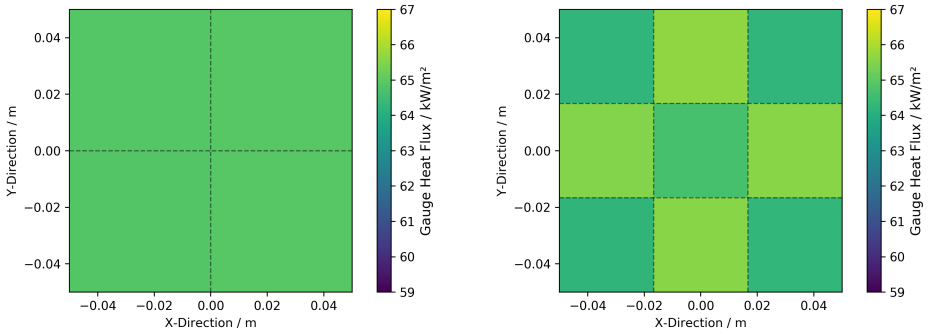

(a) Resolution: 2 by 2 cells (C2).

(b) Resolution: 3 by 3 cells (C3).

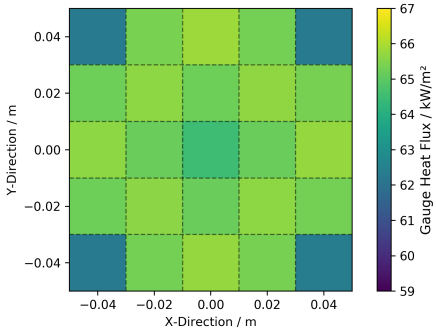

(c) Resolution: 5 by 5 cells (C5).

Figure 5: Coarse gauge heat fluxes mappings for the IMP, constructed from a high resolution simulation (C12, figure 4). Sample with an edge length of 0.1 m.

in the matter of seconds rather than minutes. Given the structure of the shuffled complex evolutionary algorithm, this is beneficial. With increasing amount of parameters, the generation size grows more than quadratic. The number of simulations to be conducted per generation Φ depends on the amount of parameters to be considered. In the work presented here, the number of complexes n_{complex} is chosen to equal the number of parameters $n_{\text{parameter}}$, see equation 1.

$$\Phi = (2 \cdot n_{\text{parameter}} + 1) \cdot n_{\text{complex}} \tag{1}$$

The number of generations was chosen to be about 150 for the micro-scale simulations and about 100 generations for the simplified cone calorimeter. In general, this is a sufficient number of generations to reach convergence.

As cost function a root mean square error (RMSE) is used. It is computed between the simulation response of a given parameter set and the experiment data used as target. The RMSE takes the whole data series into account and yields a single value as result. During the inverse modelling the optimiser minimises the RMSE, thus the lowest value is associated to the best parameter set.

Separating the reaction kinetics from the thermophysical parameters, is beneficial in two aspects. For one, it reduces the complexity of the inverse modelling itself ($n_{a+b}^2 > n_a^2 + n_b^2$). Furthermore, about two thirds of the parameters can be determined in a less costly setup. The computing time for the IMP massively depends on the fidelity of the employed simulation. Even though the number of simulations in a single IMP run is about 6 times larger for the micro-scale than the simplified cone calorimeter setup, the latter takes a good 30 times longer for the base case, as summarised in table 3. The simple cone setup with C2 resolution can be completed in about 2 weeks, while the C5 is estimated to take 10 months to over a year!

Table 3: Overview of number of optimisation parameters during different steps of the IMP. The amount of CPU cores (MPI) used equals the number of parameters. Time necessary in the bench-scale setup massively depends on the fluid cell number and size, listed here is the base case (C3). Counting of "IMP run time" begins with the start of L0 and ends with the stop of L3.

	Micro-scale	Bench-scale
Number of parameters	33	15
Generation size	2211	465
Number of generations	150	100
IMP run time (approx.)	3.5 days	> 110 days

2.6 Real-Scale Setup

As a validation step, the material parameter sets are used in a real-scale simulation setup of a parallel panel test. The results are compared to the energy release measured in the experiment, see figure 6. The parallel panel test consists of two 0.61 m wide panels facing each other with a separation of 0.3 m. In between both is a gas burner located with a width of 0.3 m and a length of 0.61 m, see validation guide [22] cases "FM Parallel Panel Experiments" and "NIST/NRC Parallel Panel Experiments", as well as the MaCFP data base [21] — the data set used here is "Test_7_PMMA_R6", labelled "PMMA R6" further on. The combustible sample, attached to the panels, extents 2.44 m above the burner surface. The burner is fed with propane gas. It reaches a quasi-steady energy release of about 60 kW, about 80 s after its ignition. After the sample is confirmed burning (sustained flaming across the panel walls), the burner is shut off. This happens about 120 s after the start of the experiment. This slows down the fire development for about half a minute. The sample material is the same cast black PMMA used throughout the MaCFP test campaign.

The simulations are conducted for the three different fluid cell resolutions introduced in section 2.4. The computational domain spans a volume of 1.2 m $\times$ 0.8 m $\times$ 4.8 m and is divided into multiple sub-domains (`MESH`). The number and dimensions of the sub-domains were adjusted compared to the FDS validation setups, from (4, 2, 12), to (3, 1, 12). Thus, the individual mesh dimensions are multiples of 10 cm and can be nicely divided following the scheme outlined in section 2.4. Furthermore, the number of meshes is reduced and the simulation can be run on a single computing node with its 64 cores.

The surface definitions are taken from the "NIST/NRC Parallel Panel Experiments" case. The sample definitions are built from the parameter sets created within this work. The simulation mode is set to LES.

Propane is used as fuel species for the gas burner in the simulation. This differs to the FDS validation setup "NIST/NRC Parallel Panel Experiments", where the combustion reaction for MMA is used for the burner and the sample. In contrast to the experiments, during the simulation the gas burner is kept at a continuous energy release of 60 kW throughout, releasing a mass flux of about 0.00732 kg/(m² s). Shutting the burner off earlier leads to fire extinction relatively fast, see discussion in section 4.3.

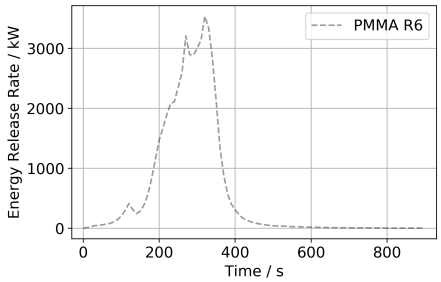

Figure 6: Fire development over PMMA panels in the parallel panel experiment.

3 Results

3.1 Micro-Scale Simulation

The first step of the parameter estimation focuses on an inverse modelling process in the micro-scale setup. Two IMP setups have been run (table 1). Both converge to their best fitness values within the first 40 generations, see figure 7. The overall fitness value is a combination of the performance in the MCC and in the TGA simulations.

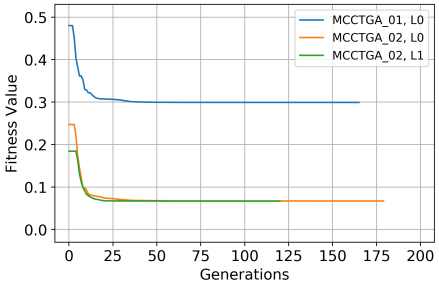

Figure 7: Fitness development of the micro-scale IMP setups. MCCTGA_02, L1, cut short due to good performance.

The responses of the best parameter sets for both IMPs are compared against the target data for both heating rates, see figure 8. The "(IMP)" marks which IMP used the respective target. The mass loss for a heating rate of 10 K/min happens at lower temperatures in the simulation for both IMPs, with MCCTGA_01 being slightly closer to its target (figure 8a). For a heating rate of 50 K/min, both yield a very similar response (figure 8b).

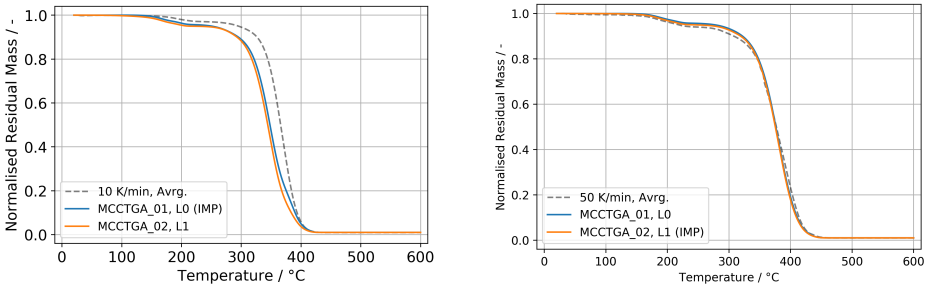

(a) Targets: MCC at 60 K/min, TGA at 10 K/min.

(b) Targets: MCC at 60 K/min, TGA at 50 K/min.

Figure 8: Normalised residual mass from TGA, for heating rates of 10 K/min and 50 K/min. Comparison of response for the best parameter sets, (IMP) indicates the respective target.

Both IMP setups are able to reproduce the target of the MCC at 60 K/min well, see figure 9.

Figure 10a shows the eight predefined decomposition reactions, labeled "PMMA 1" to "PMMA 8", after being fine tuned through the IMP. Reactions "PMMA 4" and "PMMA 8" provide significantly lower contributions compared to the other reactions (figure 10b).

Due to its better fitness value, focus is shifted to MCCTGA_02 and no further sampling limit adjustment is conducted for MCCTGA_01. MCCTGA_02 is used in the following cone calorimeter simulations.

3.2 Bench-Scale Simulation

Here, an overview of the simple cone calorimeter IMP results of the best parameter sets is presented. The full data is provided in appendix F for completeness. The best fitness values of the IMP runs are summarised in table 4. For each

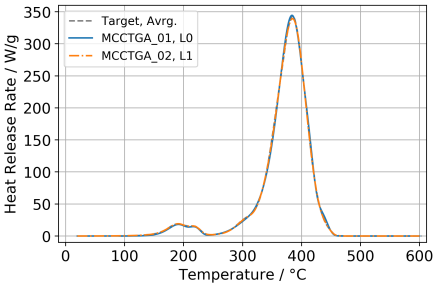

Figure 9: Heat release rate from MCC for a heating rate of 60 K/min. Comparison between experiment and best parameter set from the IMP.

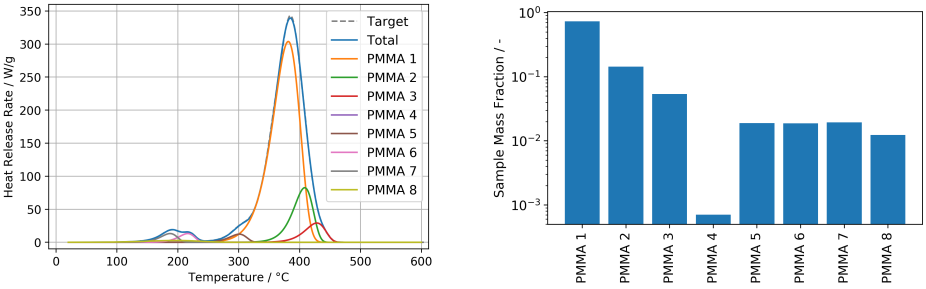

(a) Determined reactions.

(b) Reaction contributions.

Figure 10: Individual reaction steps (MCCTGA_02, L1); residue production excluded.

IMP run, 100 generations have been completed, see figure 11a and figure 28. Cone_04-L3 has the lowest fitness value, but its target is only the energy release, thus it is not directly comparably to the remaining IMPs.

Table 4: Best parameter sets of the different simple cone calorimeter IMP setups. Note: Cone_04 is lower, since it only uses energy release as target, while all others also solve for back face temperature.

IMP Setup	Limits	Repetition	Fitness Value
Cone_01	L2	43718	0.361
Cone_02	L2	38608	0.402
Cone_03	L3	17857	0.383
Cone_04	L3	39571	0.096
Cone_05	L3	13568	0.288
Cone_06	L3	45893	0.314
Cone_07	L2	35532	0.364
Cone_08	L3	32262	0.290

Figure 11 shows the responses of the best parameter sets of all the different IMP setups. For all cases, the optimiser is able to find a parameter set that reproduces the experiment data relatively well. This is emphasised by drawing all their responses without distinction, including different fluid cell resolutions (C2, C3 and C5). Cone_04 is highlighted, because it uses only the energy release as target.

With respect to the energy release, difficulties exist in reproducing the first bump at around 20 s to 50 s, the final peak at about 190 s and the following decay phase. In some cases, pronounced steps are visible towards the end of the simulations. See for example figure 29 for Cone_06. These steps are associated with the burn-out of the individual cells.

Furthermore, in all cases a small peak is visible in the beginning of the cone calorimeter simulations, at about 15 s. Cone_04 and Cone_08 capture the energy release profile best (figure 29).

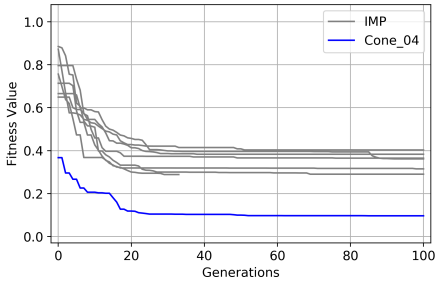

(a) Fitness development.

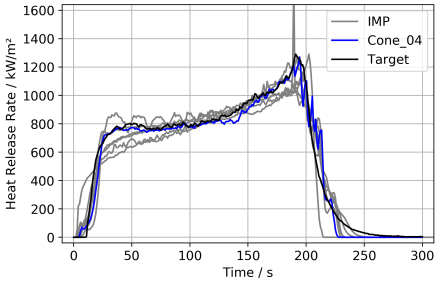

(b) Energy release.

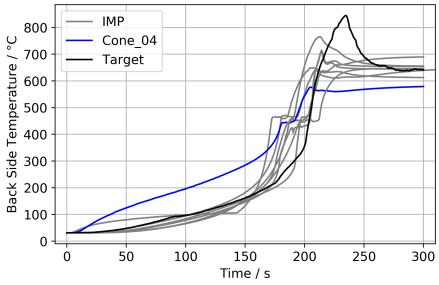

(c) Back face temperature.

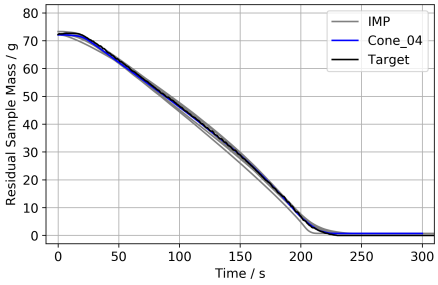

(d) Sample mass.

Figure 11: Condensed results of the IMPs. Cone_04 uses only energy release as target. Parameter set of the FDS parallel panel validation case for reference (Vali. PP). Full data provided in appendix F.

Reproducing the temperature recorded at the back face of the sample proves to be challenging, see figure 11c and figure 30. For cases where it is a target, the temperature development during the first about 160 s can be reproduced. Between about 160 s to about 270 s departures are visible, with a pronounced step around 200 s. A peak can be observed towards the end, yet less pronounced as in the experiment. Cone_04 does not have the temperature development target and is not able to reproduce a similar behaviour on its own.

The residual sample masses during the simulation are close to the experiment data, see figure 11d and figure 33.

3.3 Real-Scale Simulation

The real-scale simulations are used as validation step of the inverse modelling. As above, only selected data is shown here and the simulation results of all best parameter sets are provided in appendix H. Heat release rates in the parallel panel simulation setups are presented in figure 12.

For the smallest fluid cells (C5, figure 12a), the peaks are overall narrower and taller compared to the largest cells (C2, figure 12b). This is emphasised by comparing the peak energy release, see figure 13b. In the simulation the fire develops overall faster compared to the experiment, see figure 13a. Larger cells slow the development down slightly. In general, faster fire development leads to higher energy release, see figure 14. Total energy release (TER) of all parallel panel simulations is provided in figure 36 in the appendix.

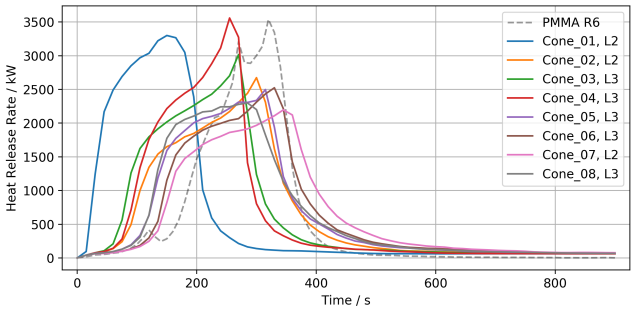

(a) Fluid cell resolution: C5.

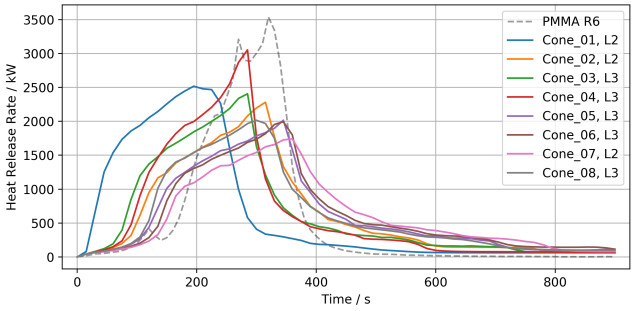

(b) Fluid cell resolution: C2.

Figure 12: Comparison between experiment and simulation of the parallel panel setup for different fluid cell sizes. Gas burner fuel is propane in the simulation. Data for fluid cell resolution C3 provided in appendix H.

4 Discussion

4.1 Micro-Scale

Both IMP setups are able to reproduce the MCC data well (figure 9). The TGA data for a heating rate of 50 K/min is better reproduced than for 10 K/min (figure 8). The deviation between simulation and experiment for 50 K/min is attributed to the non-linear heating rate in the experiment, see figure 27d. Larger differences between experiment and simulation are observable for a heating rate of 10 K/min. Here, MCCTGA_01 gets slightly closer to its target. Otherwise, the results are similar, yet happen at lower sample temperatures compared to the experiment. With the lower heating rate in the TGA (MCCTGA_01) the algorithm is not able to find a parameter set suitable for both conditions, i.e. 10 K/min in the TGA and 60 K/min in the MCC. It comes as some surprise that the IMP favours the MCC and does not position the fit somewhere in between both targets. Some bias may have been built into the setup, by manually positioning the first guess reactions based on the MCC data, or by the chosen cost function.

Possibly, some aspects of the apparatus are not captured well enough in the highly simplified micro-scale model. We know, from private communication with Karen De Lannoye, that the design of the TGA apparatus has an observable impact on the results.

The divergence could also be related to the released gas mixture, which in this contribution assumes an average heat of combustion over the course of the experiment. It is argued [34], that the first peak at about 187 °C (figure 1b) could be attributed to residual solvent within the polymer. Furthermore, radically polymerised PMMA is somewhat unstable and starts decomposition at about 220 °C, due to unsaturated end groups [27]. Even though the primary decomposition products of PMMA are MMA and carbon dioxide, the MMA is not directly involved in the gas phase combustion [27]. Some major compounds involved in the combustion of PMMA are methane, methanol, formaldehyde and acetylene, with ethylene being involved during the acetylene combustion. As an example, for pure compounds the heats of

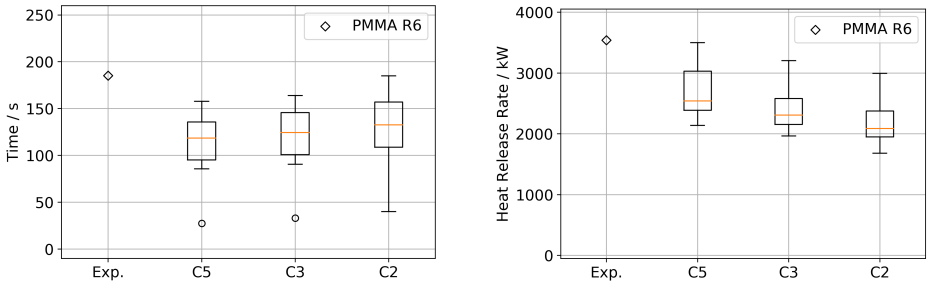

(a) Time to reach 1 MW.

(b) Peak heat release rate.

Figure 13: Peak energy release and time to reach 1 MW in parallel panel simulation setup, using the best parameter sets from IMP. Comparison between experiment (Exp) and simulation data with different radiative fractions (RF) for the gas burner reaction.

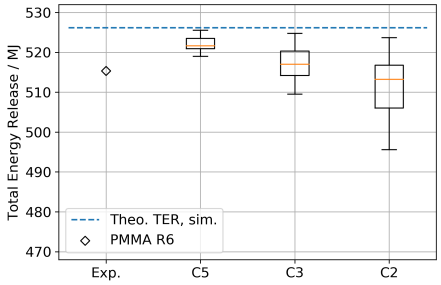

Figure 14: Total energy release of the best parameter set in parallel panel test for all IMP setups. Comparison between experiment (Exp) and simulation data with different fluid cell sizes. Simulation response with gas burner reaction of propane. Dashed line indicates theoretical total energy release of the sample in the simulation.

combustion are tabulated in the literature [35] with 50.0 MJ/kg for methane, 50.4 MJ/kg for ethylene, 19.8 MJ/kg for methanol and 24.2 MJ/kg for PMMA. In the work presented here, a variable mixture of methane, ethylene and carbon dioxide is used for the PMMA pyrolysis, that leads to an average heat of combustion of the PMMA pyrolysis products. This is an additional degree of freedom in the IMP to match the MCC and TGA data. However, fixing this mixture over all reactions could be too rigid. In future work individual mixtures could be investigated. The difference for the TGA test at 10 K/min, see figure 8, could be a manifestation of this rigidness, as low and high heating rates need to be reproduced simultaneously. A possible solution would be to use multiple gas mixtures. In an effort to reduce complexity downstream, i.e. definition of multiple chemical reactions and solving more transport equations, the mixture could be generated on-the-fly by releasing a single species per reaction. It might also be sufficient to mix only methane and carbon dioxide. Each decomposition reaction in figure 10 could be doubled. One would release methane and the other carbon dioxide, the mixture would then be controlled from the mass fraction in the surface definition. This strategy is to be investigated in future work.

Here, no IMP target is provided to explicitly match the heats of reaction for the individual decomposition reactions. This could be accomplished by using experiment data from differential scanning calorimetry (DSC). Alonso et al. [5] used TGA and DSC data as targets in their IMP setup, changing the contribution of each to the overall fitness assessment. With this, the target of higher importance is reproduced better to the detriment of the other. The employed decomposition scheme uses two consecutive decomposition reactions forming an intermediate material and a residue. A parallel decomposition scheme, as is proposed here, could be able to capture more gradual changes in the heats of reaction across the temperature range of the experiment. This could improve the overall performance of the parameter sets generated here and should be investigated in future work.

The proposed approach using gas mixtures allows to model more sophisticated technical materials. Specifically, the behaviour of fire retardant materials could be reproduced. Non-combustible gas could be released early on, which cannot be captured with a single surrogate fuel. This makes it necessary to take MCC and TGA data into account simultaneously. This could even be expanded further, by adjusting which reaction contributes most to the production of the residue. Also considering different residues, for example for intumescent materials.

Arguably, the goal to use as little decomposition reactions as possible is not achieved. Looking at figure 10, PMMA 4 (0.07%) could be removed, possibly also PMMA 8 (1.23%) – even tough it is not too far off of PMMA 6 (1.88%). It should be noted that there is an error in the definition of the pyrolysis reaction input for PMMA 4. Its heating rate is set to 80 K/min instead of the desired 60 K/min. Since the contribution of PMMA 4 is negligible, it is regarded inconsequential here. This is confirmed with a corrected IMP, see data repository (MCCTGA_2b), which virtually yields the same result.

4.2 Bench-Scale

In terms of the fitness value, Cone_08-L3 and Cone_05-L3 performed best across all IMP setups, see table 4 and figure 28. This is excluding Cone_04-L3, because it neglects the back side temperature. Adjusting the sampling limits leads mostly to better parameter sets. Occasionally, the IMPs do not find better sets within the given amount of generations. For example, L1 of Cone_03 shows worse fitness values throughout, compared to L0, see 28. The likely reason is that with each adjustment the process starts anew, combined with the randomness for choosing the individual values. With more generations, better parameter sets may be found. The impact of smaller fluid cells during the IMP is not clear. It might lead to better parameters for the Cone_05 series, yet its enormous runtime makes it not feasible to wait its completion during this work. As of now, it shows fitness values that are just marginally better than Cone_08-L3 (table 4).

Compared with previous work [8, 10], here, higher fluid cell resolutions are used to cover the cone calorimeter sample. With C3 and above, the cells become distinguishable between corners, edges and centre cells — compare the flux maps for two, three and five cells (figure 5). For the C2 configuration, each cell has essentially the same value – the average over the whole surface. This is summarised in figure 15. Higher resolutions capture the ring of higher and the substantially lower heat flux in the corners better, see figure 4. The steps in the simulations during the decay phase might be a result of it, see figure 29 between about 200 s to 250 s for Cone_06_L0. Two processes control the decay: cells burning out and the local burning behaviour, depending on the material parameters. Combining both can smooth out the decay phase. The C2 cases are primarily controlled by the parameters and show a steep drop at the end (Cone_07), because uneven sample consumption cannot be covered well. In the C3 setups the formation of pronounced steps is visible in some L0 cases, but higher limit adjustments can show a smoother decay.

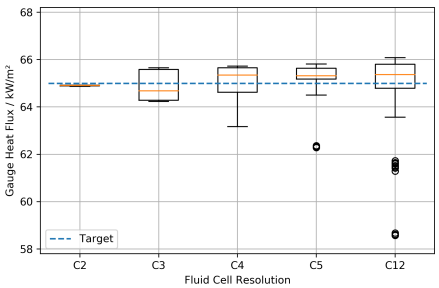

Figure 15: Gauge heat flux distribution for different resolutions (C2 to C12) across all surface cells.

This behaviour is also reflected in the back side temperature. During the decay period a spike is visible (figure 2b), until the temperature settles at a constant value, from around 280 s onward. This constant value primarily shows the influence from the heating element, without the sample. During the experiment, the sample material is consumed and at some point the thermocouples below are exposed, starting from the centre. Thus, they are able to receive the heat radiation from the flame of the surrounding sample directly, in addition to the heater radiation. Due to thermal tension, they may also bend towards the heater. All these aspects together lead to the formation of the spike.

The optimiser has difficulties to capture both, the heat release rate and the material temperature. With lower fluid cell resolution (C2, Aalto_6b in figure 30) the temperature peak between 200 s and 250 s cannot be reproduced. This is

associated to the near-uniform consumption of the sample material, see above. In the other setups, the peak can be captured for the initial sampling limits, but mostly disappears with further adjustments. Certainly, neglecting three dimensional heat conduction inside the sample, is influencing the outcome as well. On the other hand, the sample shape can change significantly during the experiment, see figure 16. Relatively early on, it creates a foam layer and starts to bend towards the heater. In experiments performed by Karen De Lannoye, the maximum height of the bump was observed to extend approximately two sample thicknesses above the original surface of a sample with a thickness of 6 mm (figure 16, right), but the behaviour can change depending on the experiment conditions. This relatively symmetrical bump can change its shape significantly during its decay. While the sample material is consumed, its surface retracts further away from the heater, compared to the beginning of the experiment. Thus, in the experiment, the received radiative flux from the heater should change. These deformations are not replicated in the simulation – the component of the radiative flux of the heater stays constant, by construction. Only the heat flux component from the flame can change. The sample deformation is likely misinterpreted as a change in mass and energy release during the inverse modelling.

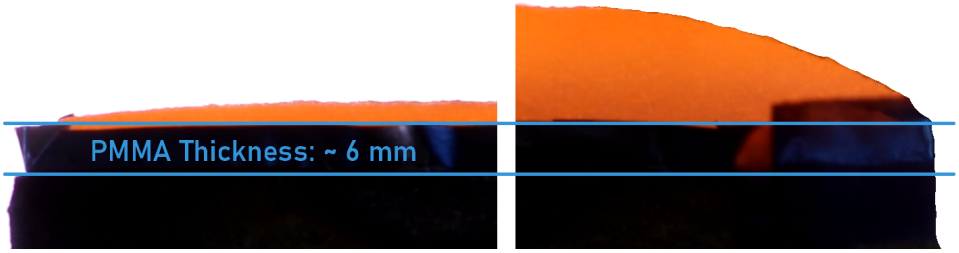

Figure 16: Formation of a bump during cone calorimeter test (50 kW/m^2) of a PMMA sample with 6 mm thickness (side view). Begin of sample deformation at about 1:51 min after experiment start (left). Peak sample deformation at about 2:41 min after experiment start (right). Images provided by Karen De Lannoye via private communication, modified (cropped) to highlight the deformation.

Given the deformation, it is fundamentally unclear where the back face temperature is actually recorded. Furthermore, changes in the rigidity of the PMMA sample (e.g. melting) such that the thermocouple tip can move into the sample, thermal expansion of the sample holder assembly and associated movement between individual components, mechanical tension on the thermocouples and others are contributing to the uncertainty. Assuming they would be tightly attached to the backing material, an air gap could form between them and a bent sample. Such a gap would be interpreted as lower thermal conductivity during the IMP. As an example, compare Cone_04 with the other IMP results in figure 11c. It only uses the energy release as target, not the back side temperature. The temperatures are higher throughout the simulation. Curiously, in the parallel panel simulation setup this behaviour appears to be beneficial, as discussed later in section 4.3. This seems to hint at incorrect temperature readings during the cone calorimeter test. If the sample separates from the thermocouple due to deformation, its recorded temperature should be lower than the actual back face temperature. Consequently, higher back face temperatures are visible in Cone_04 (figure 11c), since in the simulation it is recorded at the back face of the sample by construction. From the above, the uncertainty of the recorded temperature increases during the run time of the experiment. Reliable temperatures might only be able to be recorded for low sample temperatures during the beginning. Specifically considering the deformation, melting and consumption of the sample. Therefore, the intended separation between sample behaviour and the boundary conditions could not be achieved.

In the future, it would be interesting to assess the surface deformation of the sample during cone calorimeter tests. Maybe one could leverage methodologies used in assessing the performance of intumescent coating, e.g. [40]. This could then be used to adjust the prescribed radiative heat flux to the sample surface over time.

The conductivity and specific heat change with sample temperature in the simulation (`RAMP`). This can account for the sample deformation to some degree, when an air gap forms between sample and thermocouple. The temperatures are arbitrarily chosen and used for both parameters, except for Cone_02. At high temperatures Cone_01, 03 to 05 get relatively high values assigned by the optimiser, see figures 31 and 32. Since the material is consumed way before the 800 °C could be reached, only a very small fraction of the ramp piece between the last two points can meaningfully contribute. Thus, ramp values for 800 °C are poorly chosen and should be disregarded. The cases where the temperature points are chosen based on the MCC experiment data, see figure 3, lead to more reasonable results for the conductivity,

which is different for the specific heat. The final point is at a temperature close to the maximum the sample material can reach. Still, it seems to be a useful approach for unknown materials to align both temperature dependent values to the micro-scale data. Maybe the highest temperature value of the ramp could be chosen to be about 20 K lower than the highest meaningful value in the experiment data. This is an attempt to prevent confusion of the optimiser with temperatures that are impossible to reach, because the material is consumed. Another strategy could be to run an IMP solely to determine the ramps for some best parameter set. Thus, more parameters could be spent on the ramp alone without getting too large generation sizes.

With data provided from DBI/Lund [7], extending the conductivity ramps in Cone_08-L3 seems not to change the temperature development significantly, see figure 31. For most of the IMP setups, values for the lower temperatures are determined that are already in the vicinity of the experiment data. The conductivity ramp of Cone_02 shows a relatively narrow but high peak at 105 °C, which is used to capture the glass transition temperature of PMMA [34, 41]. It should be noted, however, that the glass transition temperature is reported at about 122 °C for cast black PMMA, while being 105 °C for extruded clear PMMA [34]. In the presented setups here, the choice of temperature values prevents finding an accurate representation of the glass transition and should be taken into account in future work.

Overall, the sample mass loss during the cone calorimeter simulation is relatively close to the experiment data, see figure 33. This behaviour is an emergent phenomenon of the steps taken with the gas mixture and gives confidence into the proposed method, since it is not an explicit target of the IMP. However, the flame height and gas temperature change with the release of the different surrogate fuel species, see appendix C. This is likely due to dilution of the surrogate fuel with carbon dioxide. Which of the presented centre line gas temperatures in figure 25b is more realistic in context of the PMMA cone calorimeter experiment studied here is unclear for now. Still, it is worth noting that the difference exists, because higher flames might have an impact on the fire spread in a simulation.

For the IMP, the fluid cell resolution of 3.3 cm (C3) seems to be beneficial. It is able to capture the uneven sample consumption, yet it runs relatively fast. However, the question arises, how will the parameters perform at higher resolutions, here C. For this, figure 17 demonstrates an exemplary comparison: a parameter set determined at a given resolution (labelled "IMP") is use at an other resolution (labelled "Check"). Some of the investigated cases show similar behaviour across all limit adjustments, see figure 17c and figure 17d. Others converge towards the higher resolution over the course of multiple limit adjustments, see figure 17a and figure 17b. All limits are provided in appendix G. Given the reduction in computational demand, this is promising.

4.3 Real-Scale

With the real-scale setup, the performance of the best parameter sets of the different IMPs (table 4) is assessed.

The fire development in the simulation is faster than the experiment for all parameter sets and fluid cell seizes, see figure 12. This could be related to the faster ramp-up of the burner in the simulation. It takes 10 s to reach the desired heat release, compared to 80 s in the experiment. Also, the burner is kept burning throughout the simulation, because the fire would extinguish otherwise (see below). Shutting the burner off in the experiment leads to a visible delay in fire development. With larger fluid cells the overall fire development is more drawn out. This could be related to a poorer resolution in the radiation field, since for example the radiation angles are not adjusted here. This is also reflected in the TER indicating that less sample material is consumed than in the experiment, see figure 14.

The peak heat release is about 30% to 40% lower in the simulation, depending on fluid cell size and parameter set, see figure 12. Notable exception is the parameter set of Cone_04. Its performance stands out, by most closely resembling the shape of experiment "PMMA R6" and reaching a similar peak HRR. This behaviour seems to be associated to neglecting the back face temperature as IMP target. In future work, it is worth to look in more detail at Cone_04. Removing the back face temperature constraint seems to be beneficial for the real-scale and may be improved with better chosen temperature values for the ramps.

During the work presented here, only the flame heat flux along the vertical centre line of the empty panels is taken into account as starting condition (figure 18). The flame heat flux data across the lower part of the panels is available via MaCFP [21], and it is compared against simulation responses for different fluid cell resolutions in figure 19. All four plots show flux data averaged over 20 s during the steady-state. The dots show the device locations during the experiment. From the simulation, the heat flux is extracted from the solid boundary directly (`GAUGE HEAT FLUX`). In the experiment, the flux is spread out nearly horizontally along the panels (figure 19a). While in the simulation, it is more focused towards the centre line, which coincides with the location of the simulated flame (figure 19b). With larger fluid cells the heat flux is more concentrated at the lower centre line (figure 19d). This indicates it is not sufficient to simply match the heat flux to the vertical centre line of the panels. To properly assess the performance of the parameter sets, the burner itself needs to be accurately modelled first. For future work it is necessary to develop a more comprehensive representation of the gas burner setup. Further investigations should incorporate the impact of

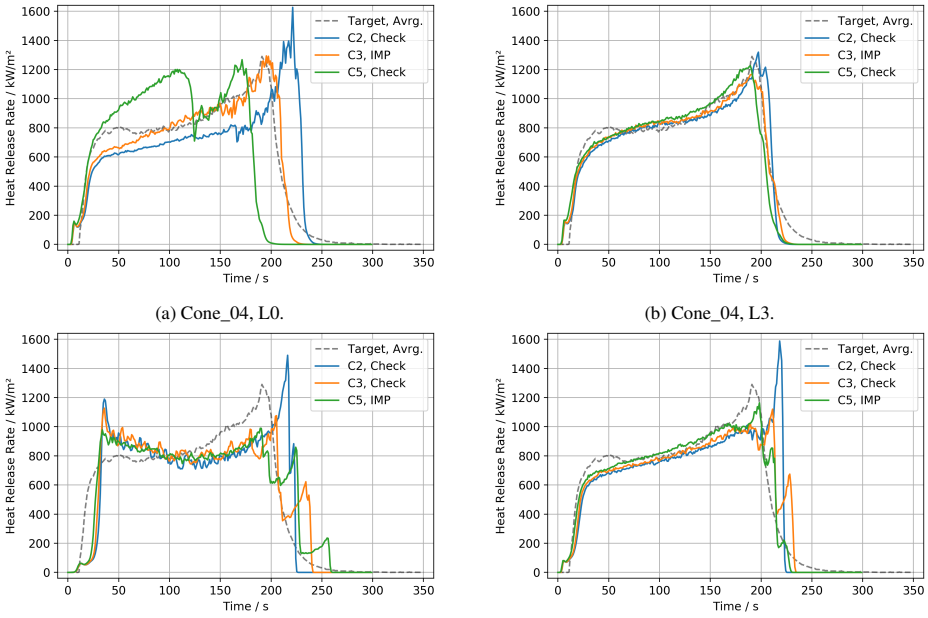

(a) Cone_04, L0.

(b) Cone_04, L3.

(c) Cone_05, L0.

(d) Cone_05, L3.

Figure 17: Comparison of the energy release of a best parameter set (IMP) across different fluid cell resolutions (Check) for the simple cone calorimeter setup.

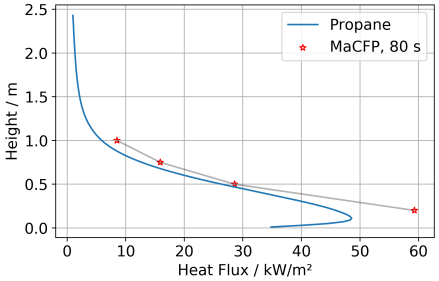

Figure 18: Centre line heat flux, from propane gas burner to empty panel.

simulation parameters like soot production, cell sizes, parameters of the radiation model and material parameters of the burner top face and empty panels.

Simulations with different burner cut-off times have been conducted. Burner cut-off times of 120 s and 220 s are chosen. In all cases the fire is not able to recover, see figure 37, even though the peak energy release in some cases is in excess of 1 MW. As an example, figure 20 shows an image of the experiment "PMMA R6" [21] and an image series captured in Smokeview, covering 60 s after the burner is shut off. The flame region is flat against the panels, about one to two cells. This might interfere with the radiative heat transfer to cells below the lower edge of the flame, as well as to the sides. A closer look at the parameters of the FDS radiation model might be necessary, for example the path length or number of radiation angles. Smaller fluid cells might be beneficial as well, due to a better resolution of the resulting

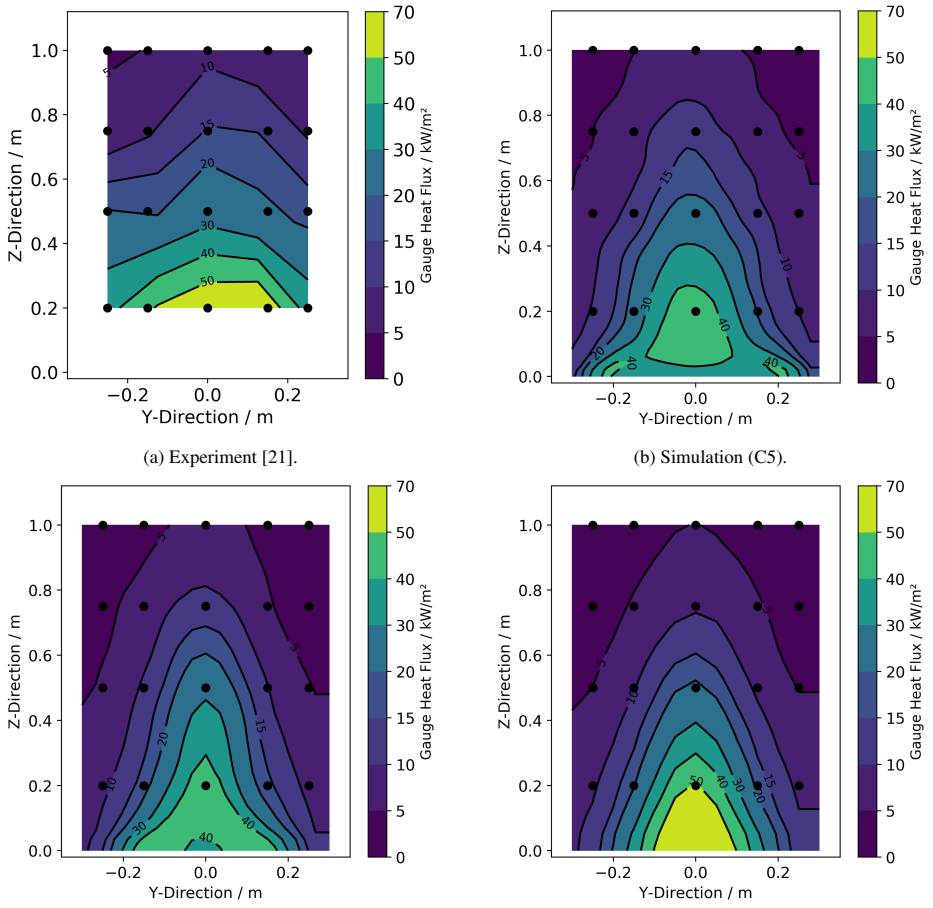

(a) Experiment [21].

(b) Simulation (C5).

(c) Simulation (C3).

(d) Simulation (C2).

Figure 19: Flame heat flux to an empty panel, for different fluid cell resolutions. The dots indicate locations of heat flux gauges during the experiment. Simulation data extracted from boundary (`GAUGE HEAT FLUX`). All show 20 s average during steady-state flaming.

temperature distribution. It should be noted further, that the radiative fraction for combustion reaction of the PMMA pyroylsis products is treated here as unknown and the FDS default is used, i.e. 35 %.

Overall, there is a clear need to investigate the conditions necessary for self-sustained fire spread in the real-scale simulation and the parameter transfer from micro- to bench-scale and further from bench- to real-scale. In the given setups here, the model seems to struggle to provide meaningful energy transfer to the cells around the reaction zone to keep the flame.

4.4 General

All IMP results are able to reproduce the cone calorimeter data well, see figure 11. Yet, in the parallel panel simulation, differences become apparent, see figure 12. Just from the cone calorimeter simulation results alone, it is not obvious how the parameter sets perform in the real-scale. This indicates that individual parameters of the material model may

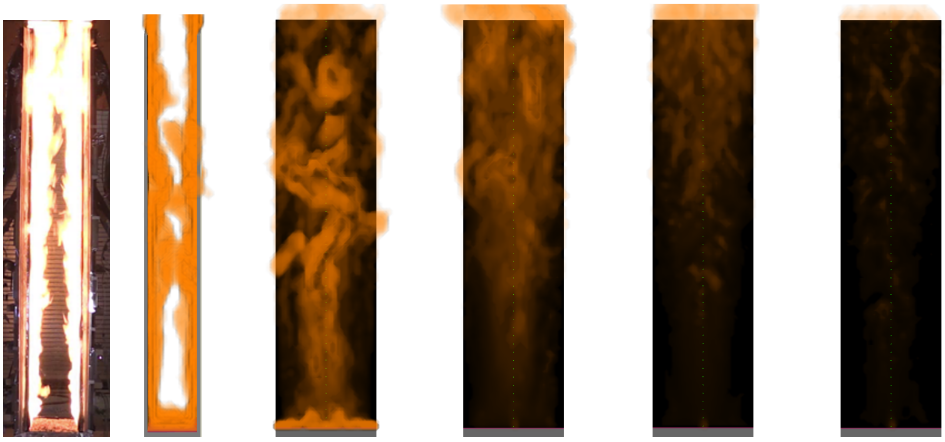

(a) 500 kW HRR [21]. (b) 120 s, side. (c) 120 s. (d) 140 s. (e) 160 s. (f) 180 s.

Figure 20: Flame extinction after burner cut-off, at 120 s and ramp down over 6 s. Pilot flame of one cell in the centre at the bottom of each panel. (Cone_03, L3, propane RF=0.15), Photograph from experiment (figure 20a) at HRR of 500 kW, close to value of burner cutoff in the simulation (figures 20b), cropped out from [21].

be differently sensitive to the simulation and experiment setup. In the cone calorimeter setup fire spread is negligible, specifically for higher radiative heat fluxes. This might mask the behaviour of some parameter. For example, the emissivity has certainly a high impact on the received energy and therefore how the sample material heats up. However, in the cone calorimeter the sample receives a constant and high flux, which might be high enough to heat up the sample fast, regardless of which value for the emissivity is chosen.

The energy transfer to the sample has a significant impact on the fire development. Specifically for the cone calorimeter setup the thermal radiation is important. More detailed investigation of the impact of the radiation model parameters in this setup is necessary. This assessment should also take the performance in the real-scale simulation into account, to ensure that the model for both setups is the same. More care should be taken when setting up the gas burner simulation model. Using individual gas phase combustion reactions for burner and sample should allow to simulate the initial sample ignition more precisely, without compromising the overall sample behaviour.

In this work, the energy release is assumed to solely take place as a gas phase combustion reaction. This may be a sufficient model for PMMA. For other materials that show significant surface reactions, like wood, this assumption might not hold.

Furthermore, experimental campaigns should incorporate medium-scale setups that focus on fire spread. This allows to test the model specifically on this aspect, which a cone calorimeter cannot provide due to its design and severe condition. It would also be useful to provide more information on the burners themselves. Specifically, their surface temperature development and emissivities over the course of the experiment.

5 Conclusions

In general, it seems attainable to simulate fire propagation in FDS, based on material parameters. Usage of a gas mixture allows to capture the MCC and TGA experiments and prevents FDS from scaling the mass introduced into the fluid domain. Thus, it is a step towards more physical parameter sets. The higher resolution in the simple cone setup can account for uneven radiative heat flux and sample consumption.

Overall, it seems clear that many parameters on all levels of this endeavour are important, and their influence needs more cohesive investigation. It is not sufficient to focus on the bench- and micro-scale experiments alone. Despite good performance during these simulations, it is not obvious how the parameters perform in the real-scale. It is necessary to look into the whole chain of setups, to understand how well the parameters eventually translate over to the real-scale. Furthermore, the impact of other model parameters, like the radiative fraction, or the radiation model in general, needs

further investigation. Finally, the landscape of experimental data is fractured specifically for real-scale setups with the same sample material as in the smaller scales. Within these constrains, the parameter set should yield a response close to the observations in the experiments at all scales. This ultimately means the parameter set needs to compensate for the simulation model and experimental shortcomings, which can hardly be accomplished by a "physical" parameter set, thus it needs to be an "effective" representation.

Data Availability

The experiment data is available from the MaCFP git repositories [7, 21] and the FDS validation suite [22]. The input for the inverse modelling, the results of the IMPs, the scripts used for data processing and the validation simulation results are provided in a Zenodo data repository [23]. A video series on how the data processing and inverse modelling is setup and used is provided on YouTube [24].

Acknowledgements

The authors thank Karen De Lannoye, for discussions on conducting the micro- and small-scale experiments and provided images. The authors thank Isaac Leventon, for discussions on conducting the parallel panel experiments. We gratefully acknowledge the computing time granted through JARA (project jjsc27) on the supercomputer JURECA [42] at Forschungszentrum Jülich and through the project on the CoBra-system, funded by the German Federal Ministry of Education and Research with the grant number 13N15497. This research was partially funded by the German Federal Ministry of Education and Research with the grant number 13N15497.

CRediT Authorship Contribution Statement

Tristan Hehnen: conceptualisation, data curation, formal analysis, investigation, methodology, software, validation, visualisation, writing – original draft preparation, writing – review and editing

Lukas Arnold: conceptualisation, funding acquisition, methodology, project administration, resources, software, supervision, validation, writing – review and editing

A Cone Calorimeter Simulation Setup

Based on Babrauskas' [36] original report on the development of the cone calorimeter, a simplified geometrical representation of the heating element is created. The simplification is primarily focused on the heating coil, which is represented as a smooth conical surface and not as a wound wire, see figure 21. The fluid cell resolution was chosen, such that the sample surface (10 cm by 10 cm) was covered with 12 by 12 cells. The geometry itself was built in Blender, using the BlenderFDS addon by Emanuele Gissi.

The heater calibration procedure is mimicked in the simulation, to determine the parameters of the boundary condition (`SURF`) of the heater. A device (`DEVC`) with the `GAUGE HEAT FLUX GAS` quantity is located in the centre of where the sample surface is supposed to be during the test. A Python script is used to automatically find an emissivity value for the heater boundary condition that leads to the 65 kW/m² at the device. Refer to the `FindTMP_FRONT.py` in the `ConeRadiationAssessment` directory of the data set [23]. The heater temperature is set, based on the temperature reported by Babrauskas, but linearly interpolated between the two enveloping values to get to the desired radiative flux. The simulation includes the gas phase, thus interactions between the radiation and the air are taken into account. The radiative flux is assessed over 20 s, after reaching a quasi-steady state. It is averaged over this time span.

Afterwards, a simulation is conducted in which an obstruction (`OBST`) is introduced to represent the sample and its holder. There is a distance of 25 mm between the sample surface and the bottom of the cone heater assembly. From the top boundary of the obstruction the radiative heat flux is recorded (`GAUGE HEAT FLUX`). Per cell, it is averaged over 20 s after reaching a quasi-steady state, same as in the previous step.

B Complex Chemistry

During the simple chemistry FDS calculates the stoichiometry itself and provides the results in the `CHID.out` file. This, however, only works if FDS is used regularly, meaning not with `TGA_ANALYSIS`. A Python script was designed that automatically finds the recent best parameter set (lowest RMSE, see section 2.5) from the micro-scale IMP and creates

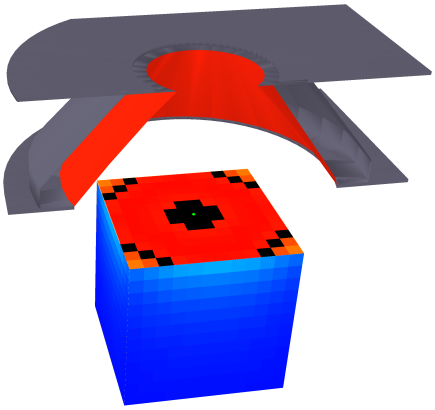

Figure 21: Geometrical model of the cone calorimeter heater, using the `GEOM` namelist. Heater surface idealised as a simple conical shape. Black areas on the sample surface receive a radiative heat flux of about 65 kW/m².

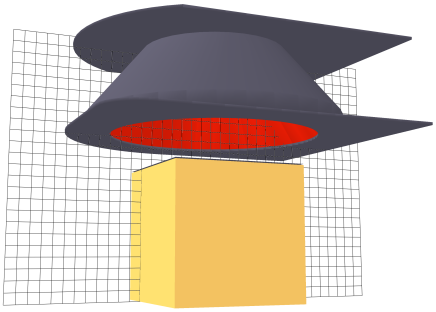

Figure 22: Geometrical model of the cone calorimeter heater, using the `GEOM` namelist. Sample surface resolved as C12.

a new FDS input file to generate a respective `CHID.out` file. After manual execution of this simulation the script can extract the needed stoichiometry information from the `CHID.out` file, build the appropriate input lines and write them to a new FDS input file. These steps are handled in the `GetChemicalReaction.ipynb` notebook, which can be found in the data repository [23]. To ensure consistency, the repetition information of the best parameter set is written to the respective FDS input files as well. For the parallel panel simulations this information can be copied over manually.

C Mass Losses and Flame Heights

An example parameter set is used to demonstrate the different mass loss rates and energy release. The cases "Cone 01" to "Cone 03" in figures 23a, 23b and 24 all use the same pyrolysis scheme. "Cone 01" and "Cone 02" use only methane as surrogate fuel. For "Cone 01" the heat of combustion in the material definition is set to 25 MJ/kg, which is about half of the value of pure methane. No heat of combustion value is provided for "Cone 02", thus it is the predefined value of 50 MJ/kg of methane. "Cone 03" uses a surrogate fuel gas mixture that consists of 26 volume percent of carbon dioxide and 74 volume percent of methane. This leads to roughly the same average heat of combustion than the 25 MJ/kg of "Cone 01". Also, the radiative fraction of the gas mixture was set to 0.20 to match the value of pure methane. Again, no HOC value is provided in the material definition, thus the released mass in the solid is transported directly to the gas domain. This highlights the distinction between the solid and gas phase side of the FDS simulation. FDS uses the heat of combustion parameter provided in the material definition to scale the mass of fuel that is introduced into the gas domain. Figure 23a shows the mass loss in the solid. All three cases experience a very similar development. In

figure 23b it can be observed that the mass introduced into the gas domain is about half for "Cone 01" compared to the others, due to the scaling of the HOC. Consequently, figure 24 shows about double the energy release for case "Cone 02" than the others.

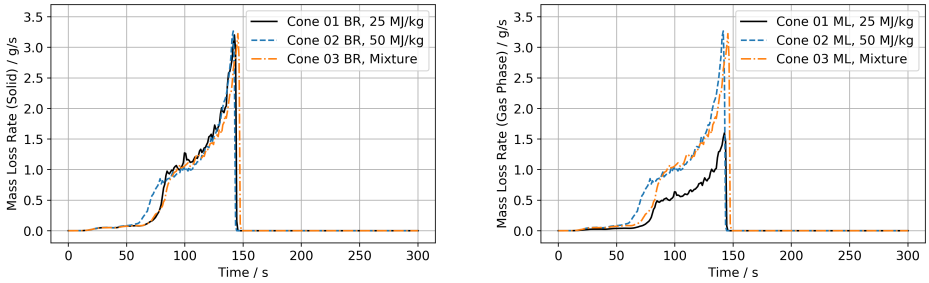

(a) Solid phase simulation.

(b) Gas phase simulation.

Figure 23: Mass loss rates for different surrogate fuel species (pyrolysis) at different locations in the same simulation. Visualising the energy release based scaling. Different heats of combustion are used as indicated, "Mixture" has a HOC of about 25.5 MJ/kg.

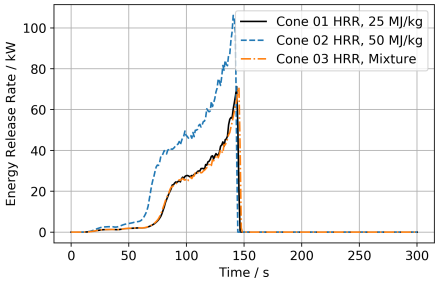

Figure 24: Energy release for different surrogate fuel species. Different heats of combustion are used as indicated, "Mixture" has a HOC of about 25.5 MJ/kg.

The different surrogate fuel strategies from above, "Cone 01" and "Cone 03", lead also to different flames. Two simulations are conducted with a constant mass release (`HRRPUA`), shown in figure 25a to mimic both setups. Gas temperatures are recorded on the vertical centre line of the flame and averaged over the second half of the simulation (30 s). This leads to differences in the flame structure as shown in figure 25b. No claim is made here as to which one is more "realistic", just the difference pointed out.

D Example Limit Adjustments

During the IMP individual parameters can get stuck at their limits. Figure 26 shows an example of this. During the initial limit definition (L0) the pyrolysis range parameter got stuck at its upper limit. Another IMP run was set up, with an expanded range (L1). Note: only the upper limit was adjusted and the lower limit was kept at its original value. Thus, the sampling space only grows larger over multiple adjustments. In the beginning, both developments are different, because not only this parameters limits are adjusted for this new run, but also for others that were stuck.

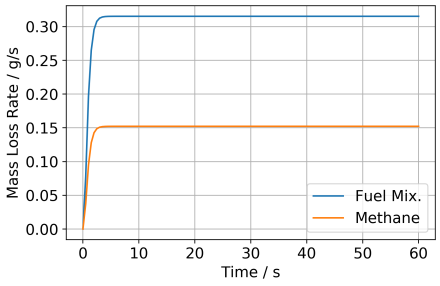

(a) Mass loss rate.

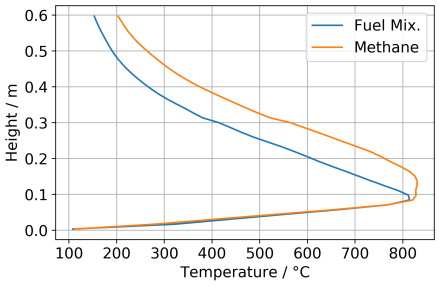

(b) Centre line temperature.

Figure 25: Simplified cone calorimeter simulation (C15) for different surrogate fuel species to compare flame heights. Mass flux adjusted to get the same energy release. Fuel mixture: methane, ethene and carbon dioxide.

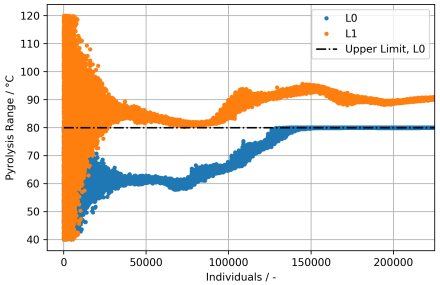

Figure 26: Example for sampling limit adjustment.

E Micro-Scale Tests

Data sets from the micro-scale tests. NIST reported that the equipment for the TGA was a Netzsch F1 Jupiter and a FAA microscale combustion calorimeter for the MCC, Sandia used a Netzsch F3 Jupiter [7].

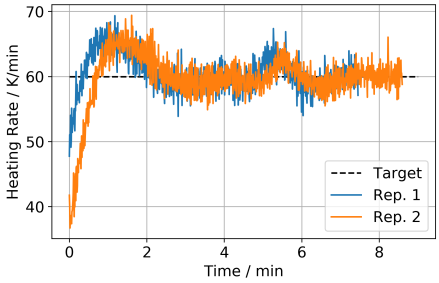

(a) MCC 60 K/min, NIST.

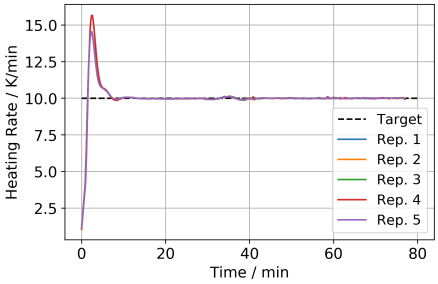

(b) TGA 10 K/min, NIST.

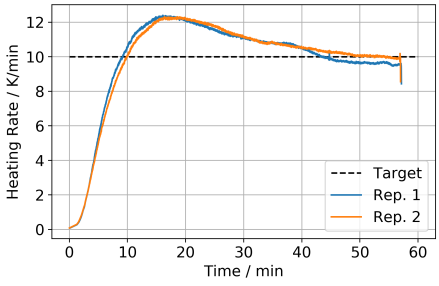

(c) TGA 10 K/min, Sandia.

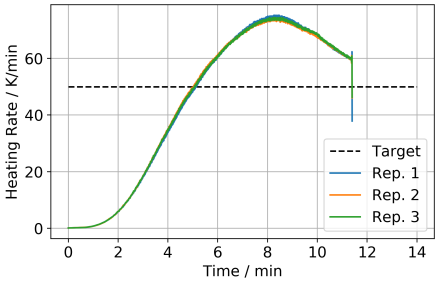

(d) TGA 50 K/min, Sandia.

Figure 27: Different heating rates of micro-scale experiments from MaCFP data base [7]

F Simple Cone Calorimeter Simulation Results

F.1 IMP Fitness Development

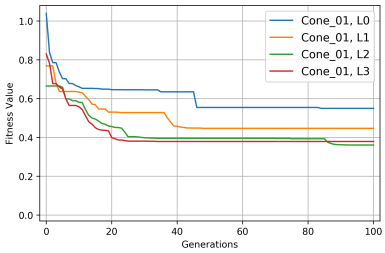

(a) IMP Setup Cone_01.

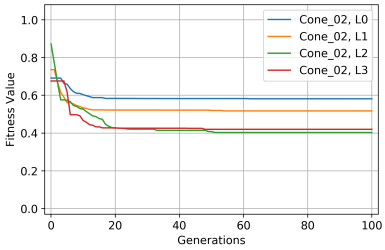

(b) IMP Setup Cone_02.

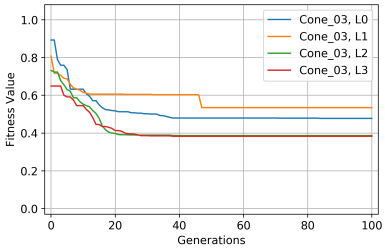

(c) IMP Setup Cone_03.

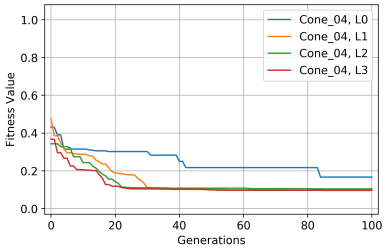

(d) IMP Setup Cone_04.

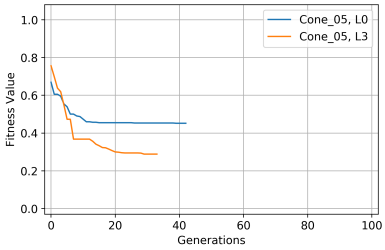

(e) IMP Setup Cone_05.

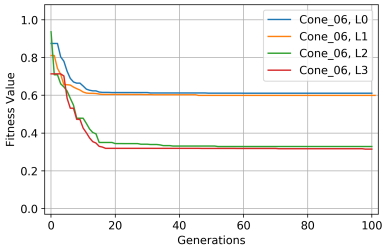

(f) IMP Setup Cone_06.

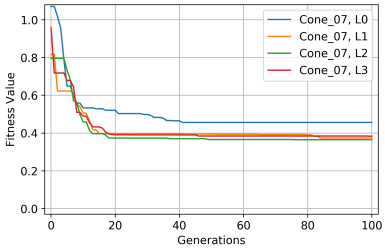

(g) IMP Setup Cone_07.

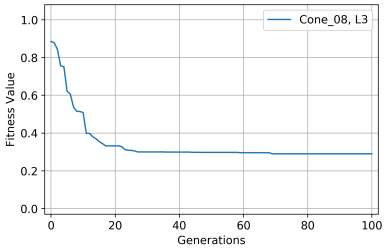

(h) IMP Setup Cone_08.

Figure 28: IMP fitness development from simplified cone calorimeter simulations at 65 kW/m².

F.2 Energy Release Rates

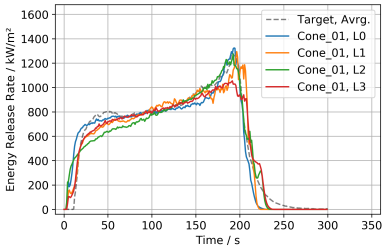

(a) IMP Setup Cone_01.

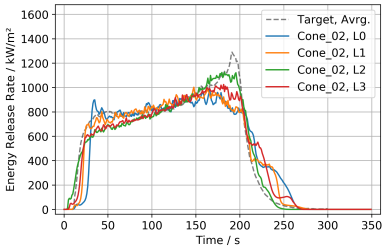

(b) IMP Setup Cone_02.

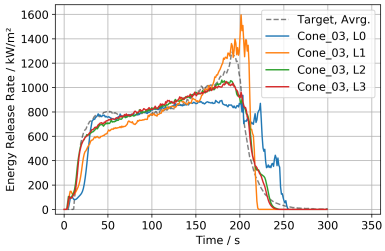

(c) IMP Setup Cone_03.

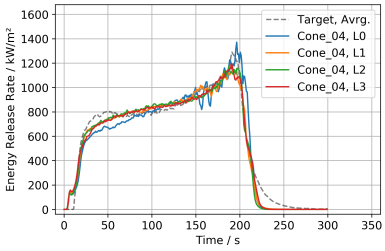

(d) IMP Setup Cone_04.

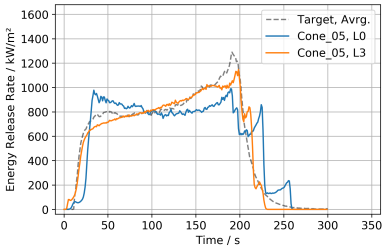

(e) IMP Setup Cone_05.

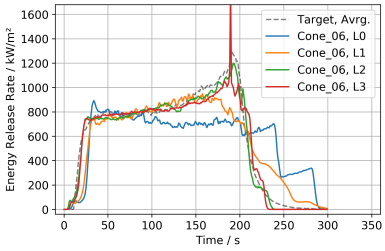

(f) IMP Setup Cone_06.

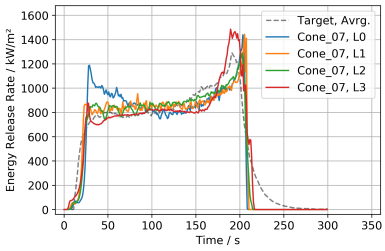

(g) IMP Setup Cone_07.

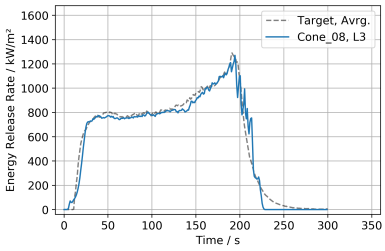

(h) IMP Setup Cone_08.

Figure 29: Energy release in simplified cone calorimeter simulation at 65 kW/m².

F.3 Back Side Temperatures

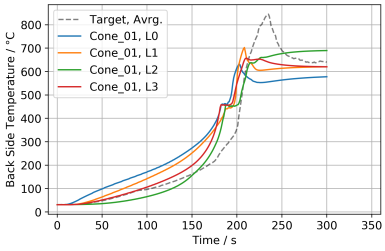

(a) IMP Setup Cone_01.

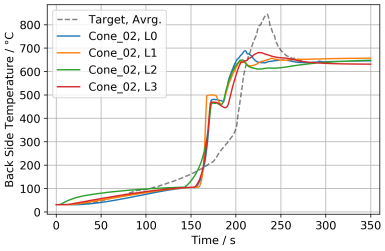

(b) IMP Setup Cone_02.

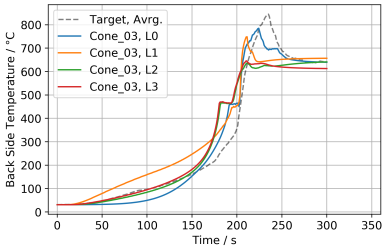

(c) IMP Setup Cone_03.

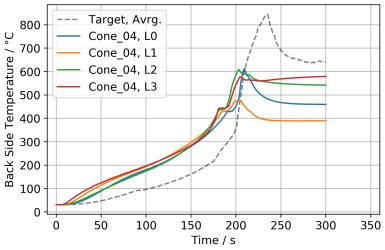

(d) IMP Setup Cone_04.

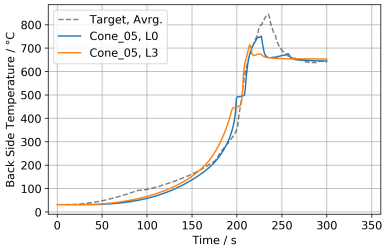

(e) IMP Setup Cone_05.

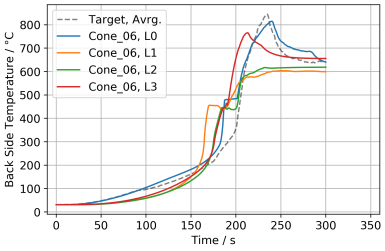

(f) IMP Setup Cone_06.

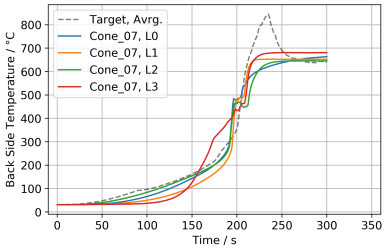

(g) IMP Setup Cone_07.

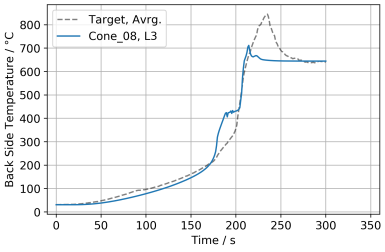

(h) IMP Setup Cone_08.

Figure 30: Back side temperature in simplified cone calorimeter simulation at 65 kW/m².

F.4 Thermal Conductivity

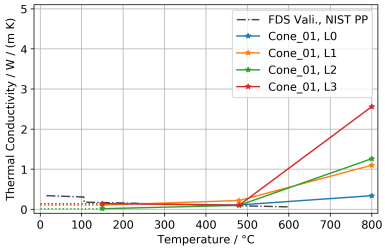

(a) IMP Setup Cone_01.

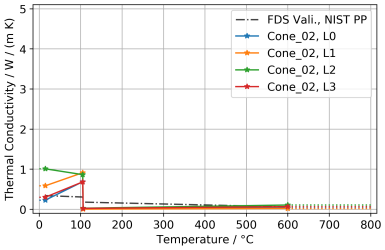

(b) IMP Setup Cone_02.

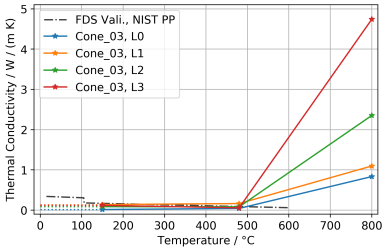

(c) IMP Setup Cone_03.

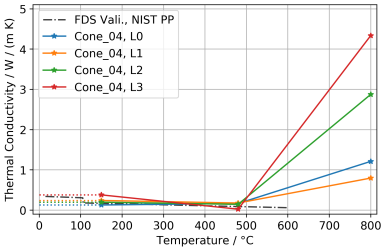

(d) IMP Setup Cone_04.

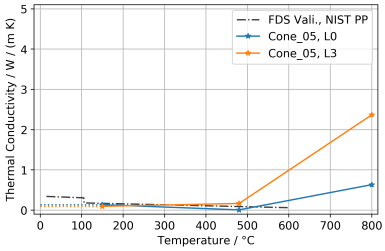

(e) IMP Setup Cone_05.

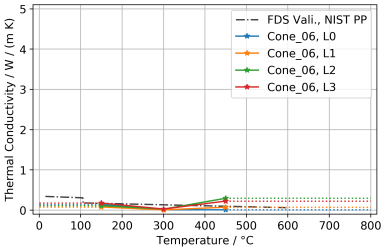

(f) IMP Setup Cone_06.

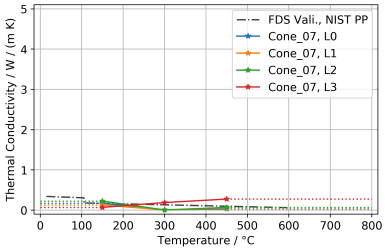

(g) IMP Setup Cone_07.

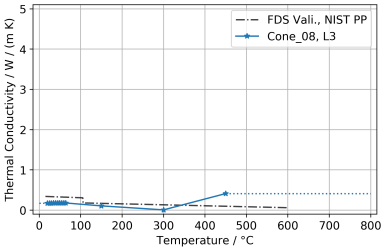

(h) IMP Setup Cone_08.

Figure 31: Thermal conductivity in simplified cone calorimeter simulation at 65 kW/m².

F.5 Specific Heat

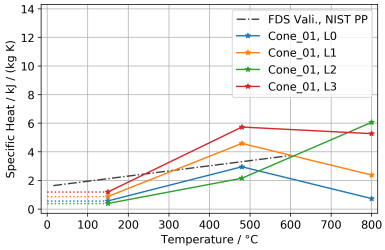

(a) IMP Setup Cone_01.

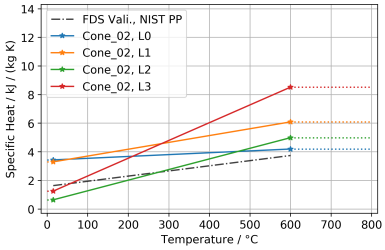

(b) IMP Setup Cone_02.

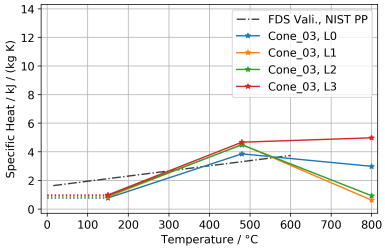

(c) IMP Setup Cone_03.

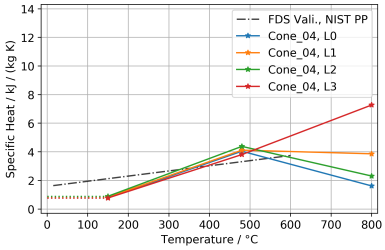

(d) IMP Setup Cone_04.

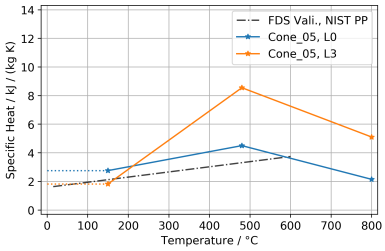

(e) IMP Setup Cone_05.

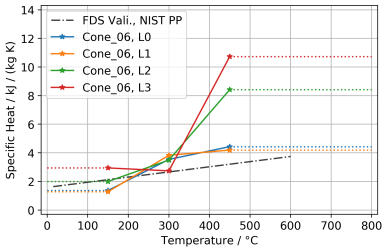

(f) IMP Setup Cone_06.

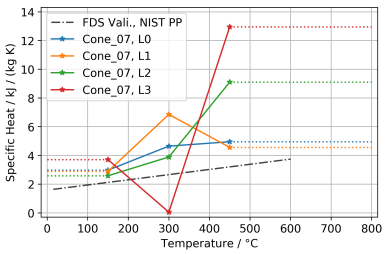

(g) IMP Setup Cone_07.

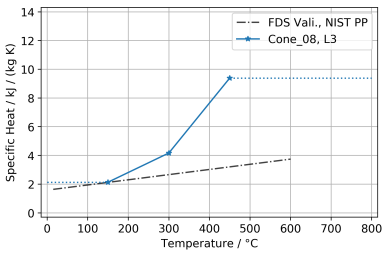

(h) IMP Setup Cone_08.

Figure 32: Specific heat in simplified cone calorimeter simulation at 65 kW/m².

F.6 Residual Sample Mass

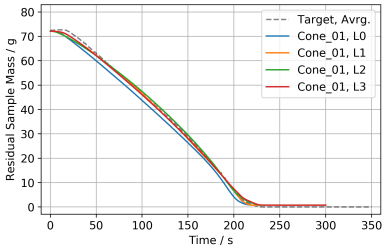

(a) IMP Setup Cone_01.

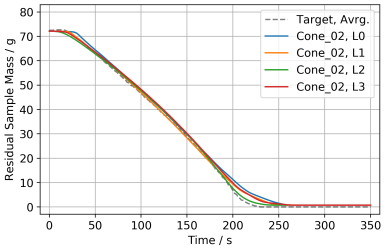

(b) IMP Setup Cone_02.

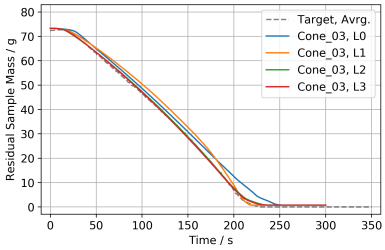

(c) IMP Setup Cone_03.

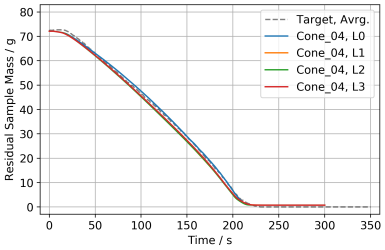

(d) IMP Setup Cone_04.

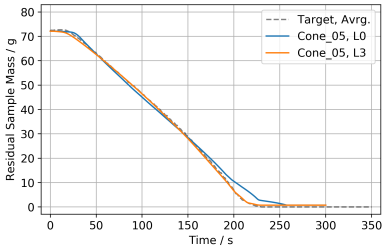

(e) IMP Setup Cone_05.

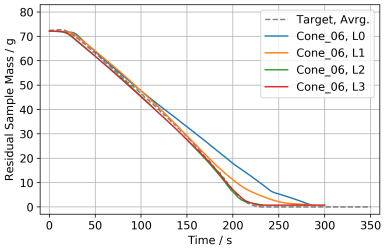

(f) IMP Setup Cone_06.

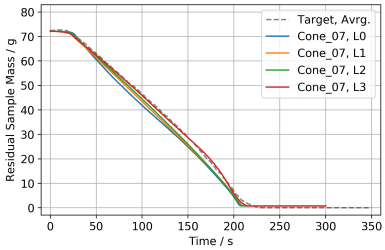

(g) IMP Setup Cone_07.

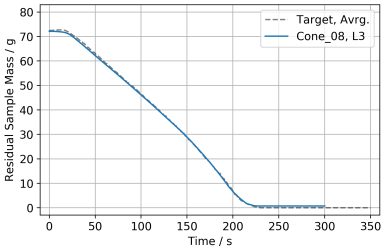

(h) IMP Setup Cone_08.

Figure 33: Residual sample mass in simplified cone calorimeter simulation at 65 kW/m².

G Simple Cone Calorimeter Simulation – Fluid Cell Convergence

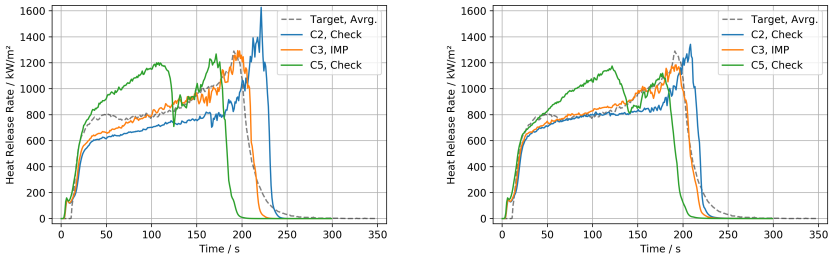

(a) Limit 0.

(b) Limit 1.

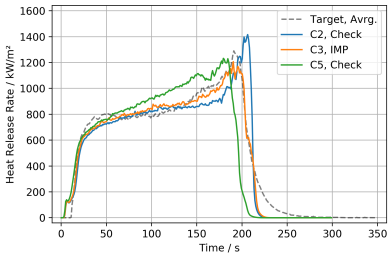

(c) Limit 2.

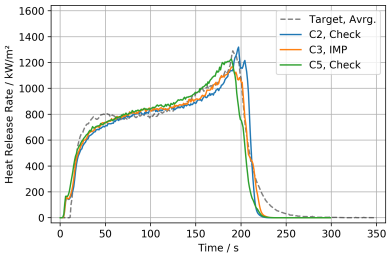

(d) Limit 3.

Figure 34: Comparison of the energy release of Cone_04 across different fluid cell resolutions for simple cone calorimeter setup. Best parameter set of IMP conducted in 3.3 cm resolution (3C), same parameter set used in 2.0 cm resolution (5C).

H Parallel Panel Simulation Results

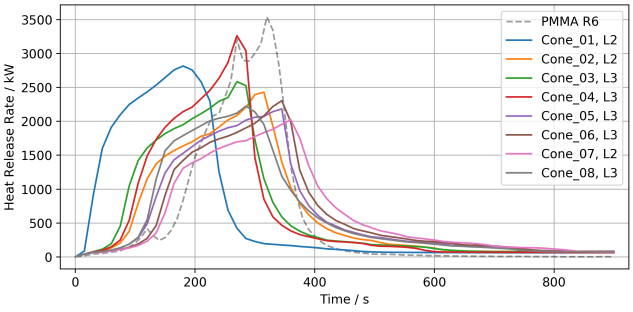

Figure 35: Comparison between experiment and simulation of the parallel panel setup for fluid cell size C3. Gas burner fuel is propane in the simulation.

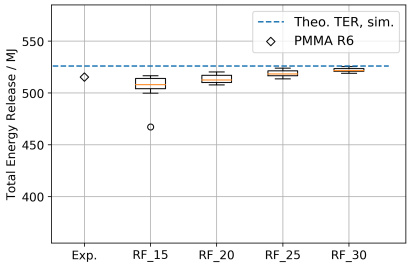

(a) Fluid cell size: 5C.

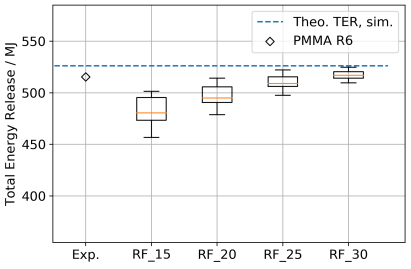

(b) Fluid cell size: 3C.

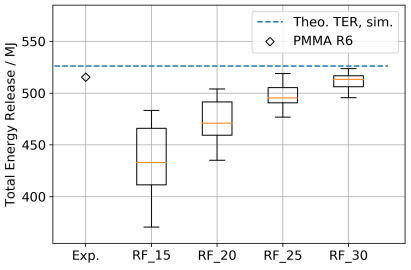

(c) Fluid cell size: 2C.

Figure 36: Total energy release (TER) of best parameter sets in parallel panel setup. Comparison between different radiative fractions (RF) and fluid cell sizes. Dashed line indicates theoretical total energy release in the simulation.

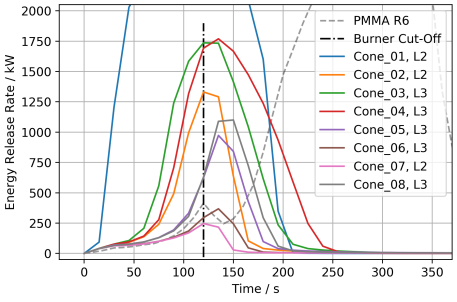

(a) Burner shut off at 120 s.

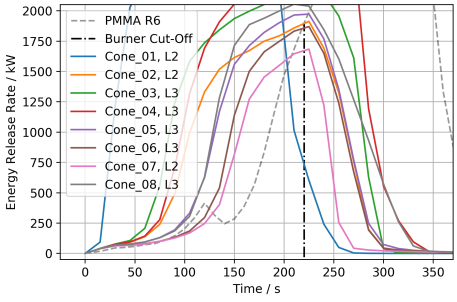

(b) Burner shut off at 220 s.

Figure 37: Parallel panel simulation with burner cut-off at 120 s and 220 s, ramp down over 6 s. Gas burner fuel is propane.

References

[1] Anna Matala. *Methods and applications of pyrolysis modelling for polymeric materials*. PhD thesis, Aalto University, Department of Mathematics and Systems Analysis Laboratory, Finland, 2013. URL http://urn.fi/URN:ISBN:978-951-38-8102-3.

[2] Yan Ding, Stanislav I. Stoliarov, and Roland H. Kraemer. Pyrolysis model development for a polymeric material containing multiple flame retardants: Relationship between heat release rate and material composition. *Combustion and Flame*, 202:43–57, 04 2019. doi:10.1016/j.combustflame.2019.01.003.

[3] Thomas Rogaume. Thermal decomposition and pyrolysis of solid fuels: Objectives, challenges and modelling. *Fire Safety Journal*, 106:177 – 188, 05 2019. doi:10.1016/j.firesaf.2019.04.016.

[4] Chris Lautenberger, Guillermo Rein, and Carlos Fernandez-Pello. The application of a genetic algorithm to estimate material properties for fire modeling from bench-scale fire test data. *Fire Safety Journal*, 41(3):204 – 214, 2006. ISSN 0379-7112. doi:https://doi.org/10.1016/j.firesaf.2005.12.004. URL http://www.sciencedirect.com/science/article/pii/S0379711205001372.

[5] Alain Alonso, Mariano Lázaro, Pedro Lázaro, David Lázaro, and Daniel Alvear. Lldpe kinetic properties estimation combining thermogravimetry and differential scanning calorimetry as optimization targets. *Journal of Thermal Analysis and Calorimetry*, 138(4):2703–2713, Nov 2019. ISSN 1588-2926. doi:10.1007/s10973-019-08199-4. URL https://doi.org/10.1007/s10973-019-08199-4.

[6] Chris Lautenberger and AC Fernandez-Pello. Optimization algorithms for material pyrolysis property estimation. *Fire Safety Science*, 10:751–764, 2011.

[7] B. Batiot, M. Bruns, S. Hostikka, I. Leventon, Y. Nakamura, P. Reszka, T. Rogaume, and S. Stoliarov. Measurement and Computation of Fire Phenomena (MaCFP) Condensed Phase Material Database. https://github.com/MaCFP/macfp-db, Commit: 7f89fd85f75cd2d4999c262f9b39f2f8109e12ef, DOI: https://doi.org/10.18434/mds2-2586.

[8] Alexandra Viitanen, Simo Hostikka, and Jukka Vaari. CFD Simulations of Fire Propagation in Horizontal Cable Trays Using a Pyrolysis Model with Stochastically Determined Geometry. *Fire Technology*, July 2022. doi:10.1007/s10694-022-01291-6.

[9] Aleksi Rinta-Paavola and Simo Hostikka. A model for the pyrolysis of two nordic structural timbers. *Fire and Materials*, 46(1):55–68, 2022. doi:10.1002/fam.2947. URL https://onlinelibrary.wiley.com/doi/abs/10.1002/fam.2947.

[10] Tristan Hehnen, Lukas Arnold, and Saverio La Mendola. Numerical Fire Spread Simulation Based on Material Pyrolysis – An Application to the CHRISTIFIRE Phase 1 Horizontal Cable Tray Tests. *Fire*, 3(3), 2020. ISSN 2571-6255. doi:10.3390/fire3030033. URL https://www.mdpi.com/2571-6255/3/3/33.

[11] Simo Hostikka and Anna Matala. Pyrolysis model for predicting the heat release rate of birch wood. *Combustion Science and Technology*, 189(8):1373–1393, 8 2017. ISSN 0010-2202. doi:10.1080/00102202.2017.1295959.

[12] Alain Alonso, David Lázaro, Mariano Lázaro, and Daniel Alvear. Numerical prediction of cables fire behaviour using non-metallic components in cone calorimeter. *Combustion Science and Technology*, 0(0):1–17, 2023. doi:10.1080/00102202.2023.2182198. URL https://doi.org/10.1080/00102202.2023.2182198.

[13] Kevin McGrattan, Simo Hostikka, Jason Floyd, Randall McDermott, and Marcos Vanella. *Fire Dynamics Simulator User's Guide*, 05 2021.

[14] Khalid Moinuddin, Qazi Samia Razzaque, and Ananya Thomas. Numerical simulation of coupled pyrolysis and combustion reactions with directly measured fire properties. *Polymers*, 12(9), 2020. ISSN 2073-4360. doi:10.3390/polym12092075. URL https://www.mdpi.com/2073-4360/12/9/2075.

[15] P. Boulet, G. Parent, Z. Acem, T. Rogaume, T. Fateh, J. Zaida, and F. Richard. Characterization of the radiative exchanges when using a cone calorimeter for the study of the plywood pyrolysis. *Fire Safety Journal*, 51: 53–60, 2012. ISSN 0379-7112. doi:10.1016/j.firesaf.2012.03.003. URL https://www.sciencedirect.com/science/article/pii/S037971121200046X.

[16] Simo Hostikka and Jesper Axelsson. Modelling of the radiative feedback from the flames in cone calorimeter. Technical report, NORDTEST, 2003. URL https://www.nordtest.info/wp/2003/10/02/modelling-of-the-radiative-feedback-from-the-flames-in-cone-calorimeter-nt-tr-540/.

[17] Lukas Arnold, Tristan Hehnen, Patrick Lauer, Corinna Trettin, and Ashish Vinayak. PROPTI – A Generalised Inverse Modelling Framework. In *Journal of Physics: Conference Series*, volume 1107, page 032016. IOP Publishing, 2018.

[18] Lukas Arnold, Tristan Hehnen, Patrick Lauer, Corinna Trettin, and Ashish Vinayak. Application cases of inverse modelling with the PROPTI framework. *Fire Safety Journal*, page 102835, 2019. ISSN 0379-7112. doi:10.1016/j.firesaf.2019.102835. URL http://www.sciencedirect.com/science/article/pii/S0379711219300438.

[19] Lukas Arnold, Tristan Hehnen, Patrick Lauer, Corinna Trettin, and Ashish Vinayak. PROPTI. Technical report, Forschungszentrum Jülich and Bergische Universität Wuppertal, Germany, March 2018. URL https://zenodo.org/record/1438349.

[20] Tobias Houska, Philipp Kraft, Alejandro Chamorro-Chavez, and Lutz Breuer. Spotting model parameters using a ready-made python package. *PLoS ONE*, 10:e0145180, 12 2015. URL doi:10.1371/journal.pone.0145180.

[21] I.T. Leventon, M.V. Heck, K.B. McGrattan, M.F. Bundy, and R.D. Davis. Experimental Measurements for Fire Model Validation - Parallel Panel Tests on PMMA. https://github.com/MaCFP/macfp-db/tree/master/Fire_Growth/NIST_Parallel_Panel, Commit: 25614bd527b658fca72265ed2940ea1287e83343, DOI: https://doi.org/10.18434/mds2-2812.

[22] Kevin McGrattan, Simo Hostikka, Jason Floyd, Randall McDermott, and Marcos Vanella. *Fire Dynamics Simulator Technical Reference Guide Volume 3: Validation*, 05 2021.

[23] Tristan Hehnen and Lukas Arnold. PMMA Pyrolysis Simulation – from Micro- to Real-Scale – Dataset. Technical report, Forschungszentrum Jülich and Bergische Universität Wuppertal, Germany, January 2023. URL https://zenodo.org/record/7065338.

[24] Tristan Hehnen. PMMA Pyrolysis and Fire Propagation in FDS. *www.youtube.com/@firesimandcoding; www.youtube.com/playlist?list=PLWziITJoPnJKtVuaVudyO2Lz-OWaCE9Co*, 2022.

[25] O.P. Korobeinichev, A.A. Paletsky, M.B. Gonchikzhapov, R.K. Glaznev, I.E. Gerasimov, Y.K. Naganovsky, I.K. Shundrina, A.Yu. Snegirev, and R. Vinu. Kinetics of thermal decomposition of PMMA at different heating rates and in a wide temperature range. *Thermochimica Acta*, 671:17–25, 2019. ISSN 0040-6031. doi:10.1016/j.tca.2018.10.019. URL https://www.sciencedirect.com/science/article/pii/S0040603118303460.

[26] Ian C. McNeill. Products of Thermal Degradation in Polymer Systems Based on Methyl Methacrylate. *International Journal of Polymeric Materials and Polymeric Biomaterials*, 24(1-4):31–45, 1994. doi:10.1080/00914039408028548.

[27] W. R. Zeng, S. F. Li, and W. K. Chow. Review on chemical reactions of burning poly(methyl methacrylate) pmma. *Journal of Fire Sciences*, 20(5):401–433, September 2002. doi:10.1177/0734904102020005482.

[28] Graig T. Bowman. Non-equilibirum radical concentrations in shock-initiated methane oxidation. *Fire Safety Journal*, page 102835, 2019. ISSN 0379-7112. doi:10.1016/j.firesaf.2019.102835. URL http://www.sciencedirect.com/science/article/pii/S0379711219300438.

[29] Victor P. Zhukov and Alan F. Kong. A compact reaction mechanism of methane oxidation at high pressures. *Progress in Reaction Kinetics and Mechanism*, 43(1):62–78, 2018. doi:10.3184/146867818X15066862094914. URL https://doi.org/10.3184/146867818X15066862094914.

[30] Victor P. Zhukov, V. A. Sechenov, and A. Yu. Starikovskii. Autoignition of a lean propane-air mixture at high pressures. *Kinetics and Catalysis*, 46(3):319–327, 2005. doi:10.1007/s10975-005-0079-7. URL https://doi.org/10.1007/s10975-005-0079-7.

[31] C.K. Westbrook, W.J. Pitz, J.E. Boercker, H.J. Curran, J.F. Griffiths, C. Mohamed, and M. Ribaucour. Detailed chemical kinetic reaction mechanisms for autoignition of isomers of heptane under rapid compression. *Proceedings of the Combustion Institute*, 29(1):1311–1318, 2002. ISSN 1540-7489. doi:10.1016/S1540-7489(02)80161-4. URL https://www.sciencedirect.com/science/article/pii/S1540748902801614. Proceedings of the Combustion Institute.

[32] H. G. Wolfhard and W. G. Parker. A new technique for the spectroscopic examination of flames at normal pressures. *Proceedings of the Physical Society. Section A*, 62(11):722–730, nov 1949. doi:10.1088/0370-1298/62/11/305.

[33] Henry J. Curran. Developing detailed chemical kinetic mechanisms for fuel combustion. *Proceedings of the Combustion Institute*, 37(1):57–81, 2019. ISSN 1540-7489. doi:10.1016/j.proci.2018.06.054. URL https://www.sciencedirect.com/science/article/pii/S1540748918302372.

[34] Gregory J. Fiola, Dushyant M. Chaudhari, and Stanislav I. Stoliarov. Comparison of Pyrolysis Properties of Extruded and Cast Poly(methyl methacrylate). *Fire Safety Journal*, 120, 2021. ISSN 0379-7112. doi:https://doi.org/10.1016/j.firesaf.2020.103083. URL https://www.sciencedirect.com/science/article/pii/S0379711219307301. Fire Safety Science: Proceedings of the 13th International Symposium.

[35] James G. Quintiere. *Principles of Fire Behavior, Second Edition*. CRC Press, 2017. ISBN 9781498735629.

[36] Vyto Babrauskas. Development of the Cone Calorimeter: A Bench-Scale Heat Release Rate Apparatus Based on Oxygen Consumption. Technical report, National Institute of Standards and Technology, Gaithersburg, MD, 1982-11-01 1982.

[37] ISO 5660-1:2015(E) — Part 1: Heat release rate (cone calorimeter method) and smoke production rate. *ISO*, 2015.

[38] Fabian Brännström. Application of fire simulation within the railway industry. In *14th International Conference and Exhibition on Fire Science and Engineering*. Interflam, July 2016.

[39] Qingyun Duan, Vijai K. Gupta, and Soroosh Sorooshian. Shuffled complex evolution approach for effective and efficient global minimization. *Journal of optimization theory and applications*, 76(3):501–521, 1993.

[40] Angus Elliott, Alastair Temple, Cristian Maluk, and Luke Bisby. Novel Testing to Study the Performance of Intumescent Coatings under Non-Standard Heating Regimes. In *Fire Safety Science*, volume 11, pages 652–665, 02 2014. doi:10.3801/IAFSS.FSS.11-652.

[41] B. Hajduk, H. Bednarski, P. Jarka, H. Janeczek, M. Godzierz, and T. Tański. Thermal and optical properties of PMMA films reinforced with Nb2o5 nanoparticles. *Scientific Reports*, 11, 2021. doi:https://doi.org/10.1038/s41598-021-01282-7. URL `https://www.nature.com/articles/s41598-021-01282-7`.

[42] Jülich Supercomputing Centre. JURECA: Data Centric and Booster Modules implementing the Modular Supercomputing Architecture at Jülich Supercomputing Centre. *Journal of large-scale research facilities*, 7(A182), 2021. doi:10.17815/jlsrf-7-182. URL `http://dx.doi.org/10.17815/jlsrf-7-182`.

Bibliography

[1] Tristan Hehnen et al. "Simulation of Fire Propagation in Cable Tray Installations for Particle Accelerator Facility Tunnels". In: *Proceedings from the 8th International Symposium on Tunnel Safety and Security ISTSS 2018*. Borås, Sweden: RISE Research Institutes of Sweden, Mar. 2018.

[2] Tristan Hehnen, Lukas Arnold, and Saverio La Mendola. "Numerical Fire Spread Simulation Based on Material Pyrolysis—An Application to the CHRISTIFIRE Phase 1 Horizontal Cable Tray Tests". In: *Fire* 3.3 (2020). ISSN: 2571-6255. URL: https://www.mdpi.com/2571-6255/3/3/33.

[3] Tristan Hehnen and Lukas Arnold. "PMMA pyrolysis simulation – from micro- to real-scale". In: *Fire Safety Journal* 141 (2023), p. 103926. ISSN: 0379-7112. DOI: https://doi.org/10.1016/j.firesaf.2023.103926. URL: https://www.sciencedirect.com/science/article/pii/S0379711223001947.

[4] Morgan J. Hurley et al. *SFPE Handbook of Fire Protection Engineering, fifth edition*. Springer-Verlag New York, Nov. 2016, pp. 1–3493. ISBN: 978-1-4939-2564-3. DOI: 10.1007/978-1-4939-2565-0.

[5] Björn Karlsson and James G. Quintiere. *Enclosure Fire Dynamics*. CRC Press, 1999. ISBN: 9780849313004.

[6] Dougal Drysdale. *An Introduction to Fire Dynamics*. Second. Southern Gate, Chichester, West Sussex PO19 8 Q, England: John Wiley & Sons, 1998.

[7] S. Simcox, N.S. Wilkes, and I.P. Jones. "Computer simulation of the flows of hot gases from the fire at King's Cross Underground station". In: *Fire Safety Journal* 18.1 (1992). Special Issue: The King's Cross Underground Fire, pp. 49–73. ISSN: 0379-7112. DOI: https://doi.org/10.1016/0379-7112(92)90047-G. URL: https://www.sciencedirect.com/science/article/pii/037971129290047G.

[8] D.D. Drysdale, A.J.R. Macmillan, and D. Shilitto. "The King's Cross fire: Experimental verification of the 'Trench effect'". In: *Fire Safety Journal* 18.1 (1992). Special Issue: The King's Cross Underground Fire, pp. 75–82. ISSN: 0379-7112. DOI: https://doi.org/10.1016/0379-7112(92)90048-H. URL: https://www.sciencedirect.com/science/article/pii/037971129290048H.

[9] H. G. Wolfhard and W. G. Parker. "A New Technique for the Spectroscopic Examination of Flames at Normal Pressures". In: *Proceedings of the Physical Society. Section A* 62.11 (Nov. 1949), pp. 722–730. DOI: 10.1088/0370-1298/62/11/305.

[10] David Morrisset, Rory M. Hadden, and Angus Law. "Quantifying the controlling mechanisms of opposed flow flame spread: Influence of orientation, material, and external heating". In: *Fire Safety Journal* 142 (2024), p. 104048. ISSN: 0379-7112. DOI: https://doi.org/10.1016/j.firesaf.2023.104048. URL: https://www.sciencedirect.com/science/article/pii/S0379711223003168.

[11] Charles H Spink. "Differential scanning calorimetry". In: *Methods in Cell Biology* 84 (2008). Review article, pp. 115–141. DOI: 10.1016/S0091-679X(07)84005-2.

[12] Richard E. Lyon and Richard N. Walters. "Pyrolysis combustion flow calorimetry". English. In: *Journal of Analytical and Applied Pyrolysis* 71.1 (2004), pp. 27–46. DOI: 10.1016/S0165-2370(03)00096-2.

[13] Richard E Lyon and Richard N Walters. "Pyrolysis combustion flow calorimetry". In: *Journal of Analytical and Applied Pyrolysis* 71.1 (2004). Practical Applications of Analytical Pyrolysis (special section), pp. 27–46. ISSN: 0165-2370. DOI: https://doi.org/10.1016/S0165-2370(03)00096-2. URL: https://www.sciencedirect.com/science/article/pii/S0165237003000962.

[14] Philip W. West. "Inorganic thermogravimetric analysis". In: *Journal of Chemical Education* 31.6 (1954), p. 334. DOI: 10.1021/ed031p334.1. eprint: https://doi.org/10.1021/ed031p334.1. URL: https://doi.org/10.1021/ed031p334.1.

[15] A. W. Coats and J. P. Redfern. "Thermogravimetric analysis. A review". In: *Analyst* 88 (1053 1963), pp. 906–924. DOI: 10.1039/AN9638800906. URL: http://dx.doi.org/10.1039/AN9638800906.

[16] Vyto Babrauskas. *Development of the Cone Calorimeter: A Bench-Scale Heat Release Rate Apparatus Based on Oxygen Consumption*. en. Tech. rep. 1982-11-01 1982.

[17] Joshua D. Swann et al. "Controlled atmosphere pyrolysis apparatus II (CAPA II): A new tool for analysis of pyrolysis of charring and intumescent polymers". In: *Fire Safety Journal* 91 (2017). Fire Safety Science: Proceedings of the 12th International Symposium, pp. 130–139. ISSN: 0379-7112. DOI: https://doi.org/10.1016/j.firesaf.2017.03.038. URL: https://www.sciencedirect.com/science/article/pii/S0379711217300541.

[18] Anna Matala. "Methods and applications of pyrolysis modelling for polymeric materials". en. PhD thesis. Aalto University, Department of Mathematics and Systems Analysis Laboratory, Finland, 2013, 85 + app. 87. URL: http://urn.fi/URN:ISBN:978-951-38-8102-3.

[19] Chris Lautenberger, Guillermo Rein, and Carlos Fernandez-Pello. "The application of a genetic algorithm to estimate material properties for fire modeling from bench-scale fire test data". In: *Fire Safety Journal* 41.3 (2006), pp. 204–214. ISSN: 0379-7112. DOI: https://doi.org/10.1016/j.firesaf.2005.12.004. URL: http://www.sciencedirect.com/science/article/pii/S0379711205001372.

[20] Aleksi Rinta-Paavola and Simo Hostikka. "A model for the pyrolysis of two Nordic structural timbers". In: *Fire and Materials* 46.1 (2022), pp. 55–68. DOI: 10.1002/fam.2947. URL: https://onlinelibrary.wiley.com/doi/abs/10.1002/fam.2947.

[21] Alexandra Viitanen, Simo Hostikka, and Jukka Vaari. "CFD Simulations of Fire Propagation in Horizontal Cable Trays Using a Pyrolysis Model with Stochastically Determined Geometry". In: *Fire Technology* (July 2022). DOI: 10.1007/s10694-022-01291-6.

[22] Patrick Lauer et al. "Performance of Optimization Algorithms for Deriving Material Data from Bench Scale Tests". In: *Fire and Evacuation Modelling Technical Conference 2016* (2016).

[23] Matala A., Hostikka S., and Mangs J. "Estimation of pyrolysis model parameters for solid materials using thermogravimetric data". In: *Fire Safety Science*. Vol. 9. 2008, pp. 1213–1223. DOI: 10.3801/IAFSS.FSS.9-1213.

[24] Chris Lautenberger and Carlos Fernandez-Pello. "Generalized pyrolysis model for combustible solids". In: *Fire Safety Journal* 44.6 (2009), pp. 819–839. ISSN: 0379-7112. DOI: https://doi.org/10.1016/j.firesaf.2009.03.011. URL: https://www.sciencedirect.com/science/article/pii/S0379711209000332.

[25] Lukas Arnold et al. "Application cases of inverse modelling with the PROPTI framework". In: *Fire Safety Journal* (2019), p. 102835. ISSN: 0379-7112. DOI: https://doi.org/10.1016/j.firesaf.2019.102835. URL: http://www.sciencedirect.com/science/article/pii/S0379711219300438.

[26] Lukas Arnold et al. "PROPTI – A Generalised Inverse Modelling Framework". In: *Journal of Physics: Conference Series*. Vol. 1107. IOP Publishing. 2018, p. 032016.

[27] Lukas Arnold et al. *PROPTI*. Mar. 2018. DOI: 10.5281/zenodo.1438349. URL: https://zenodo.org/record/1438349.

[28] Kevin B. McGrattan et al. *Cable Heat Release, Ignition, and Spread in Tray Installations during Fire (CHRISTIFIRE): Phase 1 - Horizontal Trays*. Contractor Report, NUREG/CR-7010, Vol. 1. Office of Nuclear Regulatory Research, July 2012.

[29] Kevin B. McGrattan and Scott D. Bareham. *Cable Heat Release, Ignition, and Spread in Tray Installations during Fire (CHRISTIFIRE): Phase 2 - Vertical Shafts and Corridors*. Contractor Report, NUREG/CR-7010, Vol. 2. Office of Nuclear Regulatory Research, Sept. 2013.

[30] B. Batiot et al. *Measurement and Computation of Fire Phenomena (MaCFP) Database*. https://github.com/MaCFP/macfp-db.

[31] B. Batiot et al. *Measurement and Computation of Fire Phenomena (MaCFP) Condensed Phase Material Database*. github.com/MaCFP/macfp-db, Commit: 7f89fd8, DOI: https://doi.org/10.18434/mds2-2586. 2022.

[32] Qingyun Duan, Soroosh Sorooshian, and Vijai Gupta. "Effective and efficient global optimization for conceptual rainfall-runoff models". In: *Water Resources Research* 28.4 (1992), pp. 1015–1031. DOI: https://doi.org/10.1029/91WR02985. URL: https://agupubs.onlinelibrary.wiley.com/doi/abs/10.1029/91WR02985.

[33] Qingyun Duan, Vijai Gupta, and Soroosh Sorooshian. "Shuffled complex evolution approach for effective and efficient global minimization". In: *Journal of Optimization Theory and Applications* 76.3 (1993), pp. 501–521. DOI: https://doi.org/10.1007/BF00939380.

[34] Qingyun Duan, Soroosh Sorooshian, and Vijai Gupta. "Optimal use of the SCE-UA global optimization method for calibrating watershed models". In: *Journal of hydrology* 158.3-4 (1994), pp. 265–284.

[35] Tobias Houska et al. "SPOTting Model Parameters Using a Ready-Made Python Package". In: *PLoS ONE* 10 (Dec. 2015), e0145180. URL: doi:10.1371/journal.pone.0145180.

[36] Kevin McGrattan et al. "Fire Dynamics Simulator User's Guide, FDS 6.7.6". In: *NIST Special Publication 1019, Sixth Edition* (June 2021). DOI: http://dx.doi.org/10.6028/NIST.SP.1019. URL: https://github.com/firemodels/fds/releases/tag/FDS6.7.6.

[37] Kevin McGrattan et al. "Fire Dynamics Simulator Technical Reference Guide Volume 1: Mathematical Model, FDS 6.7.6". In: *NIST Special Publication 1018-1, Sixth Edition* (June 2021). DOI: http://dx.doi.org/10.6028/NIST.SP.1018. URL: https://github.com/firemodels/fds/releases/tag/FDS6.7.6.

[38] Kevin McGrattan et al. "Fire Dynamics Simulator Technical Reference Guide Volume 2: Verification, FDS 6.7.6". In: *NIST Special Publication 1018-2, Sixth Edition* (June 2021). DOI: http://dx.doi.org/10.6028/NIST.SP.1018. URL: https://github.com/firemodels/fds/releases/tag/FDS6.7.6.

[39] Kevin McGrattan et al. "Fire Dynamics Simulator Technical Reference Guide Volume 3: Validation, FDS 6.7.6". In: *NIST Special Publication 1018-3, Sixth Edition* (June 2021). DOI: http://dx.doi.org/10.6028/NIST.SP.1018. URL: https://github.com/firemodels/fds/releases/tag/FDS6.7.6.

[40] Kevin McGrattan et al. *Fire Dynamics Simulator Users Guide, Sixth Edition*. Gaithersburg, Maryland: National Institute of Standards and Technology (NIST), Nov. 2015.

[41] Chris Lautenberger and AC Fernandez-Pello. "Optimization algorithms for material pyrolysis property estimation". In: *Fire Safety Science* 10 (2011), pp. 751–764.

[42] Anna Matala and Simo Hostikka. "Pyrolysis Modelling of PVC Cable Materials". In: *Fire Safey Science – Proceedings of the Tenth International Symposium*. DOI: 10.3801/IAFSS.FSS.10-917.

[43] Kevin McGrattan et al. *Fire Dynamics Simulator Users Guide, Sixth Edition*. Gaithersburg, Maryland: National Institute of Standards and Technology (NIST), Jan. 2017. URL: https://github.com/firemodels/fds/releases/download/FDS6.5.3/FDS_User_Guide.pdf.

[44] Tarek Beji and Bart Merci. "Numerical simulations of a full-scale cable tray fire using small-scale test data". In: *Fire and Materials* 43.5 (2019), pp. 486–496. DOI: https://doi.org/10.1002/fam.2687. eprint: https://onlinelibrary.wiley.com/doi/pdf/10.1002/fam.2687. URL: https://onlinelibrary.wiley.com/doi/abs/10.1002/fam.2687.

[45] P. Boulet et al. "Characterization of the radiative exchanges when using a cone calorimeter for the study of the plywood pyrolysis". In: *Fire Safety Journal* 51 (2012), pp. 53–60. ISSN: 0379-7112. DOI: 10.1016/j.firesaf.2012.03.003. URL: https://www.sciencedirect.com/science/article/pii/S037971121200046X.

[46] Simo Hostikka and Jesper Axelsson. *Modelling of the radiative feedback from the flames in cone calorimeter*. English. Tech. rep. NORDTEST, 2003. URL: https://www.nordtest.info/wp/2003/10/02/modelling-of-the-radiative-feedback-from-the-flames-in-cone-calorimeter-nt-tr-540/.

[47] Fabian Brännström. "Application of fire simulation within the railway industry". In: *14th International Conference and Exhibition on Fire Science and Engineering*. Interflam, July 2016.

[48] Simo Hostikka and Anna Matala. "Pyrolysis Model for Predicting the Heat Release Rate of Birch Wood". English. In: *Combustion Science and Technology* 189.8 (Aug. 2017), pp. 1373–1393. ISSN: 0010-2202. DOI: 10.1080/00102202.2017.1295959.

[49] Mark B. McKinnon and Stanislav I. Stoliarov. "Pyrolysis Model Development for a Multilayer Floor Covering". In: *Materials* 8.9 (2015), pp. 6117–6153. ISSN: 1996-1944. DOI: 10.3390/ma8095295. URL: https://www.mdpi.com/1996-1944/8/9/5295.

[50] Elena Roda et al. "Flame behaviour of magnesium and aluminium hydroxide-filled polymer composites used in power and telecom cables". In: *Plastics, Rubber and Composites* 51.4 (2022), pp. 185–195. DOI: 10.1080/14658011.2021.1962617. URL: https://doi.org/10.1080/14658011.2021.1962617.

[51] A.Yu. Snegirev. "Generalized approach to model pyrolysis of flammable materials". In: *Thermochimica Acta* 590 (2014), pp. 242–250. ISSN: 0040-6031. DOI: https://doi.org/10.1016/j.tca.2014.07.009.

[52] A. Brown et al. "Proceedings of the first workshop organized by the IAFSS Working Group on Measurement and Computation of Fire Phenomena (MaCFP)". In: *Fire Safety Journal* 101 (2018), pp. 1–17. ISSN: 0379-7112. DOI: https://doi.org/10.1016/j.firesaf.2018.08.009. URL: https://www.sciencedirect.com/science/article/pii/S0379711218301814.

[53] Gregory J. Fiola, Dushyant M. Chaudhari, and Stanislav I. Stoliarov. "Comparison of Pyrolysis Properties of Extruded and Cast Poly(methyl methacrylate)". In: *Fire Safety Journal* 120 (2021). Fire Safety Science: Proceedings of the 13th International Symposium. ISSN: 0379-7112. DOI: https://doi.org/10.1016/j.firesaf.2020.103083. URL: https://www.sciencedirect.com/science/article/pii/S0379711219307301.

[54] W. R. Zeng, S. F. Li, and W. K. Chow. "Review on Chemical Reactions of Burning Poly(methyl methacrylate) PMMA". In: *Journal of Fire Sciences* 20.5 (Sept. 2002), pp. 401–433. DOI: 10.1177/0734904102020005482.

[55] I.T. Leventon et al. *Experimental Measurements for Fire Model Validation - Parallel Panel Tests on PMMA*. https://github.com/MaCFP/macfp-db/tree/master/Fire_Growth/NIST_Parallel_Panel, Commit: 25614bd527b658fca72265ed2940ea1287e83343, DOI: https://doi.org/10.18434/mds2-2812.

[56] Isaac Leventon et al. *The Impact of Material Composition on Ignitability and Fire Growth. Volume 1: Full-Scale Burning Behavior of Combustible Solids Commonly Found in Nuclear Power Plants*. Tech. rep. Feb. 2024. DOI: https://doi.org/10.6028/NIST.TN.2282. URL: https://tsapps.nist.gov/publication/get_pdf.cfm?pub_id=933472.

[57] Vytenis Babrauskas and Richard D. Peacock. "Heat release rate: The single most important variable in fire hazard". In: *Fire Safety Journal* 18.3 (1992), pp. 255–272. ISSN: 0379-7112. DOI: https://doi.org/10.1016/0379-7112(92)90019-9. URL: https://www.sciencedirect.com/science/article/pii/0379711292900199.

[58] James G. Quintiere. *Principles of Fire Behavior, Second Edition*. CRC Press, 2017. ISBN: 9781498735629.

[59] T. Hirata, Takashi Kashiwagi, and J. E. Brown. "Thermal and oxidative degradation of poly(methyl methacrylate): weight loss". In: *Macromolecules* 18.7 (1985), pp. 1410–1418. DOI: 10.1021/ma00149a010. eprint: https://doi.org/10.1021/ma00149a010. URL: https://doi.org/10.1021/ma00149a010.

[60] T. Kashiwagi, A. Inaba, and J.E. Brown. "Differences In PMMA Degradation Characteristics And Their Effects On Its Fire Properties – 11th IAFSS Symposium". In: *Fire Safety Science* 1 (1986), pp. 483–493. DOI: https://doi.org/10.3801/IAFSS.FSS.1-483. URL: https://publications.iafss.org/publications/fss/1/483.

[61] Tristan Hehnen, Tássia L.S. Quaresma, and Lukas Arnold. "Flame Spread Simulation Over PMMA Panels, Controlled by Material Pyrolysis – MaCFP-3 Poster". In: *IAFSS, 14th International Symposium on Fire Safety Science 2023, Tsukuba, Japan*. DOI: 10.5281/zenodo.10076479. URL: https://doi.org/10.5281/zenodo.10076479.

[62] Yan Ding et al. "Determination of kinetics and thermodynamics of thermal decomposition for polymers containing reactive flame retardants: Application to poly(lactic acid) blended with melamine and ammonium polyphosphate". In: *Polymer Degradation and Stability* 129 (2016), pp. 347–362. ISSN: 0141-3910. DOI: https://doi.org/10.1016/j.polymdegradstab.2016.05.014.

[63] K. De Lannoye et al. "The influence of experimental conditions on the mass loss for TGA in fire safety science". In: *Fire Safety Journal* 144 (2024), p. 104079. ISSN: 0379-7112. DOI: https://doi.org/10.1016/j.firesaf.2023.104079. URL: https://www.sciencedirect.com/science/article/pii/S0379711223003478.

[64] Jing Li and Stanislav I. Stoliarov. "Measurement of kinetics and thermodynamics of the thermal degradation for non-charring polymers". In: *Combustion and Flame* 160.7 (2013), pp. 1287–1297. ISSN: 0010-2180. DOI: https://doi.org/10.1016/j.combustflame.2013.02.012. URL: https://www.sciencedirect.com/science/article/pii/S001021801300062X.

[65] J.E.J. Staggs. "A reappraisal of convection heat transfer in the cone calorimeter". In: *Fire Safety Journal* 46.3 (2011), pp. 125–131. ISSN: 0379-7112. DOI: https://doi.org/10.1016/j.firesaf.2010.12.002. URL: https://www.sciencedirect.com/science/article/pii/S0379711210000962.

[66] Conor G. McCoy, Jessica L. Tilles, and Stanislav I. Stoliarov. "Empirical Model of flame heat feedback for simulation of cone calorimetry". In: *Fire Safety Journal* 103 (2019), pp. 38–48. ISSN: 0379-7112. DOI: https://doi.org/10.1016/j.firesaf.2018.11.006. URL: https://www.sciencedirect.com/science/article/pii/S0379711218303035.

[67] Tássia L.S. Quaresma, Tristan Hehnen, and Lukas Arnold. "Sensitivity Analysis for an Effective Transfer of Estimated Material Properties from Cone Calorimeter to Horizontal Flame Spread Simulations". In: *Submitted to: Fire Safety Journal* (2023). DOI: https://doi.org/10.48550/arXiv.2310.02680.

[68] Nicolas Hauke. "Numerical modeling of heat transfer from gas burners to vertical surfaces". Master Thesis. Bergische Universität Wuppertal (BUW), Chair of Computational Civil Engineering (CCE), Germany, May 2024, p. 116.

[69] "ISO 5658-2:2006(en) Reaction to fire tests – Spread of flame – Part 2: Lateral spread on building and transport products in vertical configuration". In: *International Organization for Standardization (ISO)* (2006). URL: https://www.iso.org/obp/ui/en/#iso:std:36963:en.

[70] "ISO 9239-1:2010(en) Reaction to fire tests for floorings – Part 1: Determination of the burning behaviour using a radiant heat source". In: *International Organization for Standardization (ISO)* (2010). URL: https://www.iso.org/obp/ui/en/#iso:std:45781:en.

[71] Karen De Lannoye et al. "Comparison of Black and Transparent PMMA in the Cone Calorimeter". In: *ASTM SELECTED TECHNICAL PAPERS STP1642: Obtaining Data for Fire Growth Models*. Ed. by Morgan C. Bruns and Marc L. Janssens. ASTM International, Mar. 2023, pp. 150–160. DOI: 10.1520/STP164220210105.

Schriften des Forschungszentrums Jülich
IAS Series

Band / Volume 61
Artificial Intelligence Framework for Video Analytics:
Detecting Pushing in Crowds
A. Alia (2024), xviii, 151 pp
ISBN: 978-3-95806-763-9

Band / Volume 62
The Relationship between Pedestrian Density, Walking Speed and Psychological Stress:
Examining Physiological Arousal in Crowded Situations
M. Beermann (2024), xi, 117 pp
ISBN: 978-3-95806-764-6

Band / Volume 63
Eventify Meets Heterogeneity:
Enabling Fine-Grained Task-Parallelism on GPUs
L. Morgenstern (2024), xv, 110 pp
ISBN: 978-3-95806-765-3

Band / Volume 64
Dynamic Motivation in Crowds: Insights from Experiments and Pedestrian Models for Goal-Directed Motion
E. Üsten (2024), ix, 121 pp
ISBN: 978-3-95806-773-8

Band / Volume 65
Propagation of Stimuli in Crowds:
Empirical insights into mutual influence in human crowds
H. Lügering (2024), xi, 123 pp
ISBN: 978-3-95806-775-2

Band / Volume 66
Classification of Pedestrian Streams: From Empirics to Modelling
J. Cordes (2024), vii, 176 pp
ISBN: 978-3-95806-780-6

Band / Volume 67
Optimizing Automated Shading Systems in Office Buildings by Exploring Occupant Behaviour
G. Derbas (2024), 9, x, 168, ccxxiii
ISBN: 978-3-95806-787-5

Band / Volume 68
Speed-Density Analysis in Pedestrian Single-File Experiments
S. Paetzke (2025), XIII, 107 pp
ISBN: 978-3-95806-818-6

Schriften des Forschungszentrums Jülich
IAS Series

Band / Volume 69
Proceedings of the 35th Parallel Computational Fluid Dynamics International Conference 2024
A. Lintermann, S. S. Herff, J. H. Göbbert (2025), xv, 321 pp
ISBN: 978-3-95806-819-3

Band / Volume 70
Towards Improved Civil Safety: Experimental Insights into Impulse Propagation through Crowds
S. Feldmann (2025), xi, 99 pp
ISBN: 978-3-95806-828-5

Band / Volume 71
Development and Evaluation of Architecture Concepts for a System-on-Chip Based Neuromorphic Compute Node for Accelerated and Reproducible Simulations of Spiking Neural Networks in Neuroscience
G. Trensch (2025), 219, XXXV pp
ISBN: 978-3-95806-832-2

Band / Volume 72
The tube furnace as a new bench scale experiment for pyrolysis
K. De Lannoye (2025), ix, 70 pp
ISBN: 978-3-95806-839-1

Band / Volume 73
Single-file Movement: Literature Review, Empirical Analysis with Artificial Neural Networks, and Modeling
R. Subaih (2025), x, 115 pp
ISBN: 978-3-95806-843-8

Band / Volume 74
Improvement and Validation of Visibility Models in Fire Safety
K. Börger (2025), ix, 97 pp
ISBN: 978-3-95806-857-5

Band / Volume 75
Simulation of Fire Propagation, Based on Material Pyrolysis
T. Hehnen (2025), VIII, 25, xcii pp
ISBN: 978-3-95806-875-9

Weitere ***Schriften des Verlags im Forschungszentrum Jülich*** unter
http://wwwzb1.fz-juelich.de/verlagextern1/index.asp

IAS Series
Band / Volume 75
ISBN 978-3-95806-875-9

Mitglied der Helmholtz-Gemeinschaft

JÜLICH
Forschungszentrum